ABSTRACT

CONE, STEPHANIE GRACE. Age-Dependent Changes in the Structure and Function of the Anterior Cruciate Ligament during Skeletal Growth. (Under the direction of Dr. Matthew B. Fisher).

Anterior cruciate ligament (ACL) injuries are occurring at increasing rates in pediatric and adolescent populations, and current treatment approaches have sub-par results in this young demographic including high secondary tear and injury rates. These outcomes may be improved by the development of age-specific treatments designed to work with the natural growth of the musculoskeletal tissues in the knee. However, there is currently a lack of studies in the orthopaedic field on age-specific changes in the structure and biomechanical function of the ACL during skeletal growth.

The objective of this dissertation was to study changes in the angular orientation, morphology, and biomechanical function of the ACL in both healthy and injured states during skeletal growth. Specifically, ACL growth was studied in a pre-clinical large animal model, the Yorkshire pig, from birth through late adolescence. First, magnetic resonance imaging was performed on porcine stifle (knee) joints from different age groups. From these images, we found that the angular orientation of the ACL increases in both sagittal and coronal planes during growth in a similar manner to previously published findings in humans. These images were further analyzed by measuring length and cross-sectional area to determine that the ACL grows in an allometric manner, with relative cross-sectional area and length proportions changing between age groups. Additionally, we found that the ACL grows in a disparate manner compared to other soft tissues in the joint. Within the ACL, there were varied responses to increasing age between the two primary bundles, the anteromedial and posterolateral bundles. Specifically, the anteromedial bundle continued increasing in cross-sectional area throughout adolescence whereas the size of the PL bundle plateaued at the onset of adolescence. These bundle-specific

findings were echoed in initial biomechanics studies where the two bundles had roughly equal functional roles under applied tibial loads and moments during youth, but the functional demands on the anteromedial bundle increased in adolescence. Finally, we studied the immediate impact of partial and complete ACL injuries on joints from juvenile through adolescent ages. Here we found an age-dependent response to partial ACL injury, as only late adolescent joints had a detectable change in kinematics in response to applied anterior tibial loads. Complete ACL injury resulted in changes to kinematic response to both anterior loads and varus-valgus moments regardless of skeletal age. These functional changes were further assessed by calculating *in situ* joint and ACL stiffness and *in situ* joint slack, where we found an increase in overall *in situ* stiffness with increasing age. The results of this work can be used to motivate *in vivo* surgical studies on age-specific clinical treatments for pediatric ACL injuries.

Age-Dependent Changes in the Structure and Function of the Porcine Anterior Cruciate Ligament During Skeletal Growth

by
Stephanie Grace Cone

A dissertation submitted to the Graduate Faculty of
North Carolina State University
in partial fulfillment of the
requirements for the degree of
Doctor of Philosophy

Biomedical Engineering

Raleigh, North Carolina
2019

APPROVED BY:

Matthew B. Fisher Committee Chair	Jacqueline Cole
Katherine Saul	Gregory S. Sawicki External Member
Jeffrey T. Spang	

BIOGRAPHY

Stephanie Cone was born in Little Rock, Arkansas and graduated high school from Pulaski Academy. She attended the University of Arkansas – Fayetteville where she obtained a Bachelor of Science degree in Biomedical Engineering with a minor in Nanotechnology. During her undergraduate career she studied the use of biocompatible polymers with implications in soft tissue regenerative medicine working with Dr. Kartik Balachandran. In the fall of 2014, she joined the Translational Orthopaedic Research Laboratory led by Dr. Matthew Fisher in the Joint Department of Biomedical Engineering at North Carolina State University and the University of North Carolina – Chapel Hill.

ACKNOWLEDGMENTS

This dissertation would not have been possible without the mentorship, advice, and support of many people. First, I would like to thank my family for encouraging me and supporting me in following my interests and passions throughout my life. In addition to my family, I've been able to accomplish my goals because of the support of many great friends from childhood through grad school who have grown to feel like family. Thank you all for being an amazing support network!

The majority of my grad school experience has involved the members of the Translational Orthopaedics Research Lab. Thank you all for being an extra set of hands for experiments, reviewers and critics helping to improve never-ending abstracts, papers, and presentations, and most importantly – excellent friends both in lab and out in the world. Paul Warren, Lewis Gaffney, Danielle Howe and Zack Davis were the best group of co-grad students to get through long hours in lab, countless outreach events, weekly meetings (and happy hours), and the best travel buddies for conferences. Stephanie Teeter was always available whether I needed someone to help find a lost poster, run a last minute freezer thaw, or keep me from ordering 200 boxes of gloves. And finally, this work never would have been completed without the help of my undergraduate researchers. While many undergrads have been involved in these projects over the years, Emily Lambeth and Hope Piercy stand out for both shear quantity and awesome quality of their contributions. Both of you put in several years of long hours, hard work, and great insights into these studies, and the projects both within this thesis and published in other areas would not be the same without you.

This dissertation would not be nearly as meaningful and well developed without the input and advice of my committee. Thank you so much to Dr. Jacque Cole, Dr. Jorge Piedrahita, Dr. Kate Saul, Dr. Greg Sawicki, and Dr. Jeffrey Spang for always being available to talk, for

sharing your insights, and for driving me to translate my experiments into an impactful dissertation. In addition to my committee I've benefitted from the assistance of many collaborators including Dr. Lynn Fordham, Dr. Hongyu Ru, Dr. Xiaopeng Zong, Sean Simpson, and Bruce Collins. Thank you all for your help over the years.

Finally, I would like to thank my advisor – Dr. Matt Fisher. Over the past 5 years I've been fortunate to learn so many aspects of academic research directly from you – ranging from technical skills in experimentation, robotics, writing, and presenting to soft skills of time management, developing collaborations, mentoring younger students, and turning an academic network into a strong circle of friends. Thank you for always taking the time to teach me and to support me.

TABLE OF CONTENTS

LIST OF TABLES

LIST OF FIGURES

CHAPTER 1

An Introduction to Age-Related Changes in the Pediatric Anterior Cruciate Ligament

Age-specific changes in the anterior cruciate ligament (ACL) are currently not well understood, a problem of growing interest to the orthopaedic community. In this chapter, I will describe the clinical and scientific relevance of this field of study, establish the current state of scientific literature regarding these changes, and discuss the use of the porcine model for ACL studies. Section 1.3 of this chapter has previously been published as a section of a literature reviews with the following citation (3).

(3) Cone, SG, Warren, PB, Fisher, MB. Rise of the Pigs: Utilization of the Porcine Model to Study Musculoskeletal Biomechanics and Tissue Engineering During Skeletal Growth. Tissue Eng Part C Methods. 2017;23(11):763-80. doi: 10.1089/ten.TEC.2017.0227. PubMed PMID: 28726574; PMCID: PMC5689129.

1.1. Pediatric ACL Injuries: A Growing Clinical Problem

The anterior cruciate ligament (ACL) is one of the primary musculoskeletal soft tissues in the knee, acting to stabilize the knee against anterior tibial translation as well as tibial rotation (4). The ACL attaches to the lateral wall of the intercondylar notch on the distal aspect of the femur, and the anterior aspect of the tibial plateau (2, 5). The ligament is comprised of highly aligned collagen fibrils which are organized into multiple bundles. These bundles are commonly described as the anteromedial (AM) and posterolateral (PL) bundles (6, 7), as shown in Figure 1-1, although some groups report an additional intermediate (IM) bundle (8, 9).

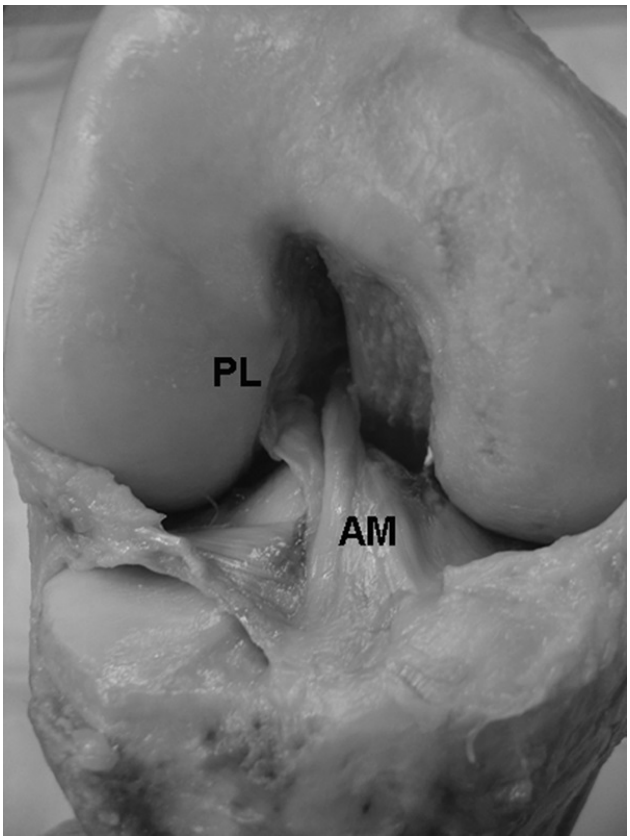

Figure 1-1. The ACL attaches to the anterior aspect of the tibia and the lateral wall of the femoral intercondylar notch, and is commonly divided into the anteromedial (AM) and posterolateral (PL) bundles as shown here. Figure reprinted from (2) with permission from Wolters Kluwer Health.

The structure of the ACL has successfully been studied though methods such as gross observation, arthroscopy, magnetic resonance imaging, and microscopic imaging in the past. However, understanding the function of the ACL has proven to be challenging due to the multidirectional nature of knee biomechanics. In order to study this tissue *in situ*, studies over the past 3 decades have employed 6-degree of freedom (DOF) robotic testing systems. The use of 6-DOF robotic systems has many benefits over more traditional single-axis tensile testing. This is due to the multi-axial nature of knee biomechanics. While the knee joint primarily moves in rotation through flexion and extension and experiences loading primarily in the anterior-posterior direction, additional loads and moments are resisted by the knee in the medial-lateral, superior-

inferior, varus-valgus, and internal-external directions. Relevant to the ACL, prior studies have shown that by limiting biomechanical studies to freedom only in the anterior-posterior direction the resulting kinematics and load distribution within the musculoskeletal soft tissues differs from a similar test allowing freedom in the other DOF (10). Furthermore, the use of 6-DOF systems allows for concurrent testing of multiple loading schemes on a single joint, leveraged within the current research as both anterior-posterior and varus-valgus testing was performed in the same joints. Many groups have employed this approach, and they have found that in mature knees the ACL resists anterior tibial loads as well as rotational loads in the varus-valgus and internal-external directions (10-19). These applications have included research on the biomechanical function of the ACL in both healthy and injured states. In this dissertation, I will describe our efforts to expand this field to incorporate age-dependent changes during skeletal growth into these applications.

When the structure of the ACL is compromised by either partial or complete injuries the stability of the knee can be compromised, impacting patients in both activities of daily living and high intensity athletics (20, 21). The standard treatment for ACL tears is surgical reconstruction, where graft tissue (autograft or allograft) is passed through tunnels in the femur and tibia in order to replace the structure of the injured ligament (22). While this approach is able to restore much of the original stability to the knee, ACL-reconstruction (ACLR) patients often incur further knee injuries to the ligaments and menisci, and experience osteoarthritis at rates nearing 50% within a decade of ACLR surgery (23, 24).

Concerningly, while ACL tears have traditionally been viewed as an issue primarily in adults, the reported incidence of ACL injuries in children and adolescents has been increasing rapidly over the past two decades. Specifically, ACLR rates are growing most rapidly in children between 10 and 13 years of age (25), and a recent study found that the average age of ACLR

patients in New York state had dropped to 17 years of age (26). ACL injuries create several immediate problems for these young patients, as in addition to the considerable pain and loss of stability associated with ACL injury, studies have shown that when students suffer from ACL injuries they frequently miss over 10 days of school, cannot return to sports for an average of 6 to 12 months, and report an average 0.3 drop in their grade point average (20, 23, 27, 28). In addition to these immediate issues, ACL injuries and ACLR surgeries are associated with worse outcomes in children and adolescents compared to adults. Secondary ACL injuries to either the graft or the contralateral ACL have been reported at rates of 29-32% in skeletally immature patients (23), or about 10X greater than the standard adult rates. Young patients also have higher rates of associated meniscal injury and suffer from similar rates of osteoarthritis to adults (24, 29).

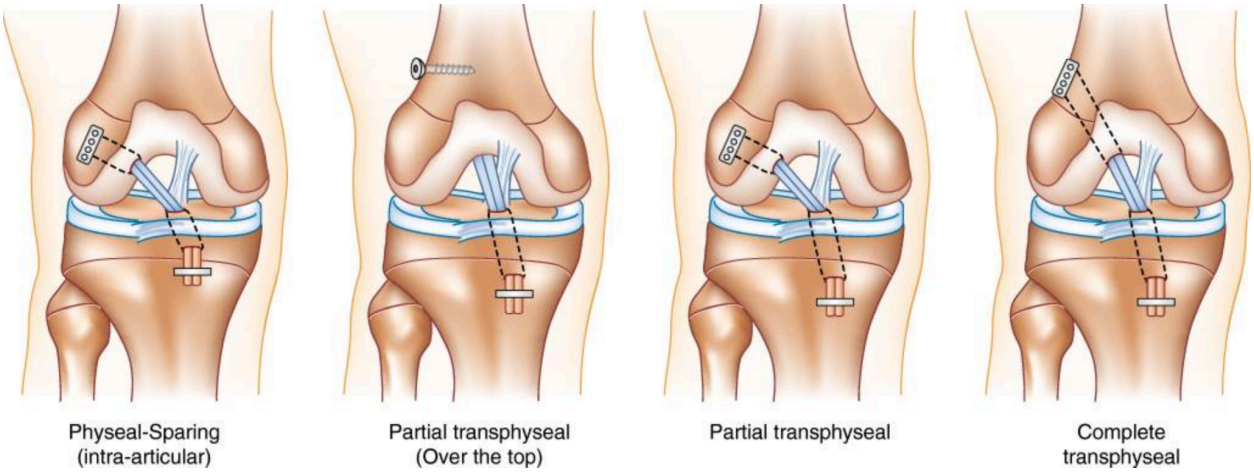

Figure 1-2. Common adaptations to ACL-reconstruction techniques are designed to avoid damage to the femoral and tibial physes, as in physeal-sparing, over the top, and partial transphyseal techniques in comparison to the complete transphyseal technique that is commonly applied in adults. Figure reprinted from (30) with permission from Springer Nature.

A potential explanation for the poor outcomes in pediatric and adolescent ACLR patients is that the ACLR surgeries traditionally used for adults do not replicate the native ACL in a growing knee as well as in mature knees (31). Furthermore, adaptations are sometimes made to

ACLR procedures for children in order to avoid injury to the growth plates (Figure 1-2) (30). While these adaptations provide protection for the femoral and tibial physes, it is possible that they compromise some of the biomechanical function intended by ACLR surgeries.

1.2. Established Age-Specific Properties of the ACL in Humans

In order to ensure that pediatric and adolescent ACLR procedures replicate age-specific tissue structure and function, we must first characterize the size, shape, and functional properties of the ACL during growth. Some studies have begun this line of research, with many studies focusing in the use of MRI to analyze tissue growth. MRI is advantageous for studying the size and shape of musculoskeletal soft tissues for several reasons. First, MRI does not involve any ionizing radiation, eliminating the exposure risks associated with methods such as x-ray and computed tomography(CT) scans (32). Second, MRI provides a 3-D view of internal soft tissues within the body in a single scan, whereas morphometric calculations from x-ray often require multiple films in order to capture images from different views. While this method can be used to create an estimate of the size and shape of ligaments, error from potential subject movement and reconstruction of images compounds with additional captures. Finally, MRI scans can be performed with many types of scan sequences in order to highlight specific tissues of interest. Common scan sequences can include T1-weighted and T2-weighted sequences with fat-suppression capabilities although more specific sequences are indicated for certain tissues of interest. Double-echo steady state (DESS) scan sequences are particularly beneficial for the knee joint, as they are capable of differentiating between the soft tissues of the knee (33).

Several groups have reported that the angular orientation of the ACL increases relative to the tibial plateau throughout growth, with increases in angle on the scale of 20° in both the sagittal and coronal planes (1, 34, 35). These changes in angular orientation may have significant

impacts on the distribution of force applied in plane with the tibial plateau between the segments of the lower limb. Additionally, one group found that the cross-sectional area (CSA) of the ACL increases earlier compared to the CSA of muscles around the knee (36). This finding suggests that musculoskeletal soft tissues in and around the knee joint respond differently to the environmental factors and mechanical stimuli initiating tissue growth. Another group found that the volume of the ACL ceases growth prior to the end of body growth assessed as body weight (37). This finding echoes the sentiment of the study reporting varied CSA growth across tissues, but expands on the findings to suggest that the ACL grows dissimilarly to the overall body, and as such to the scale of the mechanical forces transmitted through the knee joint.

Functionally, there is little information available on pediatric human tissue mechanics, however modeling studies have suggested lower tissue stiffness values in the Achilles tendon in young subjects (38), and mechanical studies on a very limited sample of pediatric cadaveric knees revealed low values of Young's modulus for pediatric ACLs (39). While direct measurements of the material properties of these tissues are limited, ongoing innovations in quantitative MRI may provide future avenues for assessing tissue mechanics *in vivo* in populations such as children and adolescents (40). Structural and functional tests can be highly invasive, so prior to studying changes in the human body, testing is often performed in a large animal model as discussed in the next section.

1.3. The Porcine Skeletally Immature Musculoskeletal Model

While there are several common large animal models for ACL studies, in this work all research was performed in Yorkshire cross-breed pigs, a large domestic pig breed. The selection of the pig model is discussed further in this section, an excerpt from *Rise of the Pigs: Utilization*

of the Porcine Model to Study Musculoskeletal Biomechanics and Tissue Engineering During Skeletal Growth (3).

In terms of fibrous soft tissues of the knee, Proffen et al. performed a comparative anatomy study of the knee joint (or equivalent stifle joint) between cow, sheep, goat, dog, pig, rabbit and human joints (41). All of the major soft tissue structures (ligaments, meniscus, etc.) were identified in all models. Unsurprisingly, differences in the limits of full extension were evident between the human knee and the animal stifle joints (0° of flexion in humans vs. 22-45° of flexion in the animals). Finer anatomical differences also existed. For example, the bundles of the anterior cruciate ligament (ACL) in the cow, sheep, and pig joints all were separated by the anterior insertion of the lateral meniscus on the tibial plateau. Based on gross anatomy alone, the authors concluded that sheep, cows, and goats had the most similar ACL to humans. In terms of dimensions, the absolute width and length measurement of the ACL were significantly similar between humans and cows, sheep, and pigs. Importantly, all species exhibited an ACL featuring multiple bundles, consistent with other work including more exotic species such as deer, bears, lions, and antelope (42, 43). Interestingly, this study found less similarity between all of the animal models and humans for the PCL. The authors proposed that this may be related to the altered biomechanical demands of the knee in bipeds and quadrupeds.

Biomechanical comparisons of the ACL in several species have also been performed (44). Specifically, the *in situ* forces in the anteromedial (AM) and posterolateral (PL) bundles under an applied anterior drawer load were compared across humans, pigs, goats, and sheep using a modified materials testing system. Relative to humans, the magnitude of force in the ACL and both bundles and the direction of force in the ACL and AM bundle were significantly different in goats and sheep. The only statistically significant difference between the pig and human was in the magnitude and direction of force in the PL bundle. The authors concluded that

the pig model was a better analog for human knees based on *in situ* biomechanics, although all three remain common pre-clinical models (45-50).

Additional studies using the porcine model within a robotic testing system illustrated how restricting degrees-of-freedom (DOF) within the knee joint under applied loads can greatly impact the direction of the force in the ACL and the relative distribution of force across the AM and PL bundles (10). Furthermore, recent studies in the human ACL have highlighted regional heterogeneity in the mechanical properties within each ACL bundle (51). It is unclear how well pigs or other large animal models match this sub-bundle biomechanical heterogeneity.

With respect to the meniscus, Proffen et al. found that pigs, sheep, and goats were most comparable to humans in regards to size, while the goat model also had similar insertion site locations to humans (41). Further studies by Takroni et al. compared human, sheep, and pig menisci and found that sheep menisci were more similar than pig menisci to human tissues in terms of tissue volume and weight, although the human menisci had significantly greater circumference than both animal models (52). In addition to studies on the body of the meniscus, inter-species comparisons have been made regarding the meniscofemoral ligaments (MFLs). The posterior MFL was present in humans, dogs, sheep, and shire horses, whereas there were no comparable tissues found for the human anterior MFL (53).

Additional studies have compared the biomechanical properties of the human meniscus to those found in baboons, cows, dogs, pigs, and rabbits (54). Across all models, the posterior region of the medial meniscus featured a lower shear modulus and aggregate modulus relative to the anterior and central regions. The authors noted that no single animal model is ideal across the board for meniscus studies, but the bovine model was most similar to humans for aggregate and shear modulus, and the canine and baboon models were the most similar to humans in terms of permeability. Studies comparing human menisci to those from pigs, sheep, dogs, monkeys,

and cows found that sheep exhibited the most similar aggregate modulus and permeability values to human data (55). Other reviews of animal models for meniscus repair have confirmed that no one model is the current gold standard, and that the specific hypothesis should be carefully considered when selecting an appropriate large animal model (56).

One challenge in the use of animal models for translational research is the definition of age equivalency. Age can be defined on several scales including chronological age, sexual age, and skeletal age (57). Within the pig model, chronological growth occurs on a significantly accelerated timeline compared to human growth. Many pig strains reach sexual maturity between 4.5 and 6 months of age (58), and this age range is often used to describe "early adolescence." Skeletal age in humans is classically measured from a left-hand radiograph, and the lack of similar bony anatomy in the porcine forelimb makes this a difficult comparison (59). Depending on the particular bone, physes in hind limbs of Yorkshire pigs close between 12 and 20 months of age (58). As such, this age range (and sometimes a little older) is often used to define the end of "adolescence." We will use the following terms to describe age: young (0-4.5 months), early adolescent (4.5-6 months), adolescent (6-18 months), late adolescent (18-24 months), and adult (>24 months).

A second consideration is that dozens of porcine strains exist. Some, such as Yorkshire pigs, are bred to gain weight rapidly for use in the food industry. Universities with agricultural programs often have closed herds of these animals. Often, the closely controlled genetics of these herds is useful from a scientific genetic standpoint (control groups can be siblings). Several strains are dubbed "minipigs," including Yucatan, Hanford, Lee-Sung, Gottingen, and Changfeng minipigs, among others (60-64). Many of these minipig lines exist in closed herds and have been bred specifically to limit rapid growth and increase docility, easing their use in biomedical research.

Several studies have examined biological differences between pig strains in terms of complications due to anesthesia (65) or the response of the skin to light due to differences in skin pigmentation (66). In terms of biomechanics, Germscheid et al. studied porcine medial collateral ligaments (MCL) and the biomechanical differences between Yorkshire and red Duroc strains (67). It was found that while MCL dimensions of both breeds were comparable to human MCLs, MCLs from the Duroc strain were larger in cross-sectional area and had lower tensile failure stress compared to MCLs from the Yorkshire strain. These findings suggest that inter-strain differences exist for the porcine model, although direct comparisons between strains have been limited to date and require further investigation.

A third consideration is the importance of the sex of the animals being studied. Unfortunately, research investigating the importance of sex in the porcine model is limited. In Gottingen minipigs ranging in age from 11-55 (mean 24) months, males had significantly higher mean cartilage thickness than females in the lateral facet of the trochlear groove (68). Separate work showed that sex, but not birth weight, had an effect on glucose intolerance in Yucatan minipigs (69). Females had a higher visceral and subcutaneous adiposity and subsequent glucose intolerance than males after 10 months of the same feeding regimen, which is consistent with human data. More recently, Kiapour et al. studied an ACL transection model in adolescent (15 months on average) Yucatan minipigs repaired either with a conventional reconstruction using a soft tissue graft or combining with a collagen-platelet-rich plasma (PRP) treatment and found several differences between sexes (70). For example, females had 19% lower yield load and 12% lower stiffness than males after 15 weeks of healing. Furthermore, in animals treated with conventional reconstruction, females had larger areas of articular cartilage damage. These data suggest that tissue engineering strategies may need to be tailored to the sex of the patient.

CHAPTER 2

Objectives

Childhood and adolescent ACL injury incidence has been increasing in the past few decades, and current treatment approaches in young patients result in sub-par outcomes. Increased incidence of secondary ACL tears, additional soft tissue injuries, and high rates of osteoarthritis motivate further research into age-specific function of the knee and the ACL specifically. In order to understand the causes of the outcomes and develop age-appropriate treatments for this patient population, we first need to improve our understanding of structural and functional changes that occur in the knee during healthy growth.

Thus, the broad objective of this thesis is to take an in depth look at changes in the structure and function of the ACL during skeletal growth. In order to address this gap, we used a pre-clinical large animal model, the Yorkshire pig. This model was selected for its proven similarity to the human ACL in both structure (41) and relative AM and PL bundle function (44). Stifle joints, the porcine knee equivalent, were collected from pigs ranging in age from birth through skeletal maturity and experiments using magnetic resonance imaging and a robotic biomechanical testing system were performed to study changes in the structure and function of these joints throughout growth. In order to approach this topic, there will be five major aims: (1) to quantify changes with age in the angular orientation of the ACL (Chapter 3), (2) to assess and compare the size and proportions of the ACL to other ligaments and tendons across ages (Chapter 4), (3) to measure changes during growth in the structure (cross-sectional area, length, and angular orientation) and function (under applied anterior loads and varus-valgus moments) of the primary bundles of the ACL along with assessing changes in knee kinematics under applied loads (Chapter 5), (4) to study the impact of partial and complete ACL injury on skeletally immature knee function (Chapter 6), and (5) to analyze changes with age in the shape

of load-deformation curves in response to applied anterior-posterior tibial loads throughout skeletal growth in both healthy and injured states (Chapter 7). Through these five aims, I describe how we intend to improve our understanding of how the tissues in the knee joint grow and how these structural changes impact the biomechanical function of the joint during skeletal growth.

CHAPTER 3

Angular Orientation of the Porcine ACL Increases with Post-Natal Growth

The initial study within this dissertation aimed to compare the porcine ACL during growth to the human ACL by measuring changes which were previously established in human literature: changes in the angular orientation of the ligament relative to the tibial plateau. Several papers have documented this change during growth in through retrospective MRI studies, finding that there are significant increases in the angle of incidence between the ACL and the tibia with the onset of adolescence (1, 35, 71). By performing this study, we hoped to find similar changes in the orientation of the porcine ACL during growth, as that would suggest continuity between age-dependent properties in the human ACL and our selected pre-clinical model, the pig.

The text in this chapter was previously published in the Journal of Orthopaedic Research, under the following citation (34) and is reprinted with permission from John Wiley and Sons.

(34) Cone SG, Simpson SG, Piedrahita JA, Fordham LA, Spang JT, Fisher MB. Orientation changes in the cruciate ligaments of the knee during skeletal growth: A porcine model. J Orthop Res. 2017;35(12):2725-32. doi: 10.1002/jor.23594. PubMed PMID: 28471537; PMCID: PMC5671372.

3.1. Introduction

Anterior cruciate ligament (ACL) injuries of the knee are increasingly common in the pediatric and adolescent populations (72). Incidence rates of ACL injury in patients under 18 years of age have been increasing rapidly, with the overall rate of ACL injury in this population nearly tripling over the past twenty years from 17.6 to 50.9 per 100,000 people aged 13-20 (26). Concurrently, the rate of ACL reconstruction in patients under 14 years old has increased by 11% every year since 2006 (25).

Clinical approaches to pediatric ACL injuries can be divided into conservative and surgical treatments. Conservative treatments avoid the risk of introducing additional damage to musculoskeletal structures (including open physes) and include functional bracing and activity modification to address the instability associated with ACL deficiency (20). Surgical reconstruction of the disrupted ACL in the pediatric patient requires modification of the traditional adult techniques to avoid direct interruption of the growth plates, and can be defined as all-epiphyseal, partial-transphyseal, transphyseal, or extraphyseal techniques depending on the graft placement (73, 74). Additionally, treatment of pediatric ACL injury is complicated by altered anatomic features relative to adult knees, requiring specialized procedures which are compatible with both the current anatomy and future anatomic changes throughout growth. Despite the modifications employed in current treatment of pediatric ACL injuries, complications include limb length discrepancy, high rates of graft failure requiring surgical revision, and early-onset osteoarthritis (OA) (73). Early onset osteoarthritis is a major concern with young patients, as the incidence of OA is approximately 50% at 10 year follow-up after ACL injury regardless of patient age (75). Between the increased pediatric injury incidence rates, challenges to surgery in growing patients, and long term risk factors, there is an increased need for improved understanding of the age-dependent structure and function of the ACL in both healthy and injured states.

One potential complication in developing age-appropriate treatments is the changing structure and function of the skeletally immature knee. Decreases in both cellularity and vascularity in the ACL with increasing age have previously been reported in skeletally immature animal models (76). Moreover, changes in matrix organization of ligaments in the knee have been found during growth, with increasing collagen alignment in older specimens (77). In humans, the angular orientation of the ACL measured relative to the tibial plateau increases

substantially from birth through adolescence (1). Specifically, the orientation in both the sagittal and coronal planes changes over time with increases in the coronal plane of approximately 20° and increases in the sagittal plane of 15°, creating a more "vertical" orientation over time. The posterior cruciate ligament (PCL) also experiences an approximately 15° increase in the relative angle of its horizontal and vertical components, and an overall decrease in the horizontal-to-vertical aspect ratio with age (1). By furthering the general knowledge of these changes in healthy patients, age-specific treatments can be designed to work within the growing joint and facilitate future changes during growth and maturation.

A unique challenge in studying pediatric ACL structure and function is the limited availability of human cadaveric specimens. As such, validated large animal models provide a mechanism to study injuries and treatments during skeletal growth (78). Relative to other animal models, the adult porcine ACL is closest to human ACL in terms of dimensional parameters such as relative ACL width and length (41). Additionally, the adult porcine ACL proved more similar to the human ACL in terms of its biomechanical properties and the direction of force under anterior tibial loading than either the sheep or the goat (44). A complicating factor in performing translational growth and development studies in a large animal model is establishing the relative ages of the models. Age can be described using several different scales, including chronological age, skeletal age, and sexual age (57). Pigs and humans experience growth on different chronological scales, with pigs experiencing far more rapid growth and shorter lifespans. Human skeletal growth is often indexed based on a left-hand radiograph (59), a system which does not easily translate to the porcine model. As such, the most commonly applied age equivalency between pigs and humans is based on a combination of skeletal age and sexual age, which defines age relative to pubertal changes. The age groups in this study are representative of the spectrum of growth, namely, newborn (0 month old), juvenile (1.5 and 3 month old), early

adolescent (4.5 month old), adolescent (6 month old), and late adolescent (18 month old) age groups (58).

In order to establish a pre-clinical large animal model for skeletally immature knee injuries, the objective of this study was to characterize the changes in the orientation of the porcine ACL and PCL during post-natal skeletal growth, and to compare these changes to corresponding human values available in the literature. Given the large changes in cruciate ligament orientation observed in humans during skeletal growth and the similarities in the ACL and PCL in skeletally mature pigs and humans, we hypothesized that the porcine model would exhibit significant changes in ACL and PCL orientation throughout skeletal growth.

3.2. Materials and Methods

3.2.1. Study Design

A total of 36 stifle (knee equivalent) joints were collected from female Yorkshire pigs (one joint per animal) at 0, 1.5, 3, 4.5, 6, and 18 months of age (n=6 per time point, Swine Educational Unit at North Carolina State University). The animals used in this study were obtained from a university owned herd, and all animals were healthy and of normal size. Swine were cared for according to the management practices outlined in the Guide for the Care and Use of Agricultural Animals in Teaching and Research and their use in the current experimental protocols was approved by the N.C.S.U. Institutional Animal Use and Care Committee (79). Animals were euthanized by one of two IACUC approved methods, intravenous injection of sodium pentobarbital, or penetrating captive bolt euthanasia followed by jugular exsanguination. The limbs were isolated from the pigs immediately following euthanasia and were stored at -20 degrees Celsius until testing.

3.2.2. Magnetic Resonance Imaging

Limbs were removed from the freezer and allowed to thaw at room temperature prior to imaging. All limbs were imaged at full extension, which in the porcine model is approximately 35 degrees of flexion. Tissues were wrapped with saline-soaked gauze for imaging. Due to the small feature size in 0 month old specimens, imaging of the 0 month old limbs was performed in a separate scanner with improved resolution relative to the scanner employed for the other age groups. MR imaging for 0 month old limbs was performed in a 9.4-Tesla Bruker BioSpec 94/30USR machine (Bruker BioSpin Corp, Billerica, MA) using a 3D fast low angle shot scan sequence (3D-FLASH, flip angle: 10°, TR: 38 ms, TE: 4.42 ms, acquisition time: 13 hours 18 minutes, FOV: 30x30x30 mm) and a 35 mm volume coil with a voxel size of 0.1x0.1x0.1 mm and no gap between slices. MR imaging for 1.5, 3, 4.5, 6, and 18 month old limbs was performed on a 7.0-Tesla Siemens Magnetom machine (Siemens Healthineers, Erlangen, Germany) with a 28 channel knee coil (Siemens Healthineers, Erlangen, Germany) using a double echo steady state scan sequence (DESS, flip angle: 25°, TR: 17 ms, TE: 6 ms, acquisition time: 24 minutes, FOV: 123x187x102 mm) with a voxel size of 0.42x0.42x0.4mm and no gap between slices. These sequences were selected as they allow for visualization of the boundaries between all musculoskeletal soft tissues within the knee joint at an adequately high resolution for post-processing and analysis.

3.2.3. Image Post-Processing

Image post-processing was performed in commercial tissue segmentation software (Simpleware 7.0, Synopsys, Chantilly, VA) using the “Distance”, “Angle”, and “Disconnected Angle” tools. All image processing and measurements were performed by a single author (SC) and analysis techniques had high intrareader repeatability (Intraclass Correlation Coefficient (ICC)=0.7113-0.9942) and interreader repeatability (ICC=0.7091-0.9702) (Table A-1-5). The

orientation and horizontal-to-vertical aspect ratios of the cruciate ligaments were collected using definitions established in the literature (1). As shown in Figure 3-2A, the sagittal angle of the ACL was collected by measuring the angle between the anterior edge of the ACL relative to the anterior-posterior line of the tibial plateau. This measurement was taken from the first full slice of the ACL approached from the medial aspect of the knee. The coronal angle of the ACL was collected from the medial edge of the ACL relative to the tibial plateau, as shown in Figure 3-2A. This measurement was performed on the first scan slice with a full image of the ACL moving from the anterior aspect of the knee.

Analysis of the posterior cruciate ligament (PCL) included measurement of the PCL angle and the horizontal-to-vertical ratio, as seen in Figure 3-3A. The PCL angle was calculated as the angle between the horizontal and vertical components of the ligament in the sagittal plane. The PCL horizontal-to-vertical ratio was calculated by dividing the length of the horizontal component by that of the vertical component, as measured from sagittal plane images.

The Blumensaat line-to-ACL angle was described as the angle between the Blumensaat line and the anterior surface of the ACL in the intercondylar notch in the sagittal plane. The angle of inclination of the intercondylar roof was the sagittal plane angle of the intercondylar roof relative to the long axis of the femur. Notch width was calculated in the coronal plane following methods established in previous literature, in which the notch width index (NWI) was defined as the ratio of the intercondylar notch width and the width of the distal femur (80-83). These widths were measured from a coronal image along the medial-lateral line which intersected the notch at one-half the total notch height.

3.2.4. Statistical Analysis

Statistics were performed using SPSS (v21.0, IBM, Armonk, NY). All specimens (36/36) were used in data analyses and statistical testing. Normality was verified for each data set with

the Kolmogorov-Smirnoff test. Analysis for all data sets consisted of a one-way analysis of variance (ANOVA) with specimen age as the independent variable. Tukey's and Games-Howell post hoc tests were used for further analysis depending on if the groups had equal or unequal variances, respectively. Overall significance was set at $p<0.05$. Data presented as mean ± standard deviation.

3.3. Results

Magnetic resonance images of porcine knees ranging from newborn to 18 month age groups revealed overall size increases, gross morphology changes, and differences in tissue orientation (Figure 3-1). In young specimens, the femur and tibia had a higher proportion of epiphyseal cartilage relative to the epiphyseal bone. By the adolescent age groups, only a thin layer of articular cartilage remained. Open growth plates were observed throughout the early adolescent stages, reaching a state of near or complete fusion by the late adolescent (18 month) age.

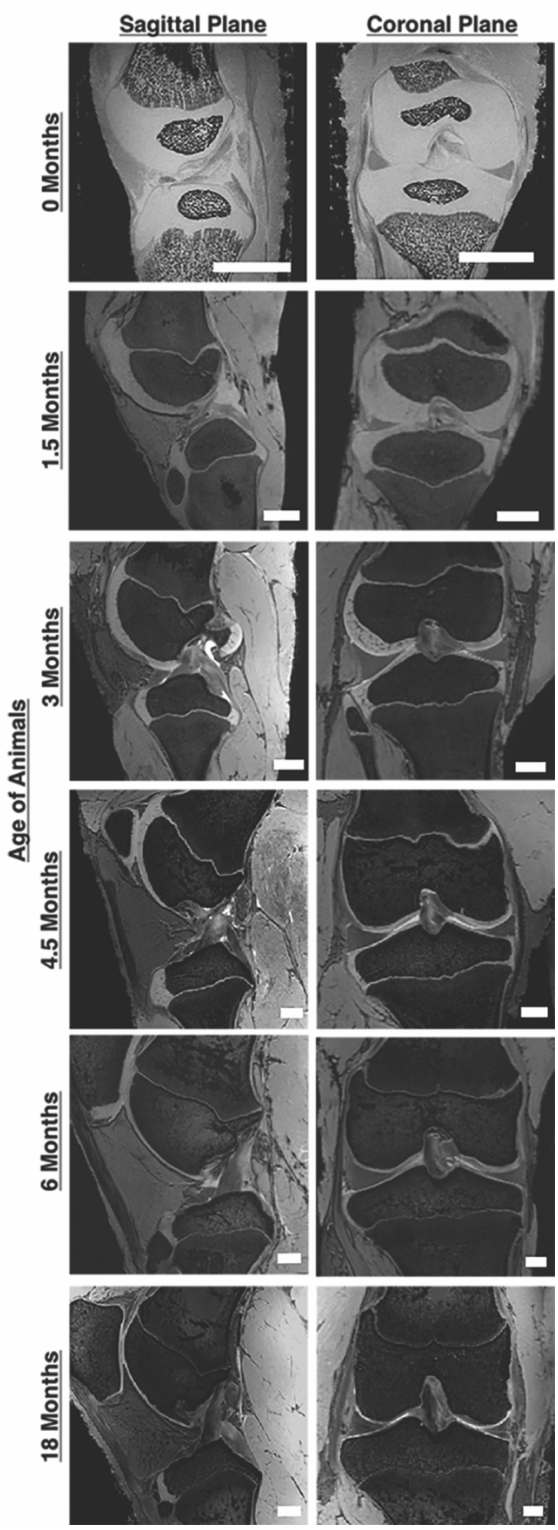

Figure 3-1. Magnetic resonance images of porcine stifle joints in the sagittal and coronal planes at 0, 1.5, 3, 4.5, 6, and 18 months of age. Scale bars are 10mm.

Analysis of the sagittal angle of the ACL relative to the tibial plateau revealed a statistically significant effect due to age (Figure 3-2B), as mean values from increased 30° in the newborn group to 60° in the 18 month old group which resulted in an overall change of 30° throughout growth. The most rapid change in sagittal angle occurred between 3 and 4.5 months (11° change between the group means over a 1.5 month timespan, $p<0.05$). Interestingly, the mean sagittal angle continued to increase by 11° between the 6 and 18 month time points ($p<0.05$). Analysis of the coronal angle revealed statistically significant effects due to age through the 4.5 month (early adolescent) age group (Figure 3-2C), with insignificant change occurring afterwards, which represented an overall increase of 41° throughout skeletal growth. Similar to the sagittal angle, the most rapid changes occurred between 3 and 4.5 months (15° change on average over 1.5 months, $p<0.05$); however, unlike the sagittal angle where major changes continued throughout adolescence, no statistically significant differences (3° and 5°) were found between 4.5 and 6, and 6 and 18 months, respectively ($p>0.05$).

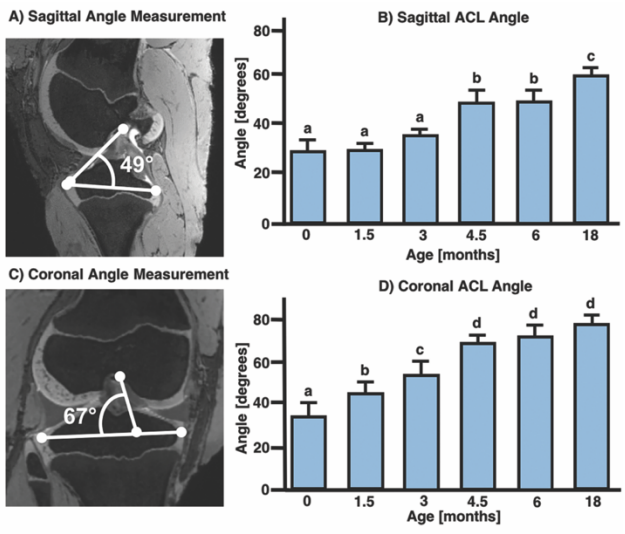

Figure 3-2. The angle of orientation of the ACL in both the sagittal and coronal planes is measured as shown in panels A and C. The sagittal angle (B) increases significantly between 3 and 18 months (late adolescence equivalent) while the changes in coronal angle (D) becomes insignificant after 4.5 months (early adolescence) in the porcine model. Data are presented as mean ± standard deviation, and age groups with different letters are statistically significant from one another. For example, for the sagittal ACL angle (panel B below), the 0 and 1.5 month age groups are not statistically different since they share a letter ($p>0.05$). The 3 and 4.5 month age groups are statistically different because they do not share a letter.

The angle of the PCL increased from 112° to 142° in the first 18 months of growth, and these changes were significant between consecutive age groups up to the 4.5 month (early adolescent) time point (Figure 3-3B). The largest changes in PCL angle occurred between 1.5 and 3, and 3 and 4.5 months of age with differences of 12° and 9° on average, respectively ($p<0.05$). No statistically significant changes were found following the onset of adolescence, with a mean difference between 6 and 18 month groups of only 2° over the course of 12 months ($p>0.05$). The PCL horizontal-to-vertical aspect ratio increased by nearly two-fold from 0.50 to 0.93 during skeletal growth, and significant changes occurred through late adolescence ($p<0.05$).

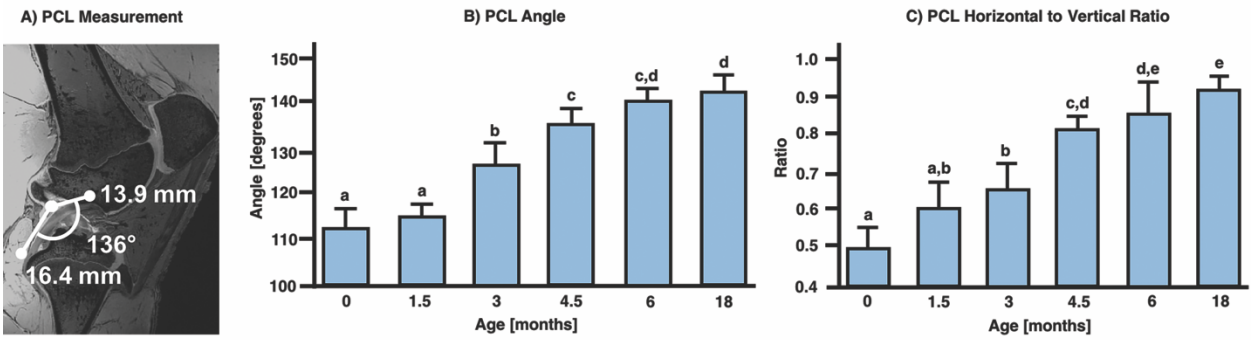

Figure 3-3. The PCL angle, measured between the horizontal and vertical components shown in panel A, increases with increasing age (B). Significant increases occur between consecutive age groups between 1.5 and 4.5 months of age, equivalent to an early adolescent age in humans. The horizontal-to-vertical ratio, calculated from these components, nearly doubles throughout skeletal growth, with significant changes occurring through late adolescence (18 months). Data are presented as mean ± standard deviation, and age groups with different letters are statistically significant from one another. For example, for PCL angle (panel B below), the 0 and 1.5 month age groups are not statistically different since they share a letter ($p>0.05$). The 1.5 and 3 month age groups are statistically different because they do not share a letter.

The angle between the Blumensaat line and the ACL decreased from 10° to 5.6° from birth to skeletal maturity in the porcine model (Table 3-1). These changes occurred gradually and only reached statistical significance across multiple time points (1.5 month to 6 months, for example), opposed to other orientation changes which are significant between sequential groups ($p>0.05$). Additionally, the angle of incidence of the intercondylar roof experienced a 5-fold decrease with increasing age (mean values of 32.9° and 5.7° at birth and 18 months, respectively) (Table 3-1); however, these changes were significant between sequential age groups through the onset of adolescence ($p<0.05$).

Table 3-1. Data on the angle between the Blumensaat line and the ACL and the angle of incidence of the intercondylar roof. Both angles decrease with increasing age. Data are presented as mean ± standard deviation, and age groups with different letters are statistically significant from one another. For example, for Blumensaat angle, the 0 and 1.5 month age groups are not statistically different since they share a letter ($p>0.05$). The 0 and 18 month age groups are statistically different because they do not share a letter.

Age [months]	Blumensaat-ACL Angle	Intercondylar Roof Angle
0	$10.0\pm1.3^{a,b}$	32.9 ± 4.3^{a}
1.5	12.4 ± 2.1^{a}	35.7 ± 5.5^{a}
3	10.8 ± 1.5^{a}	18.9 ± 6.8^{b}
4.5	$9.6\pm2.6^{a,b}$	14.4 ± 2.9^{b}
6	$7.4\pm1.2^{b,c}$	6.1 ± 1.0^{c}
18	5.6 ± 2.3^{c}	5.7 ± 3.1^{c}

The notch width aspect ratio (Figure 3-4), calculated as the ratio of the horizontal length to the vertical width of the intercondylar notch, decreased with increasing age during the juvenile age groups (0-3 months), with minimal changes throughout the remainder of skeletal growth ($p>0.05$). Specifically, 84% of the total change in aspect ratio occurred prior to 3 months of age in the porcine model. This data reflected the changing bony morphology near the cruciate ligaments, and coincided with the change in epiphysis composition from a highly cartilaginous tissue to more defined bony structure.

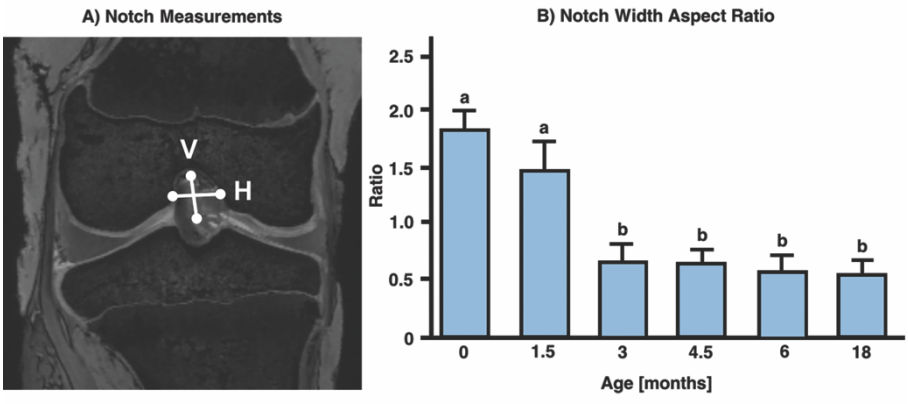

Figure 3-4. Notch width aspect ratio is calculated as a ratio of the horizontal ("H") and vertical ("V") notch measurements (A). Values decrease with increasing age, and statistically significant changes occur prior to early adolescence. Data are presented as mean ± standard deviation, and age groups with different letters are statistically significant from one another. For example, for notch width aspect ratio (panel B below), the 0 and 1.5 month age groups are not statistically different since they share a letter ($p>0.05$). The 1.5 and 3 month age groups are statistically different because they do not share a letter.

3.4. Discussion

In order to study age-specific treatments in childhood musculoskeletal injuries, including ACL tears, a pre-clinical model exhibiting age-dependent changes similar to those seen in humans must be validated. This study has established in the female porcine model that the relative angle of the ACL to the tibial plateau increases in both the coronal and sagittal planes during post-natal skeletal growth. Additionally, the angle of the PCL changes throughout skeletal growth. All of the changes occur in an age-dependent manner, in accordance with the stated hypothesis.

Humans experience significant orientation changes in the angular orientation of the ACL relative to the tibial plateau, with both the sagittal and coronal angles increasing by approximately 20° relative to the tibial plateau from early childhood through adulthood (1). Interestingly, the human data vary between male and female patients, with the sagittal angle of the ACL increasing through late adolescence in females and reaching a plateau during adolescence in male patients. These changes are concurrent with other sex-dependent

differences, as significantly smaller intercondylar notches were found in the distal femur of adolescent female pigs relative to male pigs (81). The current study found that the sagittal and coronal ACL angles also increase in the porcine model throughout skeletal growth. Moreover, female specimens in this study matched sex-specific findings in humans. The sagittal angle of the porcine ACL increases in the female pig throughout late adolescence (18 months) and human data from female subjects also change through late adolescence (17-20 years) (1). However, the coronal ACL angle increases only through an earlier stage of adolescence (6 months) in the pig. Likewise, the coronal angle of human female patients reaches a plateau at approximately 65° shortly after the onset of puberty (1). This suggests that future work in the porcine model needs to include similar characterization of soft tissue changes in a male population in order to determine the validity of the pre-clinical model for determining potential sex-based differences. Interestingly, the specific timing of these changes are similar in the human and porcine models, with major increases in the sagittal angle through late adolescence, while the coronal angle increases up to the onset of adolescence, with little change thereafter (Table 3-2).

Table 3-2. The specific timing of orientation changes in the cruciate ligaments is similar between humans and the porcine model, with continued changes in the sagittal angle throughout adolescent growth, unlike the changes in the coronal ACL angle and the PCL angle which occur primarily during the early stages of growth. Data are presented as a percentage of the total orientation change from early youth through late adolescence in each species. Age groups are as follows: [a]0-3 years, [b]10-13 years, [c]1.5-3 months, [d]4.5-6 months, [e]18-20 years, [f]18 months. Human data from Kim et al (1).

Anatomic Feature	Human Early Youth[a] to Pre-Adolescence[b]	Porcine Early Youth[c] to Pre-Adolescence[d]	Human Pre-[b] to Late-Adolescence[e]	Porcine Pre-[d] to Late-Adolescence[f]
Sagittal ACL Angle	~50%	~60%	~50%	~40%
Coronal ACL Angle	~71%	~75%	~29%	~25%
PCL Angle	~75%	~77%	~25%	~23%

While the PCL tends to be less frequently studied due to lower injury incidence rates (around 8-10% of the rate of ACL injury) (84-87), it serves as an additional comparison between the porcine model and humans. The angle between the horizontal and vertical aspects of the PCL experience a significant increase during skeletal growth (~15° increase) in human subjects.(1) Similar changes were seen in the porcine model (~30° increase). However, a comparison of horizontal-to-vertical component ratios of the PCL between human and porcine images differs with ratio decreases occurring with increasing age in humans, and ratio increases with increasing age in pigs. This disparity could be caused by several factors including different anatomy of the femur, altered loading patterns, and a major variation in the flexion angle of the joint at full extension (0° in humans, ~35° in pigs). Previous studies of pre-clinical knee models have found that the human PCL is relatively wider than the porcine PCL; however, the porcine model exhibits a similar length between the femoral and tibial insertion sites to the human knee (41).

In both human and porcine studies, the angle of incidence of the intercondylar roof decreased with increasing age, in a manner potentially related to the altered angle of the ACL (1). Intercondylar roof angle has been correlated with ACL injury and tibial spine fractures at the distal insertion of the ACL in previous literature, with significant differences in the average intercondylar roof angle between the two injury mechanisms (88). When considering the angle between the Blumensaat line and the ACL, an interesting relationship between the models appears. In human subjects, the relationship between age and angle is only statistically significant when considering values from patient 2 years old and under (1). Similarly, in the porcine model, the only statistically significant changes in this parameter are found between newborn and early juvenile age groups, with insignificant changes occurring thereafter. Anatomical differences between human and porcine knees make a comparison of notch widths difficult, as human notch width index is traditionally measured at the level of the popliteal

groove, yet a direct comparison of this anatomic landmark is not available in pigs across all age groups. However, the notch measurements in this work are taken using similar metrics to previous studies (81). As such, the notch width aspect ratio may aid in understanding growth trends in the soft tissues of the porcine knee, as the bony anatomy can affect the structure and function of soft tissues within a joint.

A limitation of this study is the inclusion of only female porcine specimens. Given the promising results of this initial work, future plans include similar studies on male pigs throughout skeletal growth in order to study the impact of both age and sex. An additional limitation of this study is the interspecies translation of ages between humans and pigs. However, using sexual maturity as a comparison scale, many similarities between pigs and humans were found in terms of ACL and PCL orientation. Additionally, the specific accuracy and repeatability measures established in this work are only applicable to *in vitro* work, and would need to be re-established for any *in vivo* tests as limb positioning would be more challenging. Finally, the study is limited by comparison of specific porcine data to approximated human data collected from the literature. Without a wide range of age-specific human scans, this limits the analysis performed in this work to a subjective comparison instead of a statistical one.

The anterior and posterior cruciate ligaments are two of the primary soft tissue stabilizers within the knee. The findings presented in this work show that major changes occur in the anatomic orientation of both ligaments throughout skeletal growth; however, orientation is only one of many factors which determine the overall function of the tissues. Other properties, including geometric measures, material properties, and intrinsic force distributions must be studied in order to develop a more complete understanding of the changes during post-natal growth and their impact on total knee behavior. Further work is needed to expand data that can be studied in both human and porcine models through non-invasive methods, including imaging

based analysis of tissue size and geometry (e.g. tissue volume, CSA, and length). These parameters can be evaluated at a higher resolution through high-strength MR imaging in both humans and the porcine model, which may be particularly important for smaller (i.e. younger) specimens (37, 89, 90). This may provide further verification that the porcine model has the potential to mimic complex processes involved in the growth of pediatric patients. Following further investigation of non-invasive parameters, characteristics including the biomechanical properties of musculoskeletal soft tissues will be investigated in the skeletally immature porcine model and/or through correlation analysis of imaging parameters and tissue properties.(40, 91)

In summary, this work demonstrates that the female porcine model experiences age-dependent changes in the orientation of the cruciate ligaments that mirror prior findings in skeletally immature humans during post-natal growth. This suggests that the porcine model may be appropriate for studying the ACL during normal growth, ACL injury, and response to clinical interventions in future studies. Given the growing prevalence of pediatric ACL injuries, an appropriate pre-clinical model will be instrumental for studying the long-term effects of ACL reconstructions, including graft remodeling and return of joint function.

3.5. Conclusions and Broader Impact

Through this study, we were able to show that the porcine ACL experiences significant increases in angular orientation in both the sagittal and coronal planes, similar to those changes seen in human growth. These changes in orientation are important in both healthy biomechanics, as the direction of the ACL determines the direction of force distribution within the knee, and in ACL reconstruction treatments, as differences in reconstruction techniques can lead to altered angular orientation of graft tissue. As such, different treatments, including those more commonly used in skeletally immature patients, may artificially create ACL orientations that are not optimal

for a given patient age. Armed with an improved understanding of the age-specific nature of ACL orientation, researchers and clinicians may be able to design treatment strategies that leverage native tissue orientation and better replicate the function of a healthy knee. Following this conclusion that the angular orientation of the ACL changes similarly in the porcine model compared to human changes, the next line of research was to study age-specific changes in the 3D morphometry of the ACL.

CHAPTER 4

ACL Morphometry Varies in an Allometric Manner During Growth

While the findings in Chapter 3 established that the angular orientation of the ACL changes with age in a similar manner to previous human studies, many questions remained regarding changes in the size and shape of the ACL during skeletal growth. Previous studies have suggested that the ACL does not grow in time either by cross-sectional area compared to muscles around the knee (36), or by volume compared to overall body weight (37). This work drove us to ask the question: is the relative size and shape of the ACL consistent throughout skeletal growth? To answer this question we analyzed the length and cross-sectional area of the ACL and other ligaments and tendons in the knee and compared parameters to classify grow as either isometric (consistent in proportions) or allometric (differing in proportions).

The text in this chapter is currently under review in the Annals of Biomedical Engineering under the following citation (92).

(92) Cone SG., Piercy, HE., Lambeth, EP., Ru, H, Piedrahita, JA., Spang, JT., Fordham, LA., Fisher, MB. Tissue-Specific Changes in the Size and Shape of the Ligaments and Tendons of the Porcine Knee During Post-Natal Growth. Ann Biomed Eng. Under Review.

4.1. Introduction

Joints within the musculoskeletal system consist of a complex combination of active and passive tissues including ligaments and tendons that have specific morphometric and mechanical properties enabling force generation and movement. Many studies have investigated early pre-natal development of ligaments and tendons (93-98). In addition, the structure, function, and biochemical makeup of ligaments and tendons undergo major changes throughout both pre-natal and post-natal growth (34, 37, 99-101). Specific changes include increasing macroscale size and

mechanical stiffness and changing orientation and shape, among others. These age-related changes are influenced by a variety of stimuli including biochemical and cell signaling as well as mechanical loading.

Pioneering work by D'Arcy Thompson (102) and many others, have reported changes in the size and shape of biological tissues, resulting in the establishment of many terms and methods for classifying objects during growth. The terms "isometry" and "allometry" describe changes in which the growth of a part do or do not match the growth of the whole, respectively (103). Further research has built on this foundation to better understand morphologic changes in the musculoskeletal soft tissues, often with a focus on differences and similarities across tissues or between species (104-106). In this work, we apply these methods of characterization to different tissues with similar structure and function within a single organ.

Additional studies have investigated specific aspects of post-natal growth within a single tissue on the macroscale. For example, the lapine medial collateral ligament (MCL) experiences growth along the full length of the tissue, with larger increases close to the tibial insertion site (107). Interestingly, differences in growth rate coefficients were found between the proximal bones of the hindlimb (femur) and forelimb (humerus) in the porcine model through 3 months of age but not between the distal bones of the same limbs (tibia and radius) (108). The same study found that both the tibia and femur experienced more rapid change in bone area relative to bone length (allometric growth), although the same trend was not found in the humerus (108). A study in human growth found that the anterior cruciate ligament (ACL) experiences linear volumetric growth up to 10 years of age, with a plateau in ACL volume during the remaining period of growth during adolescence, showing age-specific allometric growth patterns between the ACL and the body (37). Together, these studies show that ligaments undergo changes in CSA and length during post-natal growth and that tissues near the same joint can undergo

different patterns of growth. However, it is unknown if ligaments and tendons within a single joint undergo similar or different changes during post-natal growth.

The objective of this study was to analyze the post-natal morphometry of four soft tissues with similar structure and function in the same joint: the ACL, patellar tendon (PT), MCL, and lateral collateral ligament (LCL) of the knee joint. In order to address this objective, we utilized a well-described porcine model to serve as an analog for the human knee (3, 109, 110). Magnetic resonance imaging (MRI) was performed to collect high-resolution images of joints from animals of different ages, and the macroscale size and shape of each tissue of interest was analyzed. We assessed the isometry or allometry within and between each of these tissues by comparing relative changes in tissue length and CSA over time.

4.2. Materials and Methods

4.2.1. Specimen Collection

Hind limbs were collected post-mortem from 36 female Yorkshire cross-breed pigs from birth to 18 months of age (n=6/age group, total n=36). Specific age groups and estimated human equivalent age were 0 months (newborn), 1.5 months (early juvenile), 3 months (late juvenile), 4.5 months (early adolescent), 6 months (adolescent), and 18 months (late adolescent). Human age equivalencies were based on a combination of skeletal and sexual age scales in both species (58). The animals used in this study were obtained from a university owned herd, and all animals were healthy and of normal size. Swine were cared for according to the management practices outlined in the Guide for the Care and Use of Agricultural Animals in Teaching and Research and their use in the current experimental protocols were approved by the N.C.S.U. Institutional Animal Care and Use Committee (79). Hind limbs were dissected to the stifle (knee) joint and wrapped in saline-soaked gauze prior to storage at -20°C until further testing.

4.2.2. Magnetic Resonance Imaging

Limbs were allowed to thaw at room temperature prior to imaging. All limbs were imaged using MRI scanners at the Biomedical Research Imaging Center (BRIC) at the University of North Carolina – Chapel Hill. Due to the small size of the newborn hind limbs, imaging for this group was performed using a 9.4-Tesla Bruker BioSpec 94/30 USR machine (Bruker BioSpin Corp, Billerica, MA) with a 3D fast low angle shot scan sequence (3D-FLASH, flip angle: 10°, TR: 38 ms, TE: 4.42 ms, acquisition time: 13 hours 18 minutes, FOV: 30 x 30 x 30 mm) using a 35 mm volume coil and isotropic voxels of 0.1 x 0.1 x 0.1 mm with no gap between slices. Limbs from the older age groups (1.5 to 18 months) were imaged using a 7.0-Tesla Siemens Magnetom machine (Siemens Healthineers, Erlangen, Germany) with a double echo steady state (DESS, flip angle: 25°, TR: 17 ms, TE: 6 ms, acquisition time: 24 minutes, FOV: 123 x 187 x 102 mm) using a 28 channel knee coil (Siemens Healthineers) and voxels of 0.42 x 0.42 x 0.4 mm with no gap between slices.

4.2.3. Image Post-Processing

Image sequences were imported into commercial software (Simpleware 7.0, Synopsys, Chantilly, VA) and 3-dimensional (3D) models were generated for each tissue of interest (ACL, PT, MCL, LCL) (Figure 4-1). Models were refined using the "close" and "discrete Gaussian" filters and were exported from the software as .stl files. Models were translated into point clouds, which were then analyzed in a custom Matlab code. Specifically, length was defined as the magnitude of the vector between the centroids of the femoral and tibial insertion sites (ACL, MCL, LCL) or the patellar and tibial insertion sites (PT). Centroids were defined as the geometric center of the points surrounding the insertion of the soft-tissue into the bone. Length measurements were complicated by insertion sites that have a substantial directional component parallel to the length of the ligament or tendon. This included the insertions of the MCL, LCL,

and the tibial insertion of the PT, and some insertion sites extended beyond the field of view of the MRI scans for larger specimens. As such, the location of these insertion sites were measured at the edge of the insertion most proximal to the joint center since this landmark could be consistently identified in all specimens. The insertion was determined as the centroid of points collected around the tissue at this location along the tissue length. Furthermore, to avoid variability caused by the changing CSA near the bony insertions, our CSA analysis was restricted to the midsubstance of the tissues. Specifically, the CSA was measured from the central 50% (midsubstance) of the ligament or tendon by rotating the model of the tissue onto the longitudinal axis, dividing the model into slices at a 0.1 mm increments along the z-axis, measuring the area of each slice, and averaging the values within the central 50% along the length to collect a single value for each tissue.

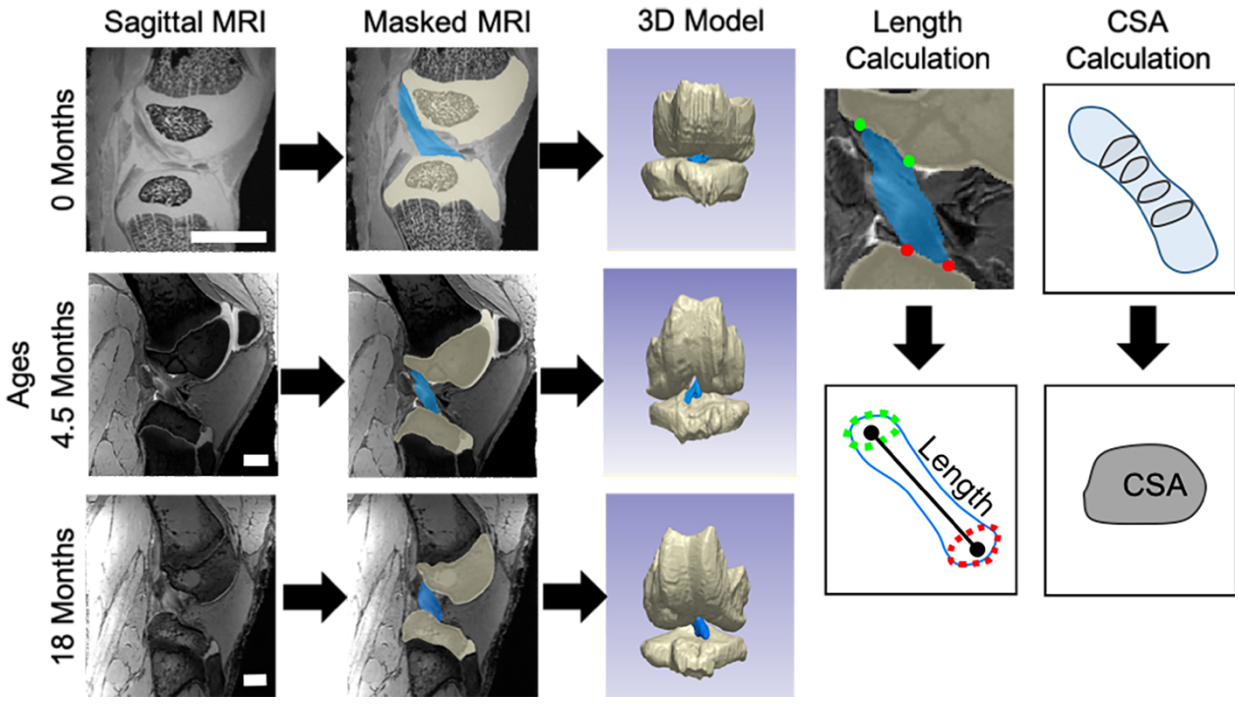

Figure 4-1. 3D models were created for tissues such as the anterior cruciate ligament (ACL) using MRI scans and segmentations of individual tissues. Images shown for newborn (0 month), early adolescent (4.5 month), and late adolescent (18 month) joints, scale bars are 10 mm. Length and cross-sectional area (CSA) calculation methods described for an ACL.

4.2.4. Analysis of Growth

Data were analyzed for each parameter (length and CSA) of each tissue (ACL, PT, MCL, and LCL) with comparisons performed between tissues and between parameters using data from all age groups. Log-log plots ($\log_{10}$) were created comparing experimental data to established isometric slopes listed in Figure 4-2. This process was done for both intra-tissue comparisons (CSA versus length) and inter-tissue comparisons (ACL versus PT, ACL versus MCL, ACL versus LCL, PT versus MCL, PT versus LCL, MCL versus LCL) for each geometric parameter. Linear regressions were performed for each plot and the slope and R^2 value were recorded.

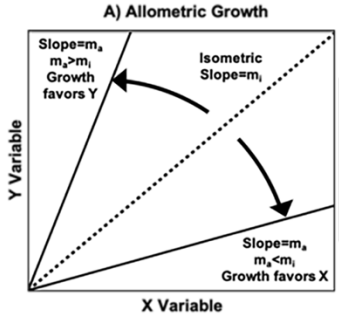

B) Isometric Slopes

X Variable	Y Variable	Isometric Slope
Length	Length	1
CSA	CSA	1
Length	CSA	2

Figure 4-2. Allometric growth within or between tissues can be assessed by plotting data on a log-log graph (A) and comparing to the slope of an isometric line. Isometric slopes are listed for all possible combinations of CSA and length (B).

4.2.5. Statistical Analysis

For comparisons between tissues, normalization of tissue size was performed by dividing the data for each geometric parameter by its respective average 18 month value for each tissue. Normality of data sets was confirmed in JMP (JMP Pro 13, SAS Institute Inc., Cary, NC). Statistical analysis of each geometric parameter consisted of a two-way ANOVA with age and tissue type as major effects and a Bonferroni method to adjust for multiplicity and significance set at $p \leq 0.05$ (JMP Pro 13, SAS Institute Inc., Cary, NC). For these analyses, tissue type was considered a within-subject variable while age was considered a between-subject variable. Analysis of the log-log plots was accomplished by comparing the slope of the linear regression

to the appropriate isometric value by an F-test by using the test statement in PROC REG Procedure (SAS 9.4, SAS Institute Inc., Cary, NC). The adjusted significance level for F-test comparisons was set at $p \leq 0.001$.

4.3. Results

4.3.1. Changes in Size During Post-Natal Growth

All of the ligaments and tendons of interest experienced significant growth in both length (Table A-2-1) and CSA (Table A-2-2) between birth and late adolescence (18 months) in this study (Figure 4-3). Increasing age resulted in significant growth in all four tissues of interest ($p<0.05$). Specifically, the length of the ACL increased 4-fold from an average of 9 mm to 35 mm from birth through late adolescence (Figure 4-3A). Simultaneously, the average length of the PT increased by 5-fold from 14 mm to 74 mm. The length of the MCL and the LCL also increased by 5-fold (Figure 4-3A). CSA increases varied across the tissue types. In the ACL, the average CSA increased 10-fold from 6 mm^2 to 57 mm^2 between birth and late adolescence (Figure 4-3B). This increase occurred alongside 24-fold (PT), 23-fold (MCL), and 16-fold (LCL) increases in the other ligaments and tendon types (Figure 4-3B). The most rapid periods of growth occurred during the juvenile and early adolescent phases (statistically significant increases between consecutive age groups are highlighted in Figure 4-3 ($p<0.05$)).

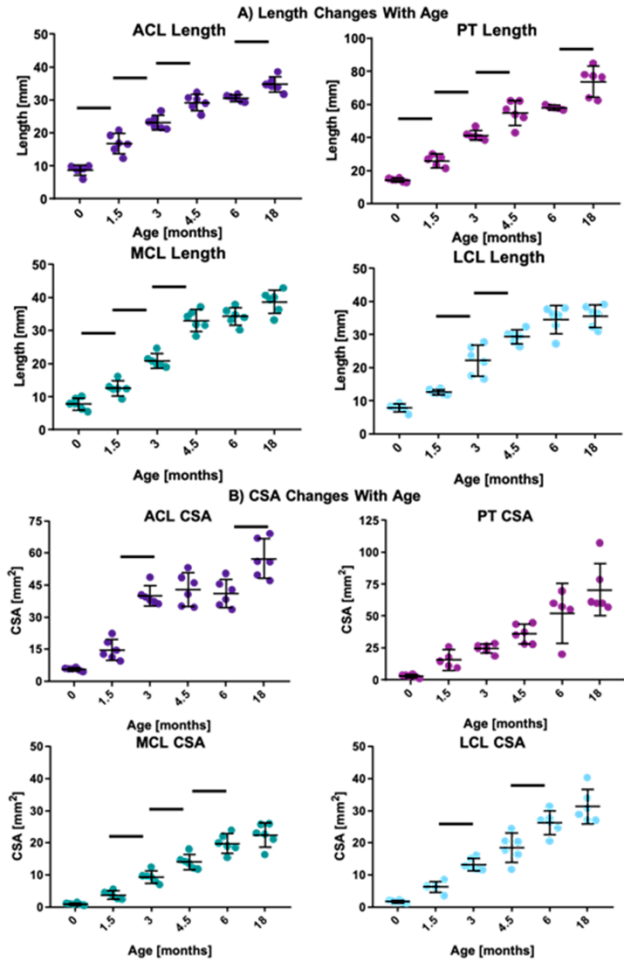

Figure 4-3. Length (A) and CSA (B) increase several fold in the ACL, PT, MCL, and LCL from birth through skeletal maturity. Data for individual specimens are presented as points while mean and 95% confidence intervals are represented by dashes and lines. Bars represent significant differences between consecutive age groups ($p<0.05$).

To compare across tissues within specific ages, values for length were normalized to the average value at 18 months for each tissue (Figure 4-4, Table A-2-3). For example, at birth, the average ACL length was 25% of the average ACL length at 18 months. Similar length values were obtained at birth for the PT, MCL, and LCL (19%, 20%, and 22%, respectively). Across all ages, these average changes in normalized tissue length were only statistically significant between the ACL and the PT, MCL, and LCL at 1.5 months of age, the ACL and the MCL at 3 months of age, and the PT and the LCL at 6 months of age ($p<0.05$).

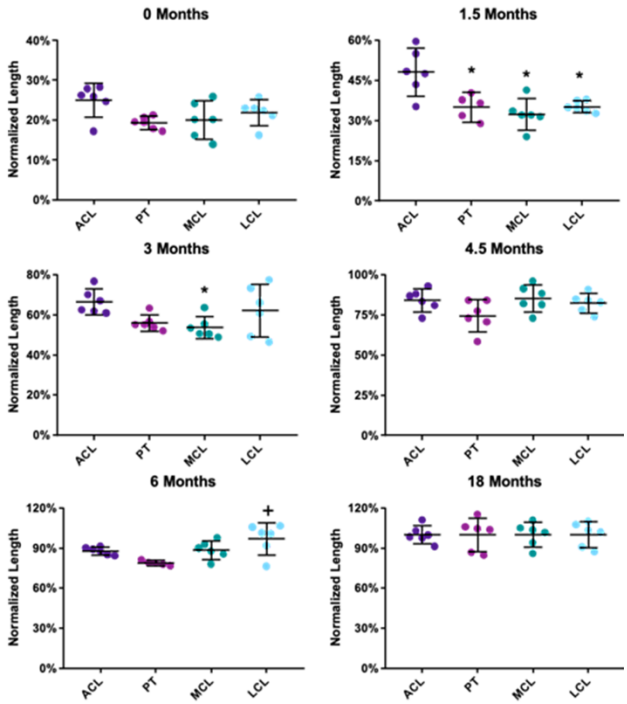

Figure 4-4. Tissue length data compared across tissues at each age normalized to the late adolescent group. Data for individual specimens are presented as points while mean and 95% confidence intervals are represented by dashes and lines. * denotes $p<0.05$ from ACL, + denotes $p<0.05$ from PT.

Values for CSA were also normalized to the average 18 month value for each tissue (Figure 4-5, Table A-2-4). At birth, major differences in the normalized CSA of the tissues were observed. Interestingly, the newborn ACL CSA was only 10% of the average 18 month group value. This normalized CSA value was much higher compared to the other tissues of interest, as the CSA values of the PT, MCL, and LCL were 4%, 4%, and 5%, respectively ($p<0.05$ vs the ACL, Figure 4-5). The ACL also had a significantly greater normalized CSA values at 0 and 3 months compared to the other three tissues, and compared to the PT at 4.5 months of age ($p<0.05$). No significant differences were found between the tissues during adolescence (6 and 18 months, $p>0.05$).

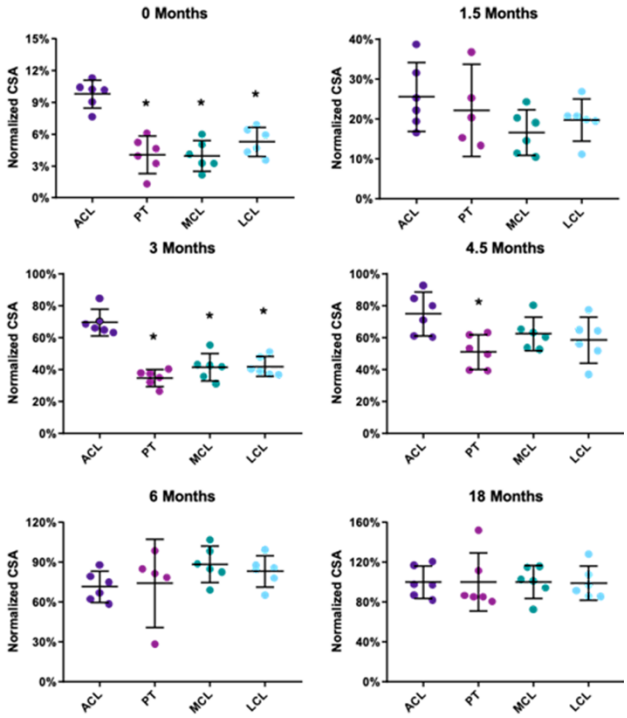

Figure 4-5. Tissue CSA data compared across tissues at each age normalized to the late adolescent group. CSA is significantly greater in the ACL compared to the other tissues ($p<0.05$) at ages including 0, 3, and 4.5 months. Data for individual specimens are presented as points while mean and 95% confidence intervals are represented by dashes and lines. * denotes $p<0.05$ from ACL.

4.3.2. Intra-Tissue Growth Behavior

Statistical analyses of log-log plots between morphometric parameters (length and CSA) for each tissue (ACL, PT, MCL, LCL) revealed differences in the modality of growth for each tissue (Figure 4-6). The slope of best fit line for the CSA versus length plot of the ACL was 1.54, which was significantly different from the isometric slope of 2 ($p<0.001$) and favored allometric increases in length over increases in CSA. The slope of the CSA versus length plot for the PT was 1.85, which was not significantly different from the isometric slope ($p=0.25$). Similarly, the slope of the MCL CSA versus length plot (1.84) did not differ from the isometric slope ($p=0.08$). However, the slope of the LCL CSA versus length plot (1.72) was significantly

different from that of an isometric slope (p=0.002) and favored greater length change over CSA change.

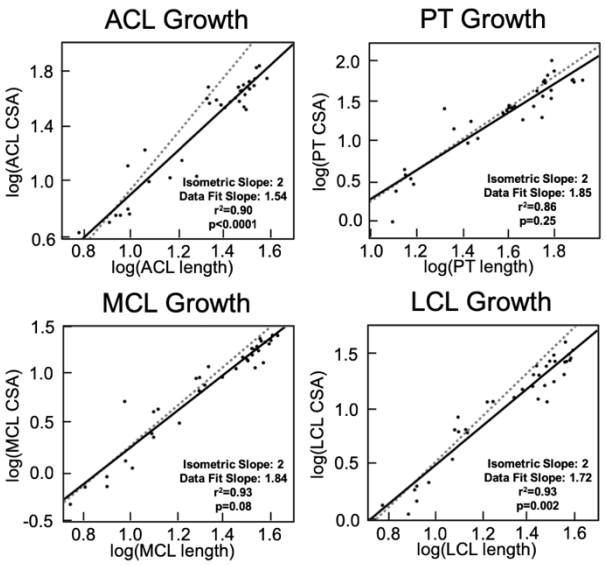

Figure 4-6. Assessment of allometric growth within each tissue. Comparisons of CSA and length for the ACL and LCL reveal allometric growth whereas the PT and MCL exhibit isometric growth. In these plots, the dashed line represents the line of isometry while the solid line represents the line of best fit for the data (R^2 values provided, $p<0.05$ denote statistical difference from isometric line, slopes denote standard and best fit lines).

4.3.3. Inter-Tissue Differences in Growth

Similar analyses were performed to compare log-log plots of morphologic growth across the four tissues of interest in the joint, with varied results depending on the parameter of interest (Figure 4-7). In terms of length, changes favored growth in the PT, MCL, and LCL over the ACL. Specifically, the slopes of the plots for the ACL relative to these tissues were 0.88 (p=0.010), 0.82 (p<0.001), and 0.88 (p=0.006), respectively. Length changes were not statistically different from an isometric slope in the PT versus MCL (slope=1.02, p=0.52), PT versus LCL (slope=0.97, p=0.39), or MCL versus LCL (slope=1.03, p=0.04) plots.

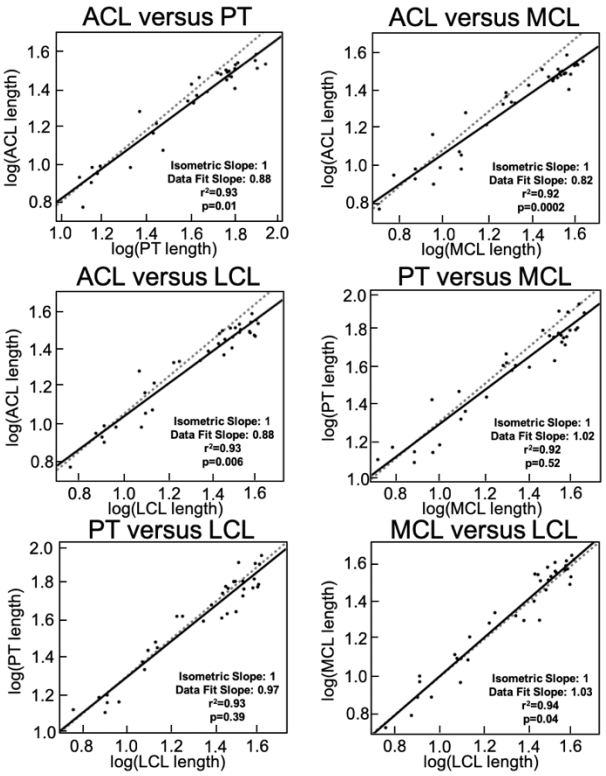

Figure 4-7. Comparisons of tissue length reveal differing rates of growth between the tissues. In these plots, the dashed line represents the line of isometry while the solid line represents the line of best fit for the data points (R^2 values provided, $p<0.05$ denote statistical difference from isometric line, slopes denote standard and best fit lines).

Comparisons of the slopes of log-log plots for CSA growth revealed some similar changes (Figure 4-8). The ACL exhibited allometric behavior relative to all three of the other tissues with a slope of 0.68 versus the PT ($p<0.001$), 0.69 versus the MCL ($p<0.001$), and 0.78 versus the LCL ($p<0.001$). In all three of these cases, changes in CSA were greater for the MCL, LCL and PT relative to the ACL. CSA changes were not statistically different from an isometric slope in plots comparing the PT versus MCL (slope=0.96, p=0.11), PT versus LCL (slope=0.85, p=0.75), or the MCL versus LCL (slope=1.10, p=0.08) plots.

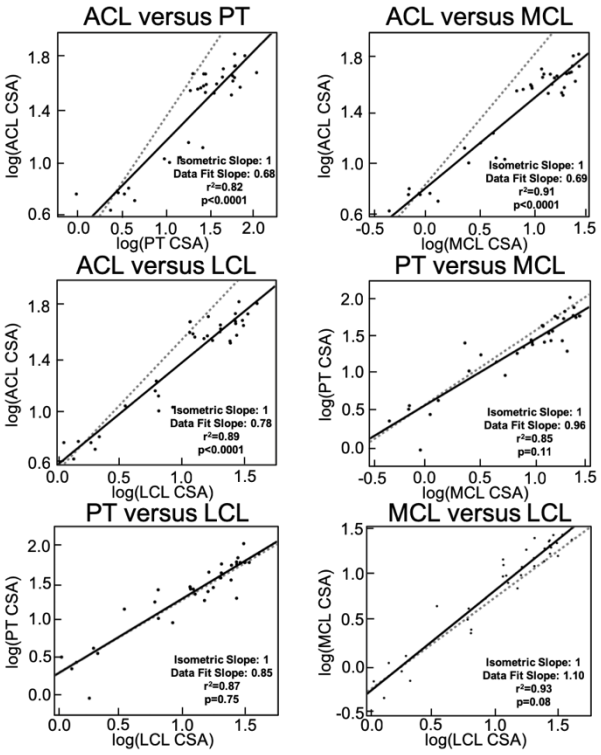

Figure 4-8. Comparisons of tissue CSA show differing rates of growth between tissues, specifically between the ACL and the other three. In these plots, the dashed line represents the mathematical line of isometry while the solid line represents the line of best fit for the data points (R^2 values provided, $p<0.05$ denote statistical difference from isometric line, slopes denote standard and best fit lines).

4.4. Discussion

While previous studies have investigated growth across body segments, this work was performed to highlight differences in growth in tissues with similar structure in a single joint. Here we presented data showing that all four ligaments and tendons studied in the knee joint increased markedly in size during growth. These changes included 4- to 5-fold increases in tissue lengths from birth through skeletal maturity alongside 10- to 20-fold increases in tissue CSA. However, changes in shape varied between tissues. Specifically, the ACL and LCL experienced allometric growth whereas the MCL and PT grew in an isometric manner. Additionally, while the increases in tissue length were similar across the tissues of interest, CSA

changes varied between tissues as the percent change in ACL CSA was lower than in the other tissues.

The age-related size increases observed in our study match more limited data in the literature. Additionally, the 2-fold changes we found from juvenile to skeletally mature groups in MCL CSA between were similar in scale to those previously reported during the same time frame in a study of rabbit MCL size (111). Related studies also reported more rapid growth in MCL CSA during the juvenile and early adolescent stages relative to later stages of growth, and our study reflected these findings as well (112). In another study in rabbits, MCL length increased by approximately one third to one half during a 10-week period of juvenile growth (107). Similarly, our findings suggested that the porcine MCL increased by just under one half of its length during a similar time frame. Our data build on these prior reports while allowing direct comparisons between tissues at a wider range of ages.

Our findings regarding the growth of the ACL suggest that there are age-specific changes in the geometric proportions of the tissue throughout skeletal growth in the pig model, and that the growth of the ACL does not parallel growth in the other tissues. Similarly, previous studies have shown that the CSA of the human ACL increases in size up to 10-12 years of age but halts in growth prior to the end of overall skeletal growth (37, 71). Additional studies comparing the growth of the human ACL to muscles surrounding the knee have shown more rapid growth in the ACL halting prior to the end of muscle growth (36). Our findings agree with these results demonstrating the allometric growth of the ACL relative to other tissues, while our findings add a more robust look into the timing of ACL growth in a relevant pre-clinical large animal model.

In order to extend these findings to the study of human growth, similar data should be analyzed in human subjects. MRI techniques have been previously employed to study the growth of musculoskeletal tissues in human populations, and some of the benefits and limitations

of this approach have been described previously. MRI was used to study growth in the pediatric shoulder, where the ability to study changes in bone and soft tissues simultaneously was highlighted (113). An additional MRI study reported age-related patterns in ligament anatomy including one reporting on the location of the femoral insertions of the collateral ligaments relative to the femoral growth plate (114). Building on works such as these and the techniques described in our study, there is an opportunity to build on our understanding of ligament and tendon growth in human populations.

Our study also relates to previous work in the porcine model focused on growth and morphometric changes of bones, while adding data regarding several soft tissues in the knee. Other groups have reported age-related changes in the growth of long bones in the hind- and fore-limbs where they found differences in CSA and length change in the bones of the hind-limb, and variations in growth coefficients between the bones of the hind-limb versus the fore-limb (108). Our findings agreed with this work suggesting that musculoskeletal tissues can undergo shape changes during growth and may occur on altered timelines relative to similar tissues. Furthermore, the porcine model has been used to study tissue mechanics during growth specifically for bone and cartilage (115-117). Thus, the porcine model may also be a valuable tool to study ligament and tendon mechanics during growth.

The findings reported here can aide in designing clinical treatments for injured ligaments and tendons. For example, when developing reconstruction treatments for the ACL in growing patients, clinicians may need to be cognizant of age-specific morphology and remaining growth in the knee. The PT is a common graft for the ACL (118); however, if the PT grows at different rates during the healing process or experiences different changes in shape this may not be as appropriate for certain age groups. In order to implement these findings in clinical treatments for human populations, this study should be repeated in a human population to confirm whether or

not these findings are species-specific. Given the non-invasive nature of MRI studies, repeating this work with a wide range of ages during growth in a human cohort may reveal interesting differences in the relative size and shape of ligaments and tendons between species and age groups, as well as any interaction between these factors.

These data also have implications in basic science research of ligaments and tendons. If developing a biomechanical model of the joint during growth, a single scaling factor cannot be applied across tissues within a single joint to create age-specific designs. Any biomechanical model of the knee should consider the corresponding relationships between length and CSA that are unique to a target age group. When considering the consequences of these findings on the field of tissue engineering and applications for ligaments and tendons, tissue-specific growth should be taken into consideration when designing tissue engineered constructs for skeletally immature patients. The study of tissue-specific changes during growth could be applied to other species and tissues. This may reveal significant differences in tissue growth in precocial and altricial species, bipedal and quadrupedal species, and across upper and lower limbs within bipedal species.

Moving forward, we plan to replicate this study in male animals in order to investigate the sex-specific changes in soft tissue morphology within the knee. Previous studies showing significant differences in injury patterns between young male and female athletes suggest that the onset of adolescence leads to a disparity in ACL behavior between the sexes (119), and this future work may elucidate the impact of structural changes on these differences. In combination with findings on the specific tissue composition and effects of altered mechanical loading on soft tissue morphogenesis, the porcine model can be used to isolate the underlying mechanisms which inform soft tissue growth in post-natal development.

Limitations of this study include the cross-sectional experimental design, as all morphological changes between ages are based on data from separate animals. Future work using a longitudinal study design may be able to expand on the power of this work by eliminating inter-specimen variation. An additional consideration is that these findings may be breed specific within the porcine species. As such, it may be informative to repeat these measurements in other common porcine models, such as the Yucatan minipig. Further limitations were introduced by the methodology for length calculations. Specifically, since the geometry of the insertion sites for the ligaments and tendons are complex (and partially out of the field of view in some cases), our length measurements were constrained to the midsubstance of the tissues. Additionally, the CSA measurements for each tissue were gathered from the midsubstance and were averaged across the tissue. Thus, our measurements represent generalized metrics of the tissue substance. Quantification of region-specific variations in size during growth would be an interesting area for exploration.

While previous work has shown growth gradients across full limbs or body segments, this has shown that similar tissues within a single joint can grow at different rates. Our findings support previous literature suggesting that age-related morphometry changes vary between tissues in the body, while increasing our understanding of this phenomenon from comparisons between body segments and multiple joints to comparisons between tissues within a single organ. This data has many potential implications in understanding musculoskeletal growth, human clinical applications, and emerging tissue engineering and regenerative medicine therapies.

4.5. Conclusions and Broader Impact

In this chapter, we have shown that the ACL experiences allometric growth through both comparison of length and CSA across ages, and when comparing changes in the ACL to changes

in the collateral ligaments and the PT. This reinforces findings from previous studies, which stated that the ACL experiences growth on a different scale compared to the total body and muscles in the leg, while building on previous findings by focusing on tissues within a single joint. This potentially highlights the effect of specific functional demands and internal cues on the growth of the ACL, as the other tissues have similar biomechanical and biochemical environments. Prior to the implementation of these findings in the clinic, this study must be confirmed in a human study. The image processing and data analysis techniques described in this chapter can be readily implemented in a retrospective human study in order to both confirm the translation between the porcine model and humans, and compare tissue growth in males and females. To extend these findings into the next chapter, the analyses used between ligaments will be applied to the anteromedial and posterolateral bundles of the ACL, and I will describe our initial biomechanical studies in joints during growth.

CHAPTER 5

Joint-Level Changes in Biomechanical Function Occur Alongside Bundle-Specific Changes in ACL Structure and Function During Skeletal Growth

While findings in the previous chapter revealed interesting changes in ACL morphometry, we were interested in studying changes within the individual bundles of the ACL during growth. The ACL is comprised bundles of collagen fibrils, and the most common division of this tissue is into two bundles: the anteromedial (AM) and posterolateral (PL) bundles. Previous studies have shown that these bundles are engaged under different applied loads and in different postures in mature cases, with the AM bundle serving a dominant functional role under applied anterior tibial loads. Additionally, we were interested in studying changes in the joint responses to applied tibial loads and moments as a function of age and flexion angle, as these parameters may shift with alterations in the biomechanical function of soft tissues including the ACL. This chapter details an investigation into changes in these joint kinematic properties and bundle-specific functional properties coupled with applications of the orientation and morphometry analyses from the prior two chapters to the AM and PL bundles throughout growth.

The text in this chapter has been provisionally accepted and is in revision at the Clinical Orthopaedic and Related Research journal under the following citation (120).

120. Cone, S.G.; Lambeth, E.P.; Ru, H.; Fordham, L.A.; Piedrahita, J.P.; Spang, J.T.; Fisher, M.B. Biomechanical Function and Size of the Anteromedial and Posterolateral Bundles of the Anterior Cruciate Ligament Change Differently with Skeletal Growth in the Pig Model. Clin Orthop Relat Res. Under Review.

5.1. Introduction

The ACL stabilizes the knee in multiple directions during activities of daily living and physically demanding athletic activities (121). Its structure is well suited to the multidirectional loads it experiences; the ACL is commonly divided into two sub-bundles: the anteromedial and posterolateral bundles (15, 122-126). The anteromedial bundle is more directly responsible for resisting anterior tibial loading and sees greater loads in deep flexion than the posterolateral bundle, while the posterolateral bundle contributes more to resisting rotational moments and in positions near full extension (121, 126, 127).

As many as 250,000 ACL injuries occur in the United States each year (128), and the incidence of ACL injury is rising in the skeletally immature population (25). Recent studies have found rapid increases in the number of ACL reconstruction procedures annually in pediatric and adolescent patients (25, 26, 129, 130), with one study reporting that the fastest growing number of ACL reconstruction procedures in boys and girls in those younger than 14 years (25). Current clinical treatments for this age group focus on restoring stability while minimizing interruption of the femoral and tibial physes for patients with considerable growth remaining (131, 132); however, these treatments may not restore normal kinematics and contact stresses in pediatric patients (31). This suggests a need for more knowledge regarding the normal function of the ACL during growth.

The size and orientation of the ACL also undergoes substantive change during growth in childhood. The ACL increases in steepness in the sagittal and coronal planes in humans during growth (1, 35). The ACL cross-sectional area increases in children up to 10 years old, with more modest changes during adolescence (36, 37). However, little is known regarding whether and how ACL function and anteromedial and posterolateral bundle function, size, and anatomic orientation change during growth.

Large-animal models are valuable when the ability to collect human data is limited, such as in pediatric cadaveric studies. Previously, the pig ACL model has been validated as a surrogate for the ACL in skeletally mature humans; the length and cross-sectional area of the healthy ACL were found to be comparable between humans and pigs (110). Additionally, the pig model better replicates human anteromedial and posterolateral bundle function under anterior tibial loads than sheep and goat models do (44). More recently, the skeletally immature pig model yielded similar changes in ACL orientation to the human ACL with growth (1, 133). Another study of ACL reconstruction and repair also employed the pig model, using both young and mature animals (134). Thus, the pig model can provide clinically useful insight into ACL function during growth.

The objectives were defined to study age-dependent changes in four parts: (1) to measure joint kinematics in response to applied anterior-posterior loads and varus-valgus moments, (2) to assess the response of the ACL under the same applied loads, (3) to compare the relative functional contributions of the anteromedial and posterolateral bundles of the ACL, and (4) to study changes in the cross-sectional area, length, and angular orientation of the bundles of the ACL.

5.2. Materials and Methods

5.2.1. Study Design

The following methods are summarized in Figure 5-1. All pigs used in this study were obtained from a university-owned herd (Swine Education Unit, NC State University) and were healthy and of normal size. The animals were cared for according to the management practices outlined in the Guide for the Care and Use of Agricultural Animals in Teaching and Research (79), and experimental protocols were approved by our local institutional animal care and use committee. Hind limbs were collected from 30 female Yorkshire crossbreed pigs at ages ranging

from 1.5 to 18 months. Age groups (n = six per group) and equivalencies to human growth were based on studies of porcine skeletal and sexual maturity (3, 58) and included: early youth (1.5 months), juvenile (3 months), early adolescent (4.5 months), adolescent (6 months), and late adolescent (18 months). Ages of animals were within a range of +/- 3 days for the early youth and juvenile groups, and within a range of +/- 7 days for the early adolescent through late adolescent groups. Sample sizes were initially determined by a power analysis based on preliminary imaging data (effect size of 2), which found that n=8 per age group would be sufficient for to detect an effect size of 2 at a power of 0.8 and adjusting for multiple comparisons. After initial testing, we observed larger effect sizes and determined that n=6 was sufficient to detect changes in major outcomes, , so animals were limited to n=6/group. Specimens were wrapped in saline-soaked gauze and stored at -20 °C.

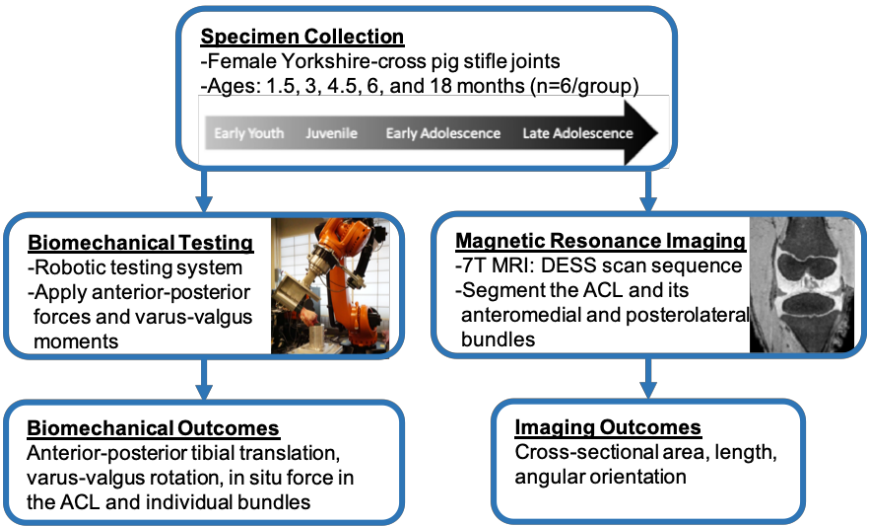

Figure 5-1. The overall methods for this manuscript are described, including specimen collection, magnetic resonance imaging, and biomechanical testing.

5.2.2. MRI

MRI analysis was performed in order to study the anatomic orientation, length, and cross-sectional area of the ACL and its anteromedial and posterolateral bundles. Hind limbs were

allowed to thaw at room temperature in preparation for MRI. Stifle joints were imaged at full extension (approximately 30°-40° of flexion) at the Biomedical Research Imaging Center at the University of North Carolina – Chapel Hill. MRI scans were performed in a 7.0-Tesla Siemens Magnetom scanner (Siemens Healthineers, Erlangen, Germany) using a double-echo steady-state sequence (flip angle: 25°; TR: 17 ms, TE: 6 ms; acquisition time: 24 minutes; FOV: 123 x 187 x 102 mm) with a 28-channel knee coil (Siemens Healthineers) and voxel size of 0.42 x 0.42 x 0.4 mm, with no gap between slices (Figure A-3-1). After imaging, each limb was wrapped in saline-soaked gauze and stored again at -20 °C.

MR images were analyzed using commercially available software (Simpleware 7.0, Synopsys, Chantilly, VA, USA) to measure the orientation and size metrics. To calculate the orientation of each bundle, we used a multiangle measurement tool to determine the angle of each bundle relative to the AP axis of the tibial plateau in both the sagittal and coronal planes, as previously reported by us and others (1, 133). Tissue length was calculated by identifying coordinates of approximately 15 evenly distributed points at the tibial and femoral insertion sites for each tissue and calculating the three-dimensional centroid for each insertion using a custom Matlab code (Matlab, Mathworks, Natick, MA). Length was then calculated as the magnitude of the vector between the centroids. Images were segmented to create three-dimensional models of each tissue, specifically the entire ACL, the anteromedial bundle, and the posterolateral bundle (Figure 5-2). Models were refined using “close” and “discrete Gaussian” filters before being exported as .stl files.

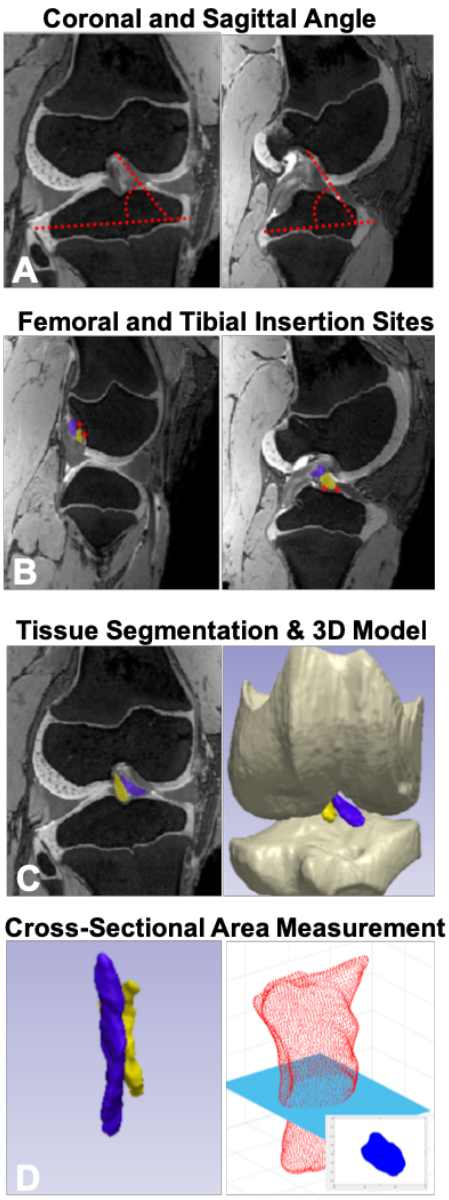

Figure 5-2. (A) Coronal and sagittal angles of the ACL bundles were measured on the most anterior (coronal, image shown) or the most medial (sagittal, image shown) slice depicting the full ACL relative to the anterior-posterior or medial-lateral plane of the tibial plateau (determined from a different MRI slice and transferred for measurement). (B) Bundle length was calculated between insertions (marked with red stars for the posterolateral bundle) based on points collected near the femoral and tibial insertion sites as shown in sagittal planes. (C) MR images were translated into three-dimensional models by creating masks for the individual tissues throughout the MRI scan and compiling the image masks to create 3D models. (D) The cross-sectional area was measured by isolating and rotating three-dimensional models of the ACL bundles, generating point clouds for each tissue, creating 2D cross-sections of these point clouds (shown in blue inset), and measuring the cross-sectional area at slices in the midsubstance of the tissue.

Cross-sectional area values were calculated from MR images in a manner similar to the method of Fujimaki et al. (89). The anteromedial and posterolateral bundles of the ACL were visualized, confirmed as inserting into the tibial plateau on the anterior and posterior side of the most medial aspect of the anterior insertion of the lateral meniscus (an anatomic feature of the porcine ACL), and transformed into individual masks (Figure A-3-2). The three-dimensional models were transformed into point clouds and imported into a custom Matlab code for further analysis. Point clouds for each tissue were rotated to align the line-of-best-fit (or long axis) to the Z-axis of a Cartesian coordinate system. The point cloud was then translated along the Z-axis to originate on the orthogonal X-Y plane, and points were projected onto planes distributed in 1-mm slices along the Z-axis. The area within the collapsed points was recorded for each slice, and the areas identified from the central 50% of the tissue were averaged to calculate the mean cross-sectional area value for the tissue.

5.2.3. Biomechanical Testing

Biomechanical testing was then performed in order to study the anterior-posterior tibial translation and varus-valgus rotation of the joints under applied loads and moments. Additionally, this testing was performed in order to study the in situ forces carried by the ACL and its anteromedial and posterolateral bundles under the applied forces and moments. Before biomechanical analysis, limbs were removed from storage and allowed to thaw at room temperature. The femur, tibia, and fibula were cut in the center of the diaphysis, and the soft tissue was removed up to the joint. The bones were fixed in molds using an epoxy compound (Everglass, Evercoat, Cincinnati, OH, USA). Joints were wrapped in saline-soaked gauze, and additional saline was applied as needed throughout testing.

Robotic testing systems have been widely used to analyze the in situ function of musculoskeletal joints and individual tissues (10, 11, 127, 135, 136). Testing was performed using a 6 degrees of freedom robotic system (KR300 R2500, Kuka, Shelby Charter Township, MI, USA) powered by a separate controller (KRC4, Kuka, Shelby Charter Township, MI, USA) combined with a 6 degrees of freedom force/moment sensor (Omega160 IP65, ATI Industrial Automation, Apex, NC, USA) and integrated and controlled via the simVitro software package (Cleveland Clinic, Cleveland, OH, USA). This system is capable of operating under both kinematic and kinetic control, with kinematic repeatability of 0.1 mm and 0.1° and load cell sensitivity of 0.25 N.

Specimens were attached to the robotic system with custom clamps, and the anatomic coordinate system of the joint was determined relative to the coordinate system of the robotic manipulator using a point digitizer with an accuracy of 0.23 mm (G2X, Microscribe, Amherst, VA, USA) as previously described (10, 127, 137). A passive path was established for each joint by increasing the flexion angle of the joint from full extension (approximately 40° of flexion, measured with a goniometer) to 90° by 1° increments while minimizing forces and moments in the other five degrees of freedom and recording the kinematics.

Once the passive path positions were established, joint kinematics under applied anterior tibial loads at 40°, 60°, and 90° and varus-valgus moments at 60° were obtained (Table 5-1). The robotic system was operated under force control to apply selected loads at 40°, 60°, and 90° of flexion. Age-specific forces and moments (Table A-3-1) were selected based on preliminary experiments to engage the connective tissues of the knee and reach the linear region of the load-displacement curve for the ACL under anterior loads. These load changes (sevenfold increase) were scaled with bone size increases (sevenfold increase). Kinematics were recorded under these applied loads and repeated in position control while force and moment data were collected. The

anteromedial bundle of the ACL was isolated and transected, and the kinematics of the intact joint were repeated to obtain force and moment data remaining in the anteromedial-deficient state. The posterolateral bundle was then transected. This order was maintained throughout testing because of our inability to access the posterolateral bundle from the anterior aspect of the joint before transecting the anteromedial bundle; however, in preliminary validation studies, blunt separation of the bundles resulted in minimal change in recorded resultant force under applied load (average of 1.7 N in the 3 month old juvenile group (n=5) and 3.8 N in the 18 month old late adolescent group (n=5)). This suggests minimal interaction between the anteromedial and posterolateral bundles. The kinematics of the intact joint were again repeated to measure the loads and moments resisted in the ACL-deficient state.

Table 5-1. Experimental protocol for robotic testing of the stifle joints of pigs.

Protocol	Data collected
(1) Intact joint Passive flexion-extension path Applied loading conditions AP40: AP load at 40° AP60: AP load at 60° AP90: AP load at 90° VV60: Varus-valgus moment at 60° Repeat kinematics (AP40, AP60, VV60, AP90) Transect AM bundle	 Passive path positions Intact kinematics (AP40, AP60, AP90, VV60) Applied forces (FAP40, FAP60, FAP90, FVV60)
(2) AM-deficient joint Repeat kinematics (AP40, AP60, AP90, VV60) Transect PL bundle	 AM-deficient forces (FAP40, FAP60, FAP90, FVV60) AM bundle in situ forces (F_{intact}-$F_{AMdeficient}$)
(3) ACL-transected joint Repeat kinematics (AP40, AP60, AP90, VV60)	 PL-deficient forces (FAP40, FAP60, FAP90, FVV60) ACL in situ forces (F_{intact}-$F_{ACLdeficient}$) PL bundle in situ forces ($F_{AMdeficient}$-$F_{ACLdeficient}$)
AP: anterior-posterior; VV: varus-valgus; AM: anteromedial; PL: posterolateral	

5.2.4. Biomechanical Data Processing

Kinematic measurements included anterior-posterior tibial translation, calculated as the anterior-posterior distance between the point of maximum applied anterior force and posterior force, and varus-valgus rotation, measured as the rotation in degrees between the maximum applied varus and valgus torques. Anterior-posterior tibial translation was normalized to the length of the tibial plateau in the sagittal plane, measured from previously collected MR images, to correct for size differences because of growth between age groups. Forces were recorded in the anterior-posterior, medial-lateral, and proximal-distal directions at the peak force or moment of each applied condition. The principle of superposition was applied to calculate the in situ forces for each force component in the anteromedial bundle, posterolateral bundle, and ACL under the applied loads in all three conditions (44, 127). Resultant forces were calculated as the result of the force vector for each tissue under each applied load. Normalized forces were calculated as a tissue-specific percentage of the overall force in the joint, measured at the peak load.

5.2.5. Primary and Secondary Outcomes of Interest

Our primary study outcomes were age-dependent changes in anterior-posterior tibial translation and varus-valgus rotation, the biomechanical contribution of the ACL under applied anterior tibial loads, and relative function of the anteromedial and posterolateral bundles of the ACL under anterior tibial loads. We tested this by applying an anterior tibial load to joints of various ages and recording the resulting deformations and sensed forces.

Our secondary study endpoints were changes in the size and angular orientation of the ACL bundles during growth. We tested these by comparing changes in tissue cross-sectional

area, length, and both sagittal and coronal tissue orientation throughout skeletal growth in the porcine model.

5.2.6. Statistical Analysis

The statistical analysis was performed using commercial software (JMP Pro 13.0, SAS Institute, Cary, NC, USA). For anterior-posterior tibial translation, normalized anterior-posterior tibial translation, and ACL force contribution, a two-way ANOVA was performed with age as an independent variable and flexion angle as a repeated measure. Varus-valgus rotation, ACL angle, bundle angle, ACL length, and cross-sectional area of the ACL were analyzed with a one-way ANOVA using age as the independent variable. Bundle contributions under varus and valgus torque, bundle angle, bundle length, and bundle cross-sectional area were analyzed using a two-way ANOVA with age as an independent variable and bundle as a repeated measure. Normalized bundle contributions to anterior tibial force were analyzed individually by bundle using a two-way ANOVA with age as the independent variable and flexion angle and bundle as a repeated measure; paired t-tests were used to compare values between bundles. For each ANOVA, Tukey's honestly significant difference post hoc analyses were performed. For all tests, the overall alpha value was set at 0.05. Data are reported in tables and supplementary material as the mean ± SD (95% CI). Figures showing individual data points and means with 95% CIs are reported in the main text, with minimal statistical markings for clarity.

5.3. Results

5.3.1. Age-Dependent Joint Kinematics

No differences in anterior-posterior tibial translation were found in response to applied loads because of age, despite increases in specimen size ($p = 0.635$) (Table A-3-2). Once it was

normalized to the length of the tibial plateau in the sagittal plane, anterior-posterior tibial translation decreased with increasing age ($p < 0.001$) (Figure 5-3). The average values for normalized anterior-posterior tibial translation in the late adolescent group (18 months) were only 50%, 56%, and 63% of that of the early youth group (1.5 months) at 40°, 60°, and 90° of flexion, respectively. These decreases occurred primarily before the onset of adolescence, with no changes during adolescence (between 4.5 and 18 months old) across all flexion angles (Table A-3-3). Varus-valgus rotation decreased with age ($p < 0.001$) (Figure 5-3) from an average of 25.4° ± 2.2° [95% C.I.: 23.1-27.8] in early youth (1.5 months) to an average of 6.3° ± 1.6° [95% C.I.: 4.6-8.0] in late adolescence (18 months) (Table A-3-4).

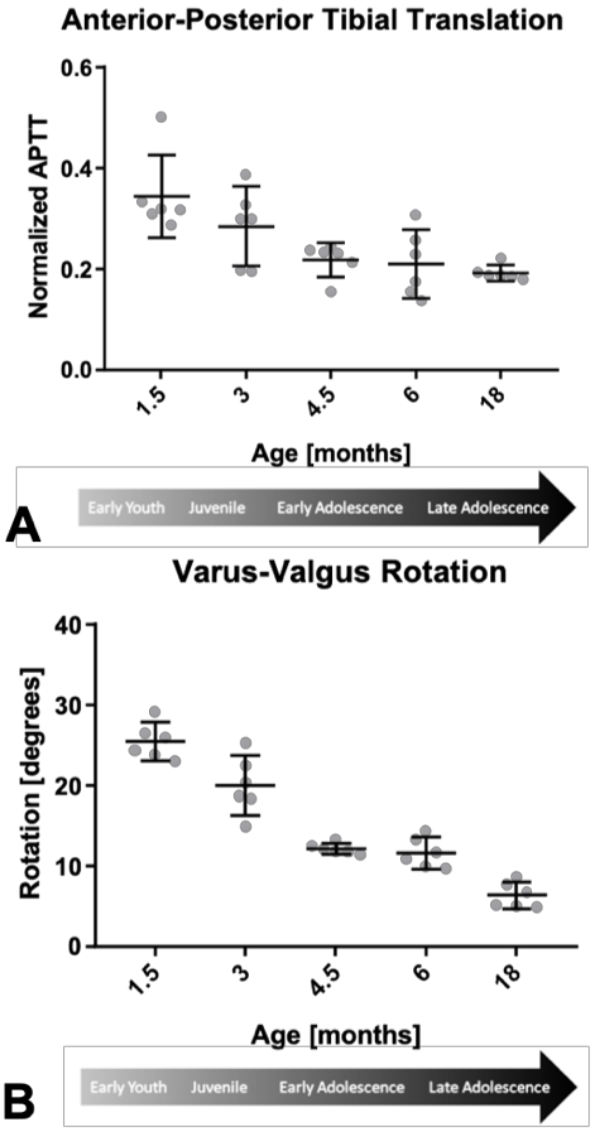

Figure 5-3. In response to applied tibial loads, **(A)** anterior-posterior tibial translation decreased with age ($p < 0.001$) when normalized to the length of the tibial plateau in the sagittal plane (data shown at 60° of flexion). Additionally, (B) varus-valgus rotation decreased with age ($p < 0.001$). The bars represent the mean and 95% CI and the points represent data from individual specimens.

5.3.2. ACL Function Under Applied Anterior Loads

The ACL served as the primary restraint to anterior tibial load in the joint throughout skeletal growth ($p = 0.630$) (Figure 5-4). The functional contribution of the ACL was measured as the percentage of the overall joint anterior force at the peak applied anterior tibial load.

Specifically, the mean contribution of the ACL ranged from 75% to 104% at 40° of flexion, 97% to 110% at 60° of flexion, and 98% to 111% at 90° of flexion across all age groups relative to the intended target load (Table A-3-5).

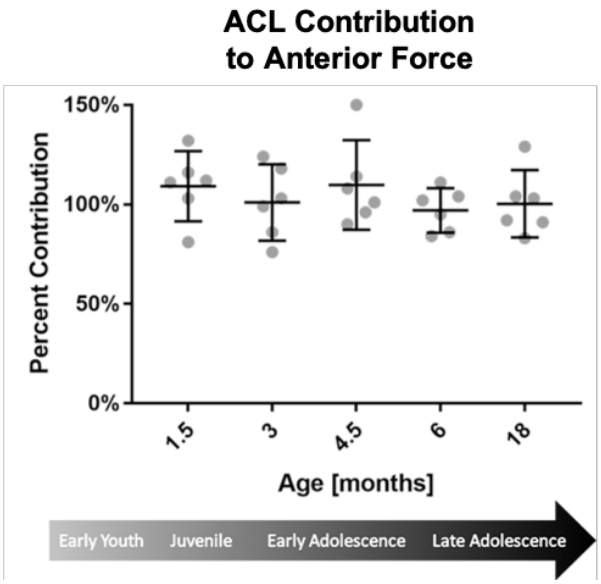

Figure 5-4. The ACL was a dominant soft-tissue restraint, reported here as a percentage of the target load, to applied anterior tibial loading, with no effect because of age ($p = 0.63$). Data are presented with a representative flexion angle (60°); the bars represent the mean and 95% CI.

5.3.3. ACL Bundle Biomechanical Function Under Applied Loads

Although the biomechanical function of the entire ACL was consistent across ages, the functional contributions of the anteromedial and posterolateral bundles shifted from both bundles having substantial but variable contributions in the younger age groups towards dominance of the anteromedial bundle under anterior loading after the onset of adolescence (Figure 5-5). In early youth (1.5 months), the average contribution of the anteromedial bundle was 44%, 50%, and 49% at 40°, 60°, and 90° of flexion, respectively. The functional contribution of the anteromedial bundle did not increase throughout youth and the onset of adolescence (6 months) ($p = 0.151$-1.000 between age groups). By late adolescence (18 months), the contributions of the anteromedial bundle had an average of 89%, 92%, and 86% of the anterior force of the ACL at

40°, 60°, and 90° of flexion, respectively (Table A-3-6). This divergence of functional contributions was such that there was a difference in contributions between the bundles by 18 months of age for all flexion angles ($p < 0.001$) (Table A-3-7).

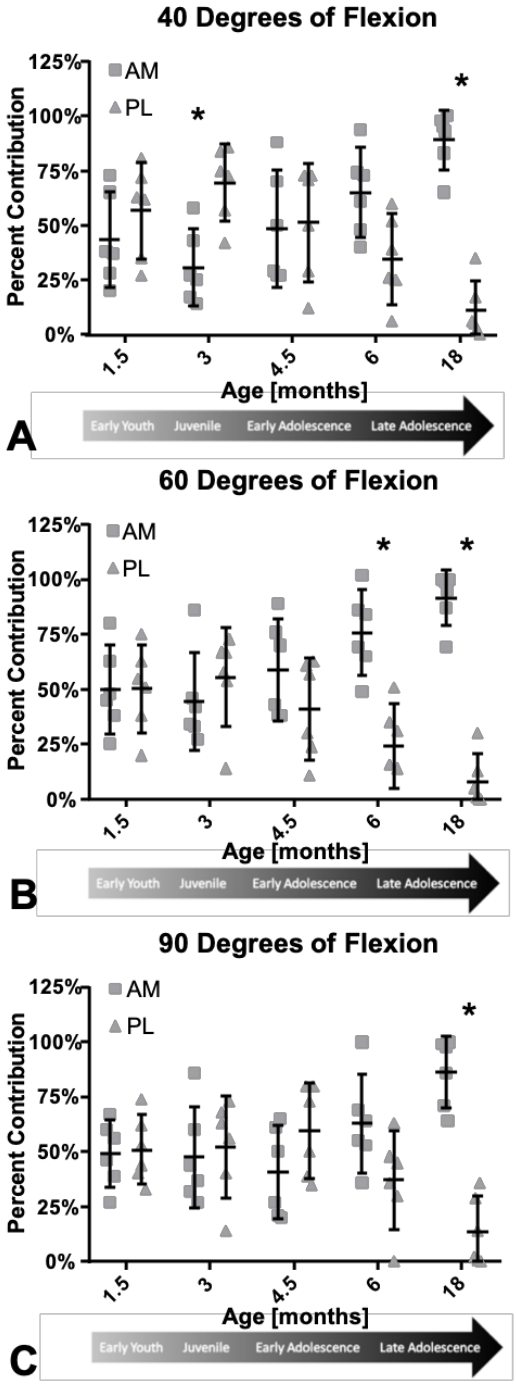

Figure 5-5. The in situ force of the anteromedial and posterolateral bundles of the ACL under applied anterior loads is shown at (A) 40°, (B) 60°, and (C) 90° of flexion (reported as a percentage of the total force in the ACL). Data varied in younger groups, with substantial forces carried by both bundles ($p = 0.04$ and $p = 0.98$ between bundles); however, after the onset of adolescence, the contribution of the anteromedial bundle became dominant under an anterior load ($p < 0.001$ for all flexion angles). The bars represent the mean and 95% CI; * $p < 0.05$ between bundles.

Under applied varus and valgus torques at 60° of flexion, the behavior of the anteromedial and posterolateral bundles also varied as a function of age ($p < 0.001$) (Figure 5-6). In the young age groups (1.5 to 3 months), biomechanical functional contributions from the anteromedial and posterolateral bundles were similar under varus and valgus loading. Beginning in early adolescence (4.5 months), the anteromedial bundle began to carry a greater portion of the resultant load under an applied varus moment ($p < 0.001$). By adolescence (6 months), the anteromedial bundle carried an average of 86% of the resultant force. In the late adolescent group (18 months), the anteromedial bundle carried 80% of the resultant force. Dissimilarly, under valgus loading, both bundles continued to have a substantial role with increased age. Highly variable behavior under valgus loads resulted in an average contribution from the anteromedial bundle that ranged between 44% and 72%, with no effect because of age ($p = 0.151$) (Table A-3-8).

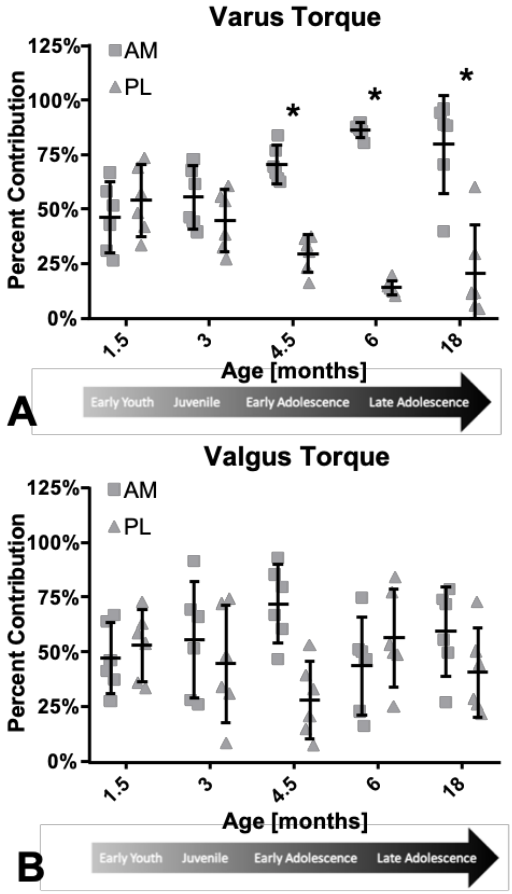

Figure 5-6. The in situ force of the anteromedial and posterolateral bundles in the ACL under applied varus and valgus moments (normalized to the total in situ force of the ACL). (A) Under varus moment, data varied in younger age groups, with both bundles carrying a portion of the forces reported as a percentage of the total force in the ACL ($p = 0.57$ and $p = 0.38$ between bundles); the anteromedial bundle playing a greater role at later ages ($p = 0.02$ and $p < 0.001$). Dissimilarly, (B) the data were highly variable throughout all age groups under an applied valgus moment, because age did not have an effect on bundle behavior ($p = 0.15$). The bars represent the mean and 95% CI; * $p < 0.05$ between bundles.

5.3.4. ACL Size and Orientation

The cross-sectional area of the ACL increased steadily with age (444% average increase from early youth to late adolescence) ($p < 0.001$) (Table A-3-9). These changes were rapid between 3 and 4.5 months old ($p = 0.002$) (Figure 5-7). Simultaneously, the ACL had a 250%

increase in length from 1.5 to 18 months of age in the pig model ($p < 0.001$) (Figure A-3-3). These increases occurred gradually throughout skeletal growth.

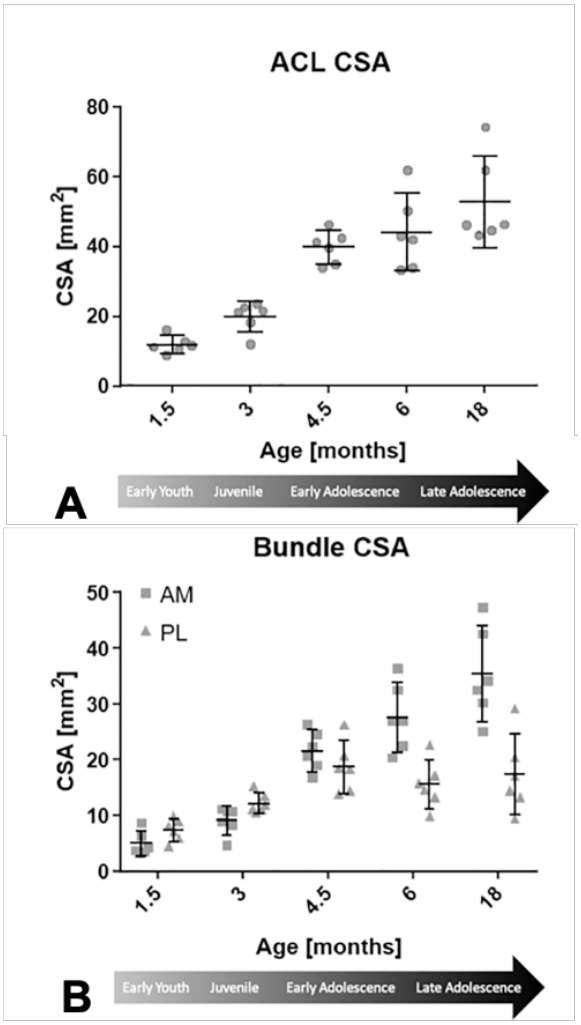

Figure 5-7. (A) The cross-sectional area of the ACL increased with increasing age ($p < 0.001$). (B) The cross-sectional area values of the anteromedial and posterolateral bundles were similar through 4.5 months old ($p = 0.04$ to 0.36), with the anteromedial bundle becoming larger in the 6- and 18-month age groups ($p = 0.003$ and $p < 0.001$, respectively). The bars represent the mean and 95% CI.

Both bundles had an increased cross-sectional area during youth ($p < 0.001$), but the anteromedial bundle had continued increases in the cross-sectional area throughout adolescence while the posterolateral bundle plateaued at the onset of adolescence. The midsubstance cross-sectional area of the anteromedial bundle increased by sevenfold from 1.5 to 18 months old ($p <$

0.001) (Figure 5-7). Simultaneously, the cross-sectional area of the posterolateral increased by only 2.3 times ($p < 0.001$) (Table A-3-9). Between bundles, the cross-sectional area values only differed in the 6- and 18-month age groups ($p < 0.001$ at 6 months; $p = 0.003$ at 18 months), with the anteromedial bundle reaching 203% of the cross-sectional area of the posterolateral bundle by 18 months old (Figure 5-7). From birth through skeletal maturity, there were similar increases in the anteromedial and posterolateral bundle lengths (262% and 284%, respectively) (Figure A-3-3). The length of the anteromedial bundle was greater than that of the posterolateral bundle in all groups between 1.5 and 18 months old ($p < 0.001$-$p = 0.002$ across ages) (Table A-3-10).

The angular orientation of the anteromedial and posterolateral bundles similarly increased with increasing age in both the sagittal and coronal planes ($p < 0.001$). In the sagittal plane, these changes occurred in similar manners across bundles, with an average increase of 29° in the posterolateral bundle (early youth: 36° ± 3° [95% C.I.: 32°-39°]; late adolescence: 66° ± 4° [95% C.I.: 62°-71°]) and 23° in the anteromedial bundle (early youth: 32° ± 3° [95% C.I.:29°-35°]; late adolescence: 55° ± 5° [95% C.I.: 50°-61°])from early youth (1.5 months) to late adolescence (18 months) (Figure 5-8). Increases occurred between consecutive age groups only at the early adolescent stage (3-4.5 months) ($p = 0.001$) (Table A-3-11). The average coronal angle of the anteromedial bundle increased by 28°, while that of the posterolateral bundle increased by 31° from youth through late adolescence (Figure 5-8). These increases occurred earlier in skeletal growth, with increases in both bundles between early youth (1.5 months) and the juvenile (3 months) stage ($p = 0.033$), and increases in the anteromedial bundle in the juvenile (3 months) and adolescent (4.5 months) stages ($p = 0.012$) (Table A-3-12).

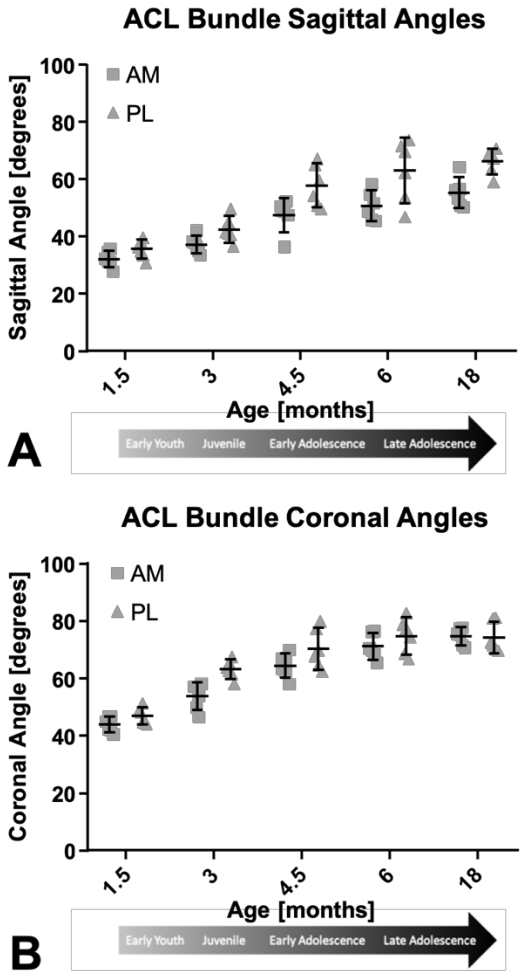

Figure 5-8. The (A) sagittal and (B) coronal angles of the anteromedial and posterolateral bundles of the ACL increased similarly with increasing age ($p < 0.001$). The bars represent the mean and 95% CI.

5.4. Discussion

Recent increases in the demand for ACL reconstructions in skeletally immature patients, coupled with initial reports of sub-optimal outcomes from traditional ACL reconstruction procedures in this population, have led to a need for age-specific studies of the native function and structure of the ACL during growth. As such, in this work we studied the joint stability, the biomechanical function of the ACL and its anteromedial and posterolateral bundles, and the structure and orientation of these bundles in a skeletally immature pre-clinical model of the knee,

the porcine stifle joint. We found that increasing age resulted in lower joint laxity under both applied anterior-posterior loads and varus-valgus moments. Additionally, we showed that the ACL carried the majority of force under an applied anterior load across ages and contributed to rotatory stability and the relative function of the anteromedial and posterolateral bundles of the ACL varied with age under anterior loading and varus torque. Near early adolescence, a shift in both relative size (cross-sectional area) and function occurred, where the anteromedial bundle had an increase in cross-sectional area and functional contribution, whereas the posterolateral bundle had a plateaued cross-sectional area and decreased functional contribution. The angular orientation of both bundles also increased with increasing age; however, the change in the orientation of the anteromedial and posterolateral bundles was similar throughout adolescence. These findings are important because the in situ functional behavior of a tissue depends on the tissue size, orientation, and intrinsic material properties, so by identifying growth stages where major structural and functional shifts occur in the ACL, we may be able to improve clinical planning to adapt for age-specific needs.

This study had several limitations. Care should be taken when trying to directly extrapolate results from a translational large-animal model to humans. However, the stifle joint in pigs has commonly been accepted as a surrogate for human knee joints, with congruence between the structure and functional properties of the ACL in mature populations (44, 110). Yet, some anatomic differences exist between the pig stifle joint and human knees. For example, testing in this study was limited to maximum extension at 40°. This resulted in a limitation because the posterolateral bundle plays a greater functional role near full extension (0°) in humans, and we were unable to study age-related changes for this flexion angle (127). Additionally, potential limitations may stem from our protocol, in which we transected the anteromedial bundle before the posterolateral bundle. While transecting the bundles in this order

was necessary for subsequent applied loading conditions not reported here, if the anteromedial and posterolateral bundles have a considerable physical interaction with one another, this may have affected the data presented in this study. Specifically, transection of the anteromedial bundle may have resulted in an underestimation of the functional contribution of the posterolateral bundle, because the principle of superposition assumes the anteromedial and posterolateral bundles are independent (44, 127). However, preliminary studies in our laboratory have confirmed that blunt separation of the bundles does not alter the forces carried by the ACL under these applied loads across a range of age groups.

Additionally, we limited our comparison to the commonly defined anteromedial and posterolateral bundles, although recent studies have highlighted the presence of three major bundles in the ACL in both humans and pigs: the anteromedial, posterolateral, and intermediate bundles (8, 138). Although the anteromedial and posterolateral bundles were easily discerned across all ages, the intermediate bundle could only be separated from the posterolateral bundle at older ages during dissection, and was not consistently discernible on MR images. For consistency across ages, the posterolateral and intermediate bundles were considered a single bundle. Reported sex-dependent differences in the incidence of ACL injury and the structural and biomechanical properties of the knee have motivated a need to investigate the effect of sex on the function of the ACL in both healthy and injured people during skeletal growth (18, 139, 140). As such, future studies should replicate this study within a male pig population to identify any sex-dependent differences in ACL function throughout growth. Additionally, noninvasive parameters, such as those collected using MRI, should be explored to enable a longitudinal approach to studying functional properties in lieu of the current cross-sectional approach (141).

Our imaging studies were limited by the resolution of our scanner and the repeatability of our analysis methods. The scanner used in this study had a resolution of 0.42x0.42x0.44 mm,

which is well below the magnitude of our reported values, and well below our between-group differences in length and cross-sectional area. Inter-viewer repeatability studies have shown that our sagittal angle measurements were repeatable within 2.6°, and our coronal angle measurements were repeatable within 2.7° across separate viewers. Again, these differences are well below the reported between-group differences in this study.

Analysis of the kinematics resulting from applied anterior-posterior loads and varus-valgus moments in this study revealed that the general joint laxity decreases considerably with increasing age in the pig model. Other studies have addressed the kinematic response of porcine joints to these loads in adolescent and skeletally mature animals, and while our study did not match the specific porcine breed, age, and loading conditions, our findings for the adolescent groups generally fit with the magnitude of anterior-posterior tibial translation and varus-valgus rotation reported previously (14, 142).

In this work we found that the ACL provided the vast majority of physical restraint to applied anterior tibial loads, not only in mature cases but throughout skeletally immature growth. These findings agreed with and built off of previous work showing that the ACL is the primary restraint to anterior tibial loads in both pig models and humans. Specifically, Xerogeanes et al. found that under 100N applied anterior tibial load, the adolescent porcine ACL restrained 95.6N ± 10.6N while the human ACL restrained 94.0N ± 4.0N (44).

Our findings regarding the functional contributions of the anteromedial and posterolateral bundles build from previous work studying the relative function of these bundles in skeletally mature human and animal models. Specifically, the relative force contributions of the anteromedial and posterolateral bundles under applied loads in adolescent (7-month-old) pigs were found to be more similar to those of humans than those of goats and sheep (44). In the aforementioned study, the anteromedial bundle carried 65% ± 21% of the in situ force of the

ACL under a 100 N applied anterior load for 6-month-old pigs, which was similar to our findings (44). Furthermore, it has been shown that the anteromedial bundle is a more considerable contributor under anterior tibial loads in the joints of skeletally mature pigs (10). However, we showed that this is not true in younger age groups. Additionally, in younger age groups, the posterolateral bundle plays a functional role under anterior tibial loads at all flexion angles in addition to applied rotational torque.

Along with our analysis of functional changes in the ACL, this study compared the cross-sectional area, length, and angular orientation of the ACL bundles during across stages of growth. While there is a paucity of functional data on the human ACL during childhood and adolescence, some comparisons have been made between anatomic changes in the ACL of pigs and humans throughout growth. These studies have shown that the angular orientation of the ACL becomes steeper relative to the tibial plateau in both the sagittal and coronal planes during skeletal growth in both species (1, 133). Additional studies in humans have found a plateau in the growth of the cross-sectional area of the ACL before the end of overall body growth (36). Previous studies in the pig model have shown that the length and width of the pig ACL was found to be similar to that of human ACL measurements (110). In our pig model, we found similar results; the cross-sectional area's growth in the ACL plateaued during adolescence. In the future, data regarding the growth of the cross-sectional area of the anteromedial and posterolateral bundles in humans should be pursued to study similarities or differences in human and pig bundle-specific changes.

These findings are clinically relevant because of the rapidly increasing numbers of ACL injuries in children and adolescents (25, 26) and the relatively high proportion of osteoarthritis and secondary injuries in this patient population (132). Although double-bundle surgeries may be difficult or impossible because of limited joint space, the information presented here direct future

clinical research to develop age-specific approaches to determine single-bundle graft size and placement with respect to the current ACL size, orientation, and function or anticipated changes in these parameters with future growth. Prior to implementing our findings into clinical practice, further work is needed to confirm the occurrence and specific timing of changes in ACL function and structure in human subjects. Previously, modifications have been made in the surgical technique used for these populations relative to adults, primarily to avoid disturbing the tibial and femoral growth plates in patients with considerable growth remaining (131). Data on the age-specific function of the bundles of the ACL could be useful in developing age-specific procedures for the treatment of childhood ACL injuries, and in this study we have determined that the relative function of the anteromedial and posterolateral bundles changes throughout skeletal growth, with both bundles playing a significant role under anterior tibial loads in youth and early adolescence. This expands on the previous understating of the field, which held that the anteromedial bundle was dominant under applied anterior tibial loads in mature cases, while the posterolateral bundle primarily functioned under rotatory movements and near full extension (44). Current adaptations for ACL reconstruction in young patients (such as all-epiphyseal and over-the-top methods) may not match the orientation and functional behavior of the ACL, and any changes in size, orientation, and function that would occur normally after surgery could further complicate effective surgical treatment (143). Further data from human studies, both clinical and cadaveric, may confirm the importance of matching age-specific function via graft selection and placement in children. The findings presented here can aid in directing future clinical studies to focus on aspects such as the timing of changes in the cross-sectional area of the ACL bundles, and direct biomechanical studies to anticipate general changes in laxity throughout growth and to focus on a redistribution of mechanical function between the bundles of the ACL.

In summary, while the overall function of the ACL as a primary stabilizer against anterior tibial load is maintained throughout skeletal growth, the individual roles of the anteromedial and posterolateral bundles undergo a major shift from shared biomechanical function in youth and early adolescence to anteromedial bundle dominant behavior after the onset of adolescence in pigs. These changes in function were coupled with changes in ACL size, with continued increase in the cross-sectional area of the anteromedial bundle and a plateau in posterolateral bundle cross-sectional area, but no differences between bundles in orientation as the bundles increased similarly throughout growth. These findings relating a shift in ACL bundle function suggest that age-specific surgical treatments with a focus on replicating the shared function of the anteromedial and posterolateral bundles during youth, and the anteromedial bundle dominance in adolescence, may result in improved functional outcomes in children; however, clinical studies are needed to confirm the relevance of these findings in humans. Moving forward, this work will be expanded to compare male and female pigs during growth, and the findings presented here will be used to motivate pre-clinical studies on the impact of partial and complete ACL injuries during skeletal growth. Additionally, the structural findings in this work can be compared to retrospective imaging databases of human growth in order to determine the similarities or differences in the timing of changes in the bundles of the ACL across species.

5.5. Conclusions and Broader Impact

Through this chapter, we have established that the age-specific changes in both biomechanical function and in structure differ between the AM and PL bundles of the ACL. Specifically, the changes in function under applied anterior tibial loads and varus tibial moments shift from shared function between bundles in youth to AM-dominant behavior in adolescence. During this shift from youth to adolescence, there is a notable difference in cross-sectional area

growth where the AM bundle experiences continued growth through adolescence while the PL bundle plateaus in early adolescence. With these stark differences established in healthy tissue function during growth, we were interested to see if there would be any changes in the functional response of joints from different ages to partial and complete ACL injuries. As such, Chapter 6 will address the impact of AM bundle and total ACL injury on joint kinematics and the functional demands on the remaining soft tissues in the joints.

CHAPTER 6

Joint Responses to Partial and Complete ACL Injuries Vary With Age

In the previous chapter we saw continued functional relevance of the ACL in resisting anterior tibial translation throughout skeletal growth, with age-dependent changes in the specific function of the anteromedial (AM) and posterolateral (PL) bundles. Given the recent increases in both partial and complete ACL injuries in young populations, we hoped to use these functional findings to motivate a study on the immediate changes in knee kinematics and the distribution of applied loads through the remaining musculoskeletal soft tissues in our skeletally immature model. This chapter describes the resulting study and the primary kinematic and kinetic findings.

The text in this chapter is in preparation for submission to the Journal of Biomechanics.

6.1. Introduction

The incidence of reported anterior cruciate ligament (ACL) injury in pediatric and adolescent patients has been steadily increasing over the past few decades (26). A recent study found that the most common age of ACL injury has dropped to 17 years of age, while the most rapid increases in injury rates occurred for 10-14 year olds (25). The skeletally immature population experience more partial ACL injuries to either the anteromedial (AM) or posterolateral (PL) bundles of the ligament in comparison to adult populations (144). The treatment of partial injuries can vary based on the extent and location of the tear (145). These decisions are informed in part by functional outcomes such as joint stability, muscle strength, or accrual of secondary injuries.

Complete ACL injury is frequently associated with secondary injuries of tissues such as the medial collateral ligament (MCL) and the medial meniscus as well as injury to the contralateral ACL (24). In pediatric age groups, chances of subsequent injury to the meniscus,

contralateral ACL, or the reconstructed graft were higher in children compared to adult values (146, 147). Studies in skeletally mature joints have shown that the loads in tissues including the MCL and medial meniscus increased in the ACL-deficient joint, leading to increased functional demands (24, 148-153). Recent work in the pig model has shown that the ACL is the primary stabilizer against anterior tibial loads throughout skeletal growth (120), so it follows that secondary stabilizers, such as the MCL and medial meniscus, would be placed under increased functional demands following an ACL injury at younger ages. However, little work has been done to assess age-dependent changes in the function of these tissues following partial or complete ACL injury during growth.

The porcine model has been established as a robust surrogate for the human ACL studies in both morphometric and functional studies in skeletally mature specimens (3, 109, 110). Previous work in our lab has found that the porcine ACL undergoes changes in its angular orientation during growth similar to the human ACL (133). We have also identified bundle- and age-dependent changes in the biomechanical function in the porcine ACL during skeletal growth (120). Specifically, under applied anterior and varus loads in the intact joint, the in-situ force carried by the PL bundle declines relative to the AM bundle from early to late adolescence. Recent work in a small set of pediatric human cadaveric specimens suggested that pediatric ACL tissue is weaker than adult tissue, and that the ACL experiences age-related microstructural changes that are disparate from those in the iliotibial band and the patellar tendon (39). However, we lack an understanding of age-dependent changes in the impact of ACL injury on joint kinetics and kinematics during growth.

Here, we assessed joint kinematics and the relative function of soft tissues in the knee under applied loads after partial and ACL transection throughout skeletal growth in the pig model. Given that the ACL is a primary stabilizer throughout growth (120), we hypothesized

that joint kinematics would increase under applied loads following partial and complete ACL injury for all age groups. Additionally, we hypothesized that the distribution of in-situ forces within secondary stabilizers would vary with age given previous reports of age-specific secondary injury rates to the medial meniscus (24, 147). To test these hypotheses, we used a robotic testing system to apply loads to porcine joints ranging from early youth to late adolescence to measure changes in anterior-posterior tibial translation and varus-valgus rotation in the joints and analyzed changes following partial and complete ACL injury in the in-situ forces within secondary tissues.

6.2. Materials and Methods

All animals in this study were obtained from a university-owned herd (Swine Educational Unit, North Carolina State University) and were healthy and of normal size. Animals were cared for according to the management practices outlined in the Guide for the Care and Use of Agricultural Animals in Teaching and Research, and experimental protocols were approved by the North Carolina State University Institutional Animal Care and Use Committee (79). Hind limbs were collected from 30 female Yorkshire cross-breed pigs at ages ranging from youth through late adolescence: early youth (1.5 months), juvenile (3 months), early adolescence (4.5 months), adolescence (6 months), and late adolescence (18 months) (n=6/group). Human age equivalencies were based on a combination of skeletal and sexual maturity (58, 133). Specimens were wrapped in saline soaked gauze and stored at -20°.

Prior to biomechanical testing, specimens were allowed to thaw at room temperature. The femur, tibia, and fibula were cut in the center of the diaphysis and all soft tissue was removed from the bones. The femur and tibia were set within custom molds using an epoxy

compound (Everglass, Evercoat, Cincinatti, OH). Joints were wrapped in saline soaked gauze with supplemental saline applied throughout testing to ensure the tissues remained moist.

Joint and tissue function were assessed using a 6 degree-of-freedom (DOF) robotic system (KR300 R3500, KUKA) operated by a separate controller (KRC4, KUKA) along with a 6-DOF force sensor (Omega160 IP65, ATI). These systems were integrated and controlled through a software package (SimVitro, Cleveland Clinic, Cleveland, Ohio), and data were processed using custom codes (Matlab2018b, Mathworks, Natick, MA). This system is capable of testing under kinematic and kinetic control with repeatability 0.1 mm and 0.25 N. We assessed repeatability in preliminary tests with joints mounted in the system. We found that the system could target forces to within 1.4±0.7N and moments to within 0.2±0.1N*m with kinematic repeatability of <0.1mm and <0.1°.

Custom clamps were used to attach each specimen to the robotic system, and a point digitizer (G2X, Microscribe) was used to define the anatomic coordinate system of the joint relative to the robotic coordinate system (10, 127, 137). A passive path was established by varying the flexion angle of the joint under kinematic control by 1° increments from full extension (40°) to flexion (90°) while minimizing forces and moments in the remaining 5 DOF.

A series of loading conditions were then applied to the joint (Table 6-1). Specifically, an anterior-posterior tibial load was applied at 40°, 60°, and 90° of flexion. A varus-valgus torque was applied at 60° of flexion. Testing under force control was performed with 4 DOF, as the flexion angle was held under kinematic control and internal-external rotation was kept under kinematic control due to the high rotational laxity in young porcine joints. Age-specific loads were determined based on the size of the footprint of the tibial plateau, measured via MRI (Table 6-2). Analyses of load-displacement curves from anterior-posterior load testing revealed that

loading levels were age-appropriate, as all specimens exceeded the toe region and none of the specimens experienced yield behavior or mechanical failure.

Table 6-1. Loading Protocol for Robotic Testing. Superscripts represent the in-situ force of a specific tissue, subscripts represent the kinematic state.

Joint State	Loading Conditions	Data Acquired
Intact Joint	Anterior-posterior tibial load (40°, 60°, 90°) and varus-valgus (60°) moment	Kinematics from intact joint (K_{intact}) In-situ force of joint (F^{intact}_{intact})
AM Bundle Transected	Anterior-posterior tibial load (40°, 60°, 90°) and varus-valgus (60°) moment	Kinematics from partial injury (K_{AMt})
	Repeat (K_{intact})	In-situ force of AM bundle ($F^{AM}_{intact}, F^{AM}_{AMt}$)
ACL Transected	Anterior-posterior tibial load (40°, 60°, 90°) and varus-valgus (60°) moment Repeat (K_{intact}, K_{AMt})	Kinematics from ACL deficient knee (K_{ACLt}) In-situ force of PL bundle and ACL ($F^{PL}_{intact}, F^{PL}_{AMt}, F^{ACL}_{intact}, F^{ACL}_{AMt}, F^{ACL}_{ACLt}$)
MCL Transected	Repeat (K_{intact}, K_{AMt}, K_{ACLt})	In-situ force of MCL ($F^{MCL}_{intact}, F^{MCL}_{AMt}, F^{MCL}_{ACLt}$)
LCL Transected	Repeat (K_{intact}, K_{AMt}, K_{ACLt})	In-situ force of LCL ($F^{LCL}_{intact}, F^{LCL}_{AMt}, F^{LCL}_{ACLt}$)
Medial Meniscus Removed	Repeat (K_{intact}, K_{AMt}, K_{ACLt})	In-situ force of medial meniscus ($F^{MMEN}_{intact}, F^{MMEN}_{AMt}, F^{MMEN}_{ACLt}$)
Lateral Meniscus Removed	Repeat (K_{intact}, K_{AMt}, K_{ACLt})	In-situ force of lateral meniscus ($F^{LMEN}_{intact}, F^{LMEN}_{AMt}, F^{LMEN}_{ACLt}$)

Table 6-2. Age-Specific Applied Loads and Moments for Robotic Testing.

Age	*Anterior-Posterior Load*	*Varus-Valgus Moment*
1.5 Months	20 N	1 N*m
3 Months	40 N	2 N*m
4.5 Months	80 N	4 N*m
6 Months	100 N	5 N*m
18 Months	140 N	7 N*m

Kinematics resulting from the applied loads and moments were recorded. Intact joint kinematics were repeated under kinematic control on the intact joint, and resulting forces and moments were recorded. The AM bundle was transected. The loading conditions were applied to the joint under force control, and resulting kinematics were recorded as AM-deficient kinematics. Both intact and AM-deficient kinematic paths were repeated on the specimen, and resulting forces and moments were recorded.

The remainder of the ACL (the PL bundle) was transected, and the loading conditions were again applied. Resulting kinematics were recorded as the ACL-transected path. The kinematics from the intact, AM-deficient, and ACL-transected paths were repeated under kinematic control on the ACL-transected joint, and all forces and moments were recorded. To determine the contributions of the remaining soft tissues of the joint (MCL, LCL, PCL, medial meniscus, and lateral meniscus), each individual tissue was transected/removed, and the kinematics from the intact, AM-deficient, and ACL-transected states were repeated while recording the resulting forces and moments.

All data was analyzed using a custom Matlab code. Anterior-posterior tibial translation (APTT) with respect to the femur was calculated as the change in position that occurred between maximum applied anterior and posterior loads. Varus-valgus rotation of the joint was calculated as the rotation of the tibia between the maximum varus and valgus moments. Normalization of APTT was performed relative to the sagittal width of the tibial plateau as measured from magnetic resonance imaging (MRI) scans (Simpleware 7.0, Synopsys, Chantilly, Virginia) (133).

Kinetic data was processed using custom Matlab codes to determine the contribution of each tissue to joint function under anterior translation, varus torque, and valgus torque (Table A-4-1). This was performed by applying the principle of superposition described previously (154). Resultant forces were calculated as the mathematical resultant of forces in the anterior-posterior,

medial-lateral, and proximal-distal directions. Force data were normalized to applied forces in the joint to facilitate comparisons across age groups. Percent contributions of the AM and PL bundles were calculated as the bundle contribution divided by the combined contribution of both bundles.

Statistical analyses were performed using commercial software (JMP Pro 13.0, SAS Institute, Cary, North Carolina). Normality was confirmed for each data set. For APTT and tissue contributions to anterior tibial translation, a multi-way ANOVA test was performed with flexion angle as a repeated measure and age and state as main effects. Varus-valgus rotation was analyzed using a two-way ANOVA with age and state as main effects. Tukey's post-hoc analysis was performed, and an overall alpha value of 0.05 was maintained. Complete summary data and statistical results are reported in the Supplemental Materials, with major findings presented in the Results section.

6.3. Results

Loss of ACL function impacted anterior-posterior tibial translation (APTT) normalized to joint size in response to applied loads (Figure 6-1 and Table A-4-2). Statistical analyses revealed significant interactions between injury state and age ($p<0.05$) as well as injury state and flexion angle ($p<0.05$). Average values for the intact joint ranged from 0.17-0.34 across flexion angles. AM bundle transection led to normalized APTT values ranging from 0.21-0.40 on average. Statistically significant increases relative to the intact joint were only found for the late adolescent (18 month old) age group (41-52% relative to the intact joint across all flexion angles tested, ($p<0.05$)). Across all ages, values for the AM-deficient group were statistically significant from the intact condition at 60° of flexion ($p<0.05$) but not 40° or 90° of flexion ($p>0.05$). Complete ACL transection further increased average normalized APTT values to

0.42-0.74. These values were approximately 2-fold higher than the intact and AM-deficient conditions across ages and flexion angles ($p<0.05$). In addition to normalized APTT, absolute values of APTT (not normalized to joint size) revealed similar differences due to partial and complete ACL transection (Figure A-4-1, Table A-4-3).

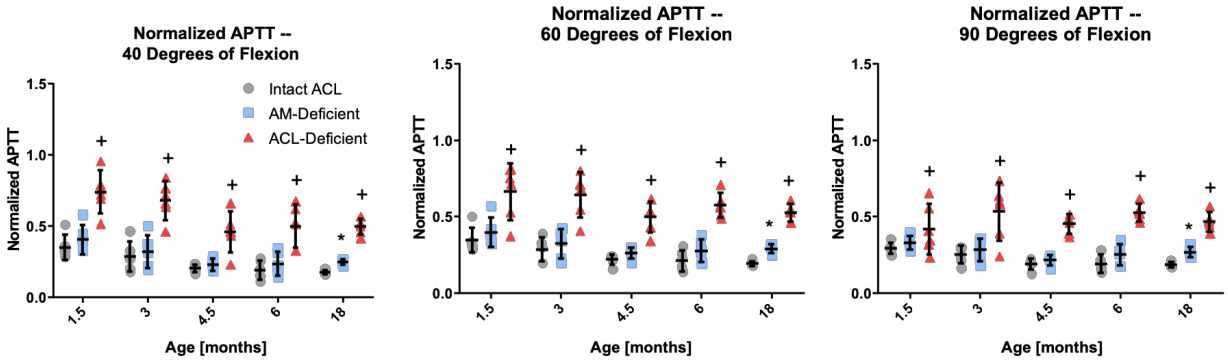

Figure 6-1. Normalized anterior-posterior tibial translation (APTT) in response to an applied anterior-posterior tibial load increased following partial and complete ACL transection. Two-fold increases occurred following complete ACL transection. Values were normalized to the anterior-posterior length of the tibial plateau. Data represented as points, with bars showing mean and 95% confidence interval. * denotes $p<0.05$ from intact state, + denotes $p<0.05$ from intact and AM deficient states.

ACL transection also resulted in increased varus-valgus rotation (Figure 6-2, Table A-4-4). AM bundle transection resulted in 0.5°-1.5° increases from the intact state ($p<0.05$, Table A-4-4), while increases due to complete ACL transection ranged from approximately 3°-5° compared to intact values across ages ($p<0.05$). In addition to increases due to injury, varus-valgus rotation decreased with increasing age regardless of injury state ($p<0.05$). For the intact state, varus-valgus rotation decreased from an average of 25.4° in youth to 6.3° in late adolescence. For the ACL-transected state, values decreased from 30.1° in youth to 10.6° in late adolescence.

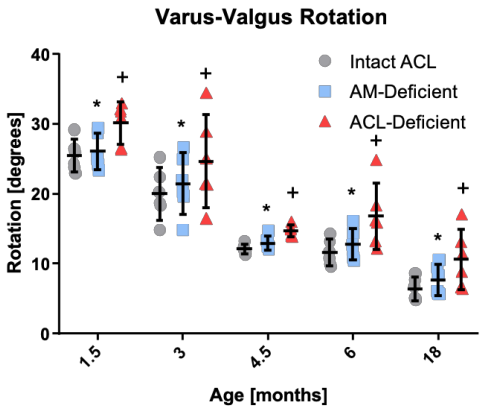

Figure 6-2. Varus-valgus rotation increased under applied moments following both partial and complete ACL transection across ages. Data represented as points, with bars showing mean and 95% confidence interval. * denotes $p<0.05$ from intact state, + denotes $p<0.05$ from intact and AM deficient states.

In addition to changes in kinematic parameters, we studied the force distribution across tissues. In the intact state, the ACL served as the primary soft tissue stabilizer to anterior tibial translation across ages and flexion angles, carrying 75-111% of the applied anterior load (Table A-4-5). Division of this load across the AM and PL bundles varied with age, with substantial contributions from both the AM and PL bundles in younger age groups and the AM bundle resisting the majority of the anterior load in adolescence (average 80-91% across flexion angles, Figure 6-3, Figures A-4-2, A-4-3, Tables A-4-6, A-4-7). Following AM bundle transection, the PL-bundle carried 79-101% of the applied anterior load under anterior tibial translation across all age groups at 60° of flexion (Figure 6-3). Similarly, at 60° and 90° of flexion, the average PL bundle contribution dropped no lower than 88% following AM bundle transection (Table A-4-7). While the contributions of the other soft tissues are minimal in both intact and partial injury states, they are substantial following ACL transection.

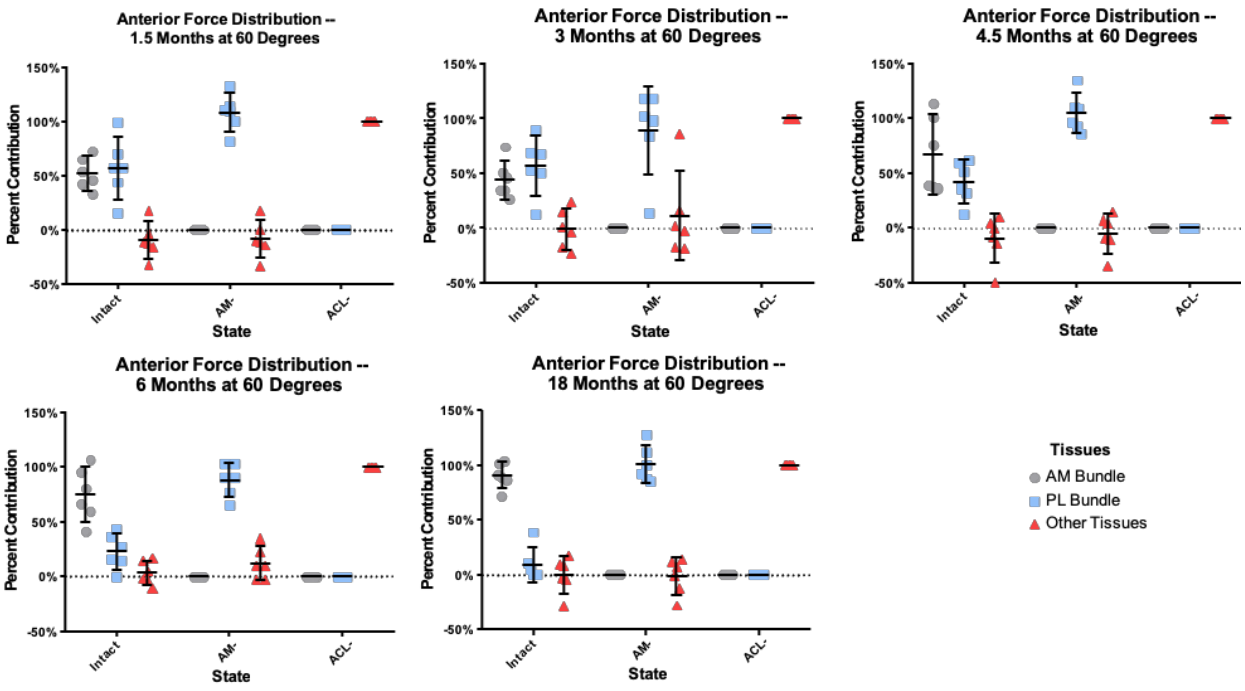

Figure 6-3. In-situ force contributions of the AM and PL bundles of the ACL relative to all other soft tissues in response to an applied anterior-posterior tibial load are shown for all ages for the intact, AM-deficient, and ACL-transected states at 60° of flexion normalized to the total force carried in the joint. The PL bundle resists the majority of the load across ages in the partial transection state, and other tissues carry all of the functional contributions in the ACL-transected state. Data represented as points, with bars showing mean and 95% confidence interval. Percent contribution is normalized to the total anterior force resisted by the joint under an applied load.

As such, we assessed the in-situ forces of specific secondary stabilizers, namely the medial meniscus and the MCL, after ACL transection. Although the demand under anterior translation on secondary soft tissues did not increase following AM-bundle transection, the contributions of the MCL and medial meniscus increased significantly following complete ACL transection (Figure 6-4, Figures A-4-5, A-4-6). In the ACL transected state, the MCL carried the greatest proportion of the applied anterior tibial load across ages, an average of 52-90% of the total load across flexion angles and ages (Figure 6-4, Table A-4-8). The medial meniscus also played a substantial role, carrying up to 35% of the anterior load on average in the ACL transected state. Of note, the contribution of the MCL was greater at 90° of flexion than either 40° ($p<0.05$) or 60° ($p<0.05$) of flexion in the ACL transected state. The contribution of the

medial meniscus was greater at 40° ($p=0.01$) and 60° ($p<0.01$) compared to 90° of flexion (Table A-4-9).

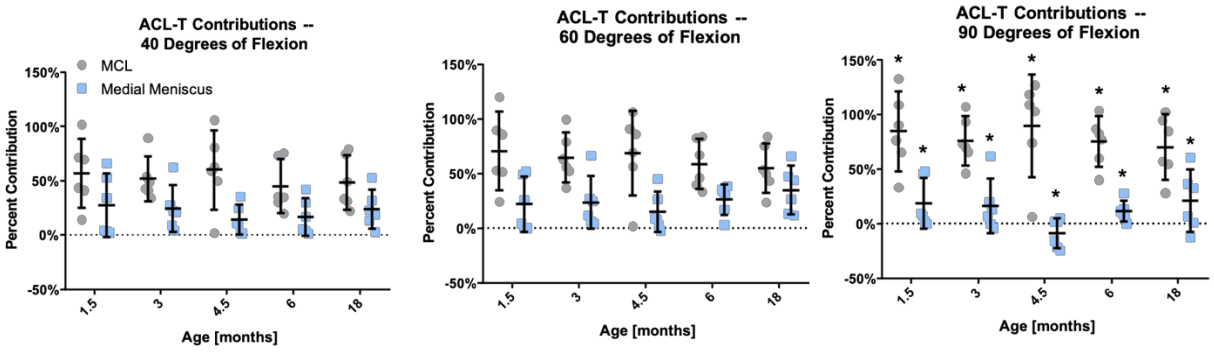

Figure 6-4. The MCL and medial meniscus carry the majority of in-situ force within the ACL-transected joint under an applied anterior tibial load across age groups. Data represented as points, with bars showing mean and 95% confidence interval. Percent contribution is normalized to the total force resisted by the joint under an applied load. * denotes $p<0.05$ from both 40° and 60° of flexion.

6.4. Discussion

In this study, we analyzed changes in joint function in the porcine model during growth following partial and complete ACL injury. Under applied anterior-posterior tibial loads, complete ACL transection resulted in greater anterior-posterior tibial translation throughout skeletal growth, and partial ACL transection resulted in increased translation only in adolescence. Under varus-valgus moments, both complete and partial ACL transection led to increased varus-valgus rotation at all ages. Together, these findings partially affirmed our first hypothesis that joint kinematics would increase following partial and complete ACL transection for all age groups. While the ACL was the primary restraint to anterior tibial loads across ages, the PL bundle was the primary restraint following AM bundle transection. After complete ACL transection, the MCL and medial meniscus consistently provided the majority of functional restraint across flexion angles and age groups. This finding was contrary to our second

hypothesis that the role of the secondary stabilizers following ACL transection would vary with age.

This study reported the immediate ex-vivo changes in kinematic resulting from loss of ACL function. We reported a 50% increase in anterior-posterior tibial translation following partial ACL injury only in the late adolescent group and 2- to 3-fold increases due to complete ACL injury across all ages. A human cadaveric study using biplanar radiography and manual joint manipulation found that complete, but not partial, ACL transection resulted in a significant 1.5- to 2-fold increase in anterior tibial translation under anterior tibial loads (155). Previous studies testing human specimens on robotic testing systems have also found that anterior translations doubled following ACL transection (17) while a porcine study reported that anterior tibial translations tripled following ACL transection (12). Additionally, we found an increase in varus-valgus rotation following both partial (5-20% increases) and complete (20-70% increases) ACL injuries at all ages. Another study found significant 2-fold increases in varus-valgus rotational laxity in ACL-sectioned knees in passive flexion-extension paths (156). Although our results suggest difficulty in detecting partial ACL injuries in younger joints through clinical exams, prior studies in human patients reported greater sensitivity to partial ACL injuries in skeletally immature patients through clinical examination (76.5%) compared to MRI analysis (52.9%) (157). The sensitivity of clinical exams such as a Lachman test to partial ACL injuries is similar in mature patients, with a meta-analysis of 8 studies reporting an average sensitivity of 68% (158). However, more sophisticated imaging in combination with clinical examinations may also allow better identification of partial ACL injuries (159). A study employing 3T MRI scanners to diagnose partial ACL injuries found that sensitivity for partial ACL tears was 77%, representing a significant improvement from the earlier value in MRI sensitivity, matching the reported sensitivity of clinical examination by Kocher et al. (160).

With increasing numbers of pediatric and adolescent ACL injuries in recent years, an improved understanding of the functional properties of the soft tissues of the knee is increasingly necessary. A need for subsequent reconstruction has been noted in cases of injuries affecting >50% of the midsubstance of the ACL and also in injury mainly to the PL bundle (144). Previous studies have considered the importance of the ACL in stabilizing the knee against anterior tibial translation, reporting that the ACL provides the majority (85-125%) of the overall restraint in both humans and animals (44, 49, 120). The increased role of the PL bundle following an AM bundle injury, and that of the MCL and medial meniscus following complete ACL transection may provide insight into the cause of secondary injuries in young patients with partial ACL injuries., although more work is needed. Along these lines, a recent study in an in-vivo sheep model reported that AM bundle transection had varied results in joint kinematics and cartilage health between animals, with noticeable effects on some animals and minimal changes in others (161). Furthermore, our findings on the function of the AM and PL bundles under anterior tibial translation in the intact adolescent joint were in line with previous reports showing that that 60-70% of the force carried in the ACL was carried through the AM bundle in adolescent pigs (44).

In this study, we did not find age-related differences in the immediate loading of the MCL and medial meniscus. Age-specific differences in secondary injuries following ACL injury have been reported. Specifically, patients over the age of 15 suffered from medial meniscus tears at a higher rate (29). However, additional factors related to different species, patient age and weight or time to surgery may contribute to this discrepancy (24, 29). Our findings regarding increased resultant loads in the medial meniscus following ACL transection are in agreement with a previous study which found significant increases in the resultant loads in the medial meniscus in ACL deficient knees compared to intact knees (149). Future in-silico and in-vivo

studies will aim to investigate the impact of tissue adaptation to ACL injury throughout skeletal maturity, which is particularly relevant within joints that are still growing.

This work used a large animal model, the Yorkshire cross-breed pig. The porcine ACL has closer structural and functional properties to human ACL properties in comparison to other large animals, and our mature age group corresponded well to previously published works on porcine ACL function (3, 109, 110). As with all studies involving large animal models, differences exist relative to humans in terms of growth timeline, locomotion modality, and body size. Another limitation of this study is the inclusion of only specimens from female animals, and in the future, a similar study will be completed in a male population to assess the effect of sex on parameters measured in this study. Additionally, this study involved only passive soft tissue restraints, whereas the behavior of the joint in-vivo is influenced by the activity of the muscles crossing the tibiofemoral joint. Finally, we only studied partial ACL injury to the AM bundle, although comparison to injuries to the PL bundle would be an interesting direction for future studies.

In conclusion, in response to applied loads, partial ACL injury led to increased anterior tibial translation only in late adolescence and increased varus-valgus rotation at all ages. Complete ACL injury led to increased translation and rotation at all ages. The PL bundle, not the MCL or medial meniscus, carried the majority of load in case of a partial ACL injury to the AM bundle. However, with the additional loss of PL bundle function, the MCL and medial meniscus provided functional restraint against anterior translation. These findings add to our understanding of the knee joint during growth and may aid in clinical assessment and treatment of ACL injuries in skeletally immature patients.

6.5. Conclusions and Broader Impact

Through this study, we found age-dependent kinematic responses to a partial ACL injury, with consistent responses to complete ACL injury. Specifically, partial ACL injury affected tibial rotation in response to applied varus-valgus moments across all ages, but increased tibial translation in response to applied anterior loads only in the skeletally mature group. Complete ACL injury resulted in increased laxity in all loading conditions tested. Interestingly, the medial meniscus and MCL were engaged in the complete injury case across age groups with no age-specific behavior detected in immediate changes in biomechanics. This suggests that there may be differences either due to chronic damage or between our porcine model and the human condition as previous literature suggests that secondary injuries to these tissues occur in an age-dependent manner. The functional studies in both this chapter and the previous chapter were limited to analysis at the maximum applied load or translation; however, *in vivo* knee loading often occurs somewhere within the working range. Additionally, by investigating changes in the shape of the load-deformation curve under applied anterior-posterior tibial loads we may be able to better understand the clinical implications of these changes in biomechanical function. As such, in the final aim of this dissertation we investigated differences between the endpoints of the load-deformation curve in both healthy and injured joints.

CHAPTER 7

The Shape of the Load-Deformation Curve Under Applied Anterior-Posterior Tibial Loads Varies With Both Age and Injury During Growth

Findings in the biomechanical studies from the previous two chapters suggest that the overall kinematic response of the knee, as well as the specific function of the multi-bundle ACL, vary with age throughout skeletal growth. However, in order to begin understanding the mechanisms of these changes we need to look deeper into the biomechanics of these tissues under applied loads. The parameters such as anterior-posterior tibial translation of the joint and anterior force carried in the ACL are measured from the maximum and minimum points of the load-deformation curves created from anterior-posterior tibial translation in response to loads applied to the tibia. In this chapter, we aimed to use metrics of *in situ* slack and *in situ* stiffness to describe the functional behavior of these joints and tissues throughout the application of these external loads.

The text in this chapter is in preparation for submission to the Journal of Biomechanical Engineering.

7.1. Introduction

Traumatic sports injuries requiring treatment, including knee injuries such as partial and complete anterior cruciate ligament (ACL) tears, impact roughly one third of all children in the United States (162). In a recent study, 60% of injuries treated in patients between 5-17 years of age were in the lower extremity, with ACL tears representing 9% of all injuries in the study. Interestingly, this injury was the 6th most common primary diagnosis in children between 5-12 years of age and the 2nd most common injury in 13-17 year old patients (163). Treatments for ACL injuries can range from conservative approaches such as functional bracing and physical

therapy to surgical reconstruction or repair, depending on both the severity of the injury and the remaining skeletal growth of the patient (20). Specifically, partial tears affecting <50% of the tissue and injuries in young patients have been suggested for conservative treatment in previous studies (144). While the intent of these conservative treatments is to improve joint stability by strengthening neuromuscular control, the ongoing instability may contribute to irreparable damage to the articular cartilage, potentially contributing to the near 50% incidence rates of osteoarthritis within 10 years of initial injury (23). Although joint instability is well established as an issue in knee injuries, less work has been done in quantifying changes in joint stability throughout skeletal growth, particularly in cases of partial and complete ACL-deficiency.

Joint instability, or laxity, can be assessed as the kinematic displacement of one bone relative to another in response to an applied load. Knee laxity is frequently studied under applied anterior-posterior tibial loads, resulting in a measure of anterior-posterior tibial translation (APTT) relative to the femur (14, 164). APTT is commonly assessed in patients via manual clinical exams (165) or in situ in cadaveric joints using force-sensing 6 degree-of-freedom (DOF) robotic systems in the lab (13, 127, 166, 167). Through these approaches, previous studies have established that the instability associated with complete ACL injuries results in an increased APTT under maximum applied anterior-posterior tibial loads (127, 168). In addition to work measuring APTT as an effect of ACL injury, a previous study by our lab has shown that skeletal growth (120) can have a considerable effect on APTT, with decreased laxity in older age groups when normalized to the size of the joint (anterior-posterior tibial plateau length) although differences were not significant in non-normalized cases.

While APTT provides an end-point measurement of joint laxity, few studies have reported on the shape of the anterior-posterior tibial load-translation curve between these end-points. A recent paper by Imhauser et al. established parameters for describing this behavior for

knees and knee ligaments at sub-maximum loads, and related their findings back to the laxity of the joints under applied tibial loads (169). This work described in situ slack as the relative motion in the joint between the points where the soft tissues began carrying considerable force in opposing directions, and in situ stiffness as the slope of the linear region of the load-translation curve after the slack region (169). Their work was able to correlate in situ slack of the cruciate ligaments to anterior-posterior laxity, and both in situ slack and in situ stiffness of the medial collateral ligament to valgus laxity (169). These findings led us to ask whether in situ slack and stiffness could be used to describe age- and injury-related changes in joint function during skeletal growth.

As such, the objective of this study was to assess the effect of age and injury on the shape of the load-translation curve of both the joint and the ACL under applied anterior-posterior tibial loads during skeletal growth in a porcine model. In order to do so, we used a force-sensing robotic system to apply loads to joints ranging from early youth to skeletal maturity and recorded both the 6-DOF kinematics and 6-DOF kinetics throughout loading. Load-translation plots were created for each joint and the ACL, and the in situ slack and in situ stiffness were compared across ages and states.

7.2. Methods

7.2.1. Specimen Collection

Hind limbs were collected from 30 female Yorkshire cross-breed pigs from birth through skeletal maturity (1.5, 3, 4.5, 6, and 18 months of age, n=6 per age group). These ages were equivalent to early juvenile, juvenile, early adolescent, adolescent, and late adolescent groups in humans, respectively, based on a combination of skeletal and sexual age scales in both species (58). The animals used in this study were obtained from a university owned herd, and all

animals were healthy and of normal size. All swine were cared for according to the management practices outlined in the Guide for the Care and Use of Agricultural Animals in Teaching and Research and their use in the current experimental protocols were approved by the N.C. State University Institutional Animal Care and Use Committee (79). Hind limbs were dissected to the stifle (knee) joint and wrapped in saline-soaked gauze and stored at -20° C. To prepare the joints for testing, the joints were thawed at room temperature overnight. The femur, tibia, and fibula were cut at the mid-diaphysis and the bones on either side of the joint were fixed within an epoxy compound in custom molds. The joints were wrapped in saline-soaked gauze and stored again at -20°C.

7.2.2. Biomechanical Testing

Biomechanical tests were performed using a 6-DOF (degree of freedom) robotic testing system (KR300 R2500, Kuka, Shelby Charter Township, MI) powered by a controller (KRC4, Kuka, Shelby Charter Township, MI) along with a 6-DOF force/moment sensor (Omega160 IP65, ATI Industrial Automation, Apex, NC). This system was integrated and controlled using a commercial software package (simVitro, Cleveland Clinic, Cleveland, OH). The robotic system used in this study can operate under both kinematic and kinetic control and has a kinematic repeatability of 0.1mm and 0.1° and a load cell sensitivity of 0.25 N. Joints were attached to the robotic system using custom clamps with the femur attached to a clamp fixed to the floor and the tibia attached to the end effector of the robot. The anatomic coordinate system of the joint was defined relative to the coordinate system of the robotic manipulator as described previously using a 3D point digitizer (G2X, Microscribe, Amherst, VA) (15, 120, 127).

The following robotic protocol is summarized in Table 1. A passive path was determined for each joint by changing the flexion angle of the joint from full extension (40° in the pig stifle

joint) to 90° of flexion in 1° increments while minimizing the forces and moments in the other 5-DOF. The kinematics of each passive position were recorded for each flexion angle. Joint kinematics were then recorded for the intact joint under applied anterior-posterior tibial loads at full extension (40°), 60°, and 90° of flexion. These "intact" kinematic paths were repeated under kinematic control and the resulting forces were recorded. The anteromedial (AM) bundle of the ACL was then transected and the anterior-posterior loads were applied again at 40°, 60°, and 90° of flexion. The resulting "AM-deficient" kinematic paths and the intact kinematic paths were repeated in this state. Then the remainder of the ACL (the posterolateral (PL) bundle) was transected and the anterior-posterior loads were applied in the ACL-deficient state. The ACL-deficient kinematics were then repeated along with the AM-deficient and intact kinematics.

Table 7-1. Robotic loading protocol.

Joint State	Robotic Command	Kinematic Outputs	Kinetic Outputs
Intact Joint	Passive flexion-extension path	Passive Path Positions	
Intact Joint	Anterior-posterior loads	Intact Kinematics	
Intact Joint	Repeat intact kinematic path		Intact path forces
AM-Deficient Joint	Anterior-posterior loads	AM-Deficient Kinematics	
AM-Deficient Joint	Repeat intact path		AM-bundle *in situ* forces
AM-Deficient Joint	Repeat AM-deficient path		AM-deficient path forces
ACL-Deficient Joint	Anterior-posterior loads	ACL-Deficient Kinematics	
ACL-Deficient Joint	Repeat intact path		ACL *in situ* forces
ACL-Deficient Joint	Repeat AM-deficient path		PL-bundle *in situ* forces
ACL-Deficient Joint	Repeat ACL-deficient path		ACL-deficient path forces

7.2.3. Biomechanics Data Processing

Force and translation data were plotted against one another to create the load-translation plot represented in Figure 1. Anterior-posterior tibial translation, *in situ* forces in the AM bundle, *in situ* forces in the PL bundle, and *in situ* forces in the ACL. APTT was calculated as the distance in the anterior-posterior plane between the point of maximum translation under applied

anterior and posterior tibial loads (Figure 1). *In situ* forces in the AM bundle, PL bundle, and the ACL were calculated using the principle of superposition to calculate the force components in 3-DOF under applied anterior tibial loads (15, 127). Resultant forces were then calculated as the resultant of the force vector for each tissue.

Biomechanical data at sub-maximum loads were assessed under applied anterior-posterior loads in a manner similar to that published by Imhauser *et al* (169). Force and displacement data were collected at intermediate points defined at increments of 20% of the peak applied load for each specimen (Figure 7-1). A custom Matlab code was developed to fit data to bi-phasic curves in the anterior and posterior regions with an exponential fit ranging from the passive path position to a transition point and a linear fit from that transition point to the maximum load position. This process was iterated with each of the intermediate points defined as the transition point. The transition point resulting in the greatest combined r^2 value from the exponential and linear regions was selected, and a single curve combining the curve-fits of the exponential and linear regions. The process of selecting and generating a bi-phasic curve was repeated between the passive path position and the maximum applied posterior drawer. A point of maximum curvature was determined for the new plot, and this was defined as the engagement point of the tissue. In situ slack was defined as the distance between the engagement point in the anterior and posterior directions. The stiffness of the tissue of interest, e.g. knee or ACL, was defined as the slope of the linear region of the plot under anterior load.

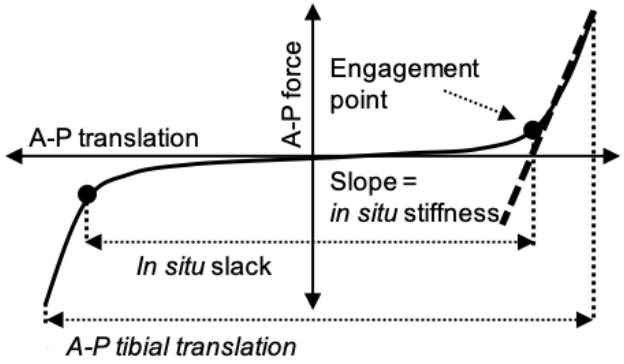

Figure 7-1. Schematic depicting the load-translation curve of the joint under anterior (positive) and posterior (negative) tibial translation and parameters determined from the curve.

7.2.4. Statistical Analysis

Statistical analysis was performed with commercial software (JMP Pro 13.0, SAS Institute, Cary, NC). Analyses for APTT, *in situ* slack, and *in situ* stiffness consisted of multi-way ANOVA tests with Tukey's post-hoc analysis using age as a between subjects effect, and flexion angle and injury state as repeated measures with significance set at $p<0.05$. *In situ* stiffness of the joint and the ACL were compared via linear regression. Slope of the line, the r^2 value, and p value are reported.

7.3. Results

7.3.1. Joint Biomechanics

Average anterior-posterior load-translation curves for the joints at all age groups are shown in Figure 7-2. Data is shown for 60° of flexion, but similar behavior was found at 40° and 90° of flexion (Figure A-5-1). These plots reveal a shift from shallow, linear curves in juvenile groups to steep, non-linear curves in late adolescence. These changes are partly driven by an increase in the age-specific target loads in both anterior and posterior directions (20 N in early youth to 140 N in late adolescence). However, concurrent with these 7-fold increases in load, there are no meaningful changes in APTT.

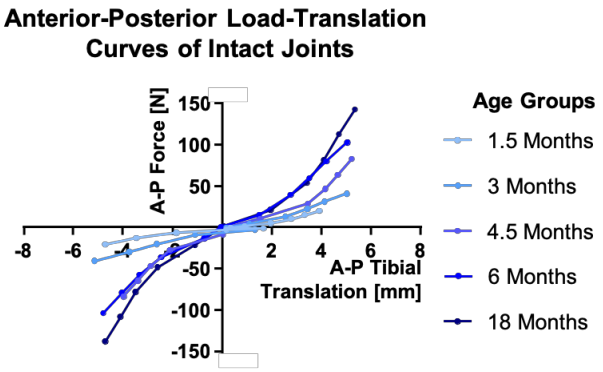

Figure 7-2. The anterior-posterior (A-P) load-translation curves of intact joints vary with age. Individual points represent group averages. For both the x- and y-axes, the posterior direction is negative, while the anterior direction is positive. Data presented at 60° of flexion.

In order to better understand these changes in the shape of the load-translation curve, the *in situ* slack and *in situ* stiffness was calculated for each joint. First, analysis of the *in situ* joint slack versus age shows that the overall slack length of the joints (the length between anterior and posterior engagement points) did not vary substantially with age (Figure 7-3). Specifically, *in situ* slack length slack ranged from 3.2 ± 1.1 mm to 5.5 ± 0.8 mm across ages and flexion angles (Figure 7-3, Table A-5-1). Statistical analysis of the *in situ* joint slack revealed that there were no significant differences due to age at any flexion angle tested ($p>0.05$) (Figure 7-3, Figure A-5-2).

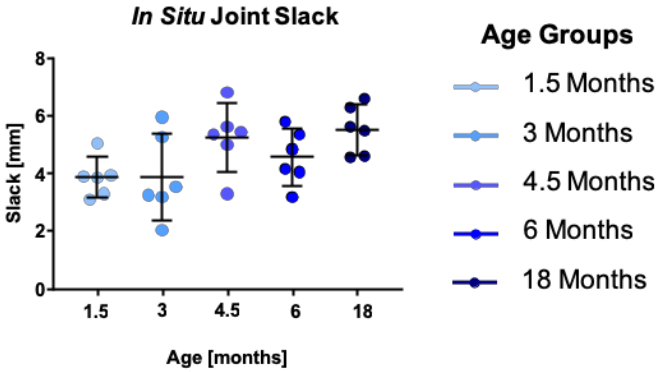

Figure 7-3. In situ joint slack did not vary substantially across age groups. Points represent data from separate specimens, bars represent mean ± 95% C.I.

In situ joint stiffness increased between 1.5 and 18 months of age as shown in Figure 7-4. Increases of 4-fold to 5-fold were observed with age, as group averages ranged from 9 N/mm to

17 N/mm in juvenile age groups while group averages ranged from 31 N/mm to 72 N/mm in adolescent age groups across all flexion angles. The greatest increase between consecutive time points occurred at the onset of adolescence, between 3 and 4.5 months of age. Statistically significant changes occurred due to age ($p<0.05$) but not flexion angle ($p>0.05$) (Figure A-5-3, Table A-5-2). Relative to juvenile age groups (1.5 and 3 months), these increases were statistically significant in adolescent (4.5-18 month) age groups ($p<0.05$). There were no statistically significant differences detected between the adolescent age groups ($p>0.05$).

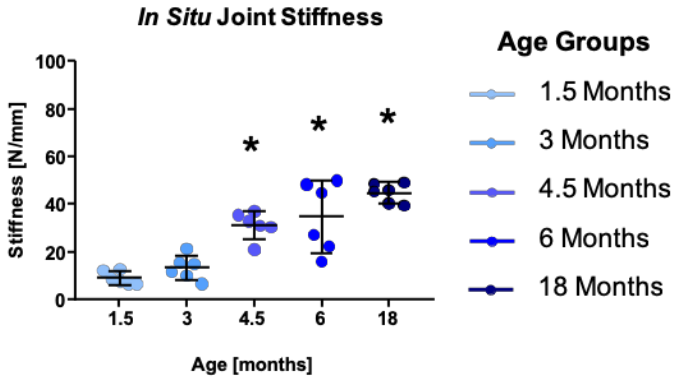

Figure 7-4. In situ joint stiffness increases with increasing age across flexion angles. Points represent data from separate specimens, bars represent mean ± 95% C.I. * represents statistically significant difference from both 1.5 and 3 month age groups. Data presented at 60° of flexion.

7.3.2. ACL Biomechanics Change During Skeletal Growth

The anterior load-translation curves derived from the anterior load carried by the ACL were also evaluated (Figure 7-5). Visually, the engagement of the ACL under anterior tibial translation is evident across age groups, as the slope increased with increasing anterior tibial translation. With increasing age, the shape of the ACL curve varies from a shallow curve in the juvenile groups to a steep curve in late adolescence. Similar changes were seen across flexion angles (Figure A-5-4).

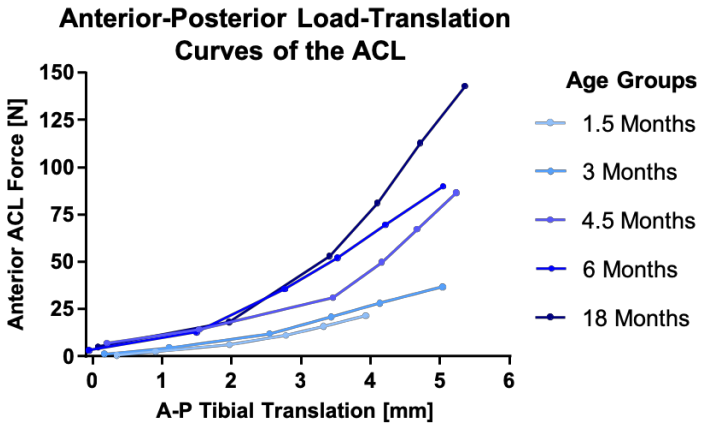

Figure 7-5. The anterior-posterior (A-P) load-translation curves of ACLs under applied anterior tibial loads vary with age. Individual points represent group averages. For both the x- and y-axes, the posterior direction is negative, while the anterior direction is positive. Data presented at 60° of flexion.

These qualitative assessments matched quantitative measures of *in situ* ACL stiffness (Figure 7-6). Between 1.5 and 18 months of age, *in situ* ACL stiffness increased by 4-fold to 5-fold. Specifically, *in situ* ACL stiffness ranged from an average of 9 N/mm in early youth to 45 N/mm in late adolescence across flexion angles. Similar to changes in *in situ* joint stiffness, significant increases occurred primarily between juvenile and adolescent groups, with no significant change following the onset of adolescence ($p>0.05$). Higher values were found at 90° of flexion compared to 40° and 60° of flexion ($p<0.05$) (Table A-5-3, Figure A-5-5).

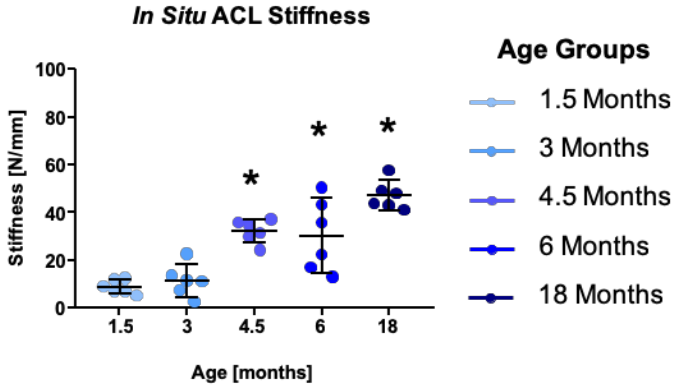

Figure 7-6. ACL stiffness increases as a result of increasing age. Points represent data from separate specimens, bars represent mean ± 95% C.I. * represents statistically significant difference from both 1.5 and 3 month age groups. Data presented at 60° of flexion.

7.3.3. Relationship of ACL Stiffness and Joint Stiffness Throughout Skeletal Growth

In order to assess the relationship between the *in situ* stiffness of the joint and the *in situ* stiffness of the ACL throughout skeletal growth, the two parameters were plotted and the linear correlation was assessed (data at 60° of flexion shown in Figure 7-7). The *in situ* ACL stiffness was closely correlated to the *in situ* stiffness of the joint for all flexion angles. At 60° of flexion the resulting slope was 1.01 (r^2=0.91, p<0.001) suggesting equal change in the two parameters (Figure 7-7). At full extension (40° of flexion), the slope was 0.71 (r^2=0.81, p<0.001), while at 90° of flexion, the slope was 1.08 (r^2=0.93, p<0.001) (Figure A-5-6).

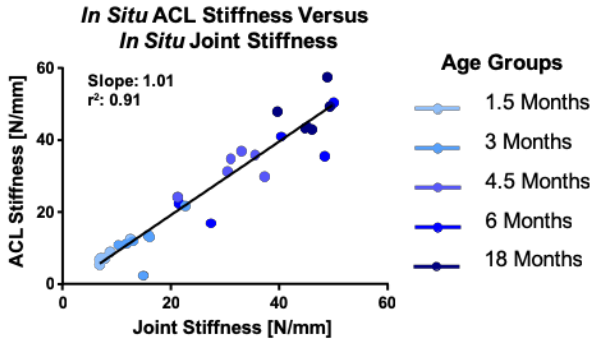

Figure 7-7. Line of best fit for ACL stiffness versus joint stiffness reveals a close correlation between the two parameters across all ages at 60° of flexion.

7.3.4. Impact of Partial and Complete ACL Injury on Joint Biomechanics

Building from the analysis of age-related changes in the load-translation curve for *in situ* parameters of the intact joint during growth, the next analysis assessed the impact of partial (AM bundle) and complete (total ACL) transections on these biomechanical parameters. The impact of injury on *in* situ slack is shown in Figure 8. Although age alone did not impact *in situ* joint slack in the intact joint, the introduction of partial and complete ACL transections did result in significant changes to this parameter. Specifically, *in situ* slack increased 2-fold to 4-fold between the intact and ACL-transected states across ages and flexion angles (p<0.05) (data in Table A-5-4, additional flexion angles shown in Figure A-5-7). AM bundle transection resulted

in significant increases in *in situ* joint slack only in the late adolescent case ($p<0.05$). Comparing between injury states, *in situ* joint slack was significantly greater with complete injury relative to partial injury regardless of age ($p<0.05$).

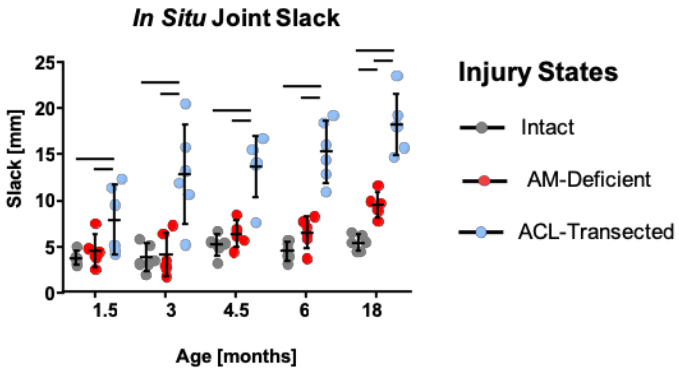

Figure 7-8. In situ joint slack increases as a result of complete ACL injury across age groups, and as a result of partial ACL injury in late adolescence. Points represent data from individual specimens, bars represent mean ± 95% C.I. Top bars represent statistically significant differences between states. Data presented at 60° of flexion.

The impact of injury on *in* situ stiffness is shown in Figure 7-9. In *situ* joint stiffness decreased significantly following the introduction of ACL injury to the joints in many cases. Specifically, complete ACL transection resulted in 3- to 4-fold decreases in total joint stiffness relative to the intact state across all ages and flexion angles ($p<0.05$ in 3-18 month age groups). Meanwhile, relative to the intact state, AM bundle transection resulted in a 67-86% decrease in *in situ* joint stiffness in the 6- and 18-month age groups ($p<0.05$), while there were no statistically significant changes between these states in the younger groups ($p>0.05$). Comparing between injury states, joint stiffness decreased significantly with complete ACL injury relative to partial ACL injury in age groups between 3 and 18 months ($p<0.05$). Data for all flexion angles are provided in Table A-5-5 and Figure A-5-7.

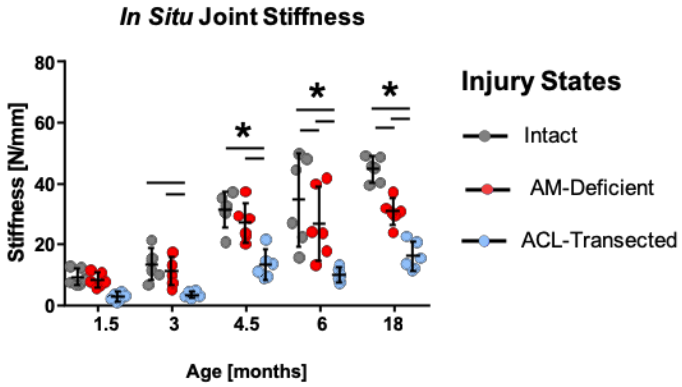

Figure 7-9. In situ joint slack decreases as a result of complete ACL injury across age groups (3-18 months) and as a result of partial ACL injury in adolescence (6-18 months). Points represent data from individual specimens, bars represent mean ± 95% C.I.. Bars over data represent statistically significant differences between states. Data presented at 60° of flexion.

7.4. Discussion

In this work using a porcine model, we found that the shape of the load-translation curves of joints changes under applied anterior tibial loads throughout skeletal growth. While there was a lack of significant changes in the low-load region of these curves, represented by the *in situ* slack, increasing age resulted in 4-fold to 5-fold increases to the slope of the high-load portion of the load-translation curve, represented by the *in situ* joint stiffness. Additionally, the *in situ* ACL stiffness increased by a similar amount throughout skeletal growth. Combined with the lack of significant changes in the toe region of these curves, represented by the *in situ* slack, this differences suggests a change in the shape of the load-translation curve during growth. Additionally, we report that the *in situ* slack increases and the *in situ* stiffness decreases with complete ACL injury across all ages and with partial (AM bundle) injury in adolescent and late adolescent groups.

The findings presented here fit with the current understanding of changes in joint laxity with skeletal growth. Specifically, previous studies in humans show greater joint laxity in the knee in children and adolescents compared to mature populations (170-172). Furthermore, a study by Ford et al. analyzed active knee stiffness from computational models measured in the

sagittal plane during the stance phase of a jump landing task (38). This group reported ~5-7% increases in knee stiffness in within the same adolescent subjects over a period of one year. Moreover, post-pubertal subjects (14.5 ± 1.4 years) had stiffness values ~15% higher than pubertal subjects (12.4 ± 0.9 years). In this study we found increases in joint stiffness of ~10% between early adolescent and adolescent age groups. Our work has expanded on and reinforced this body of knowledge by reporting changes in an *in situ* measure of joint slack and stiffness at ages ranging from early youth to late adolescence in a common pre-clinical model for the knee.

There is less information available regarding the function of the skeletally immature ACL. Through this analysis of ACL function throughout the load-translation curve, we have developed an improved understanding of how its function changes with age. The ACL acts to stabilize the porcine stifle joint against anterior tibial loads across ages, with similar low-load (or "toe region") behavior across age groups, but major increases in the *in situ* stiffness describing the high-load portion of the load-translation curve. The stiffness values reported for the late adolescent group in this work were similar to mature human values reported by Imhauser et al., as our adolescent and late adolescent *in situ* ACL stiffness values ranged from 24 - 52 N/mm across ages and flexion angles, while the *in situ* ACL stiffness for skeletally mature humans reported by Imhauser et al. was 33 N/mm at 30° of flexion (169), suggesting that both the tissue properties and methods are repeatable across research groups.

In addition to studies reporting the effect of growth on joint mechanics, some studies have worked to quantify the effects of partial and complete ACL injury on knee biomechanics. Specific to comparisons of partial and complete ACL tears, one study found that clinicians were able to diagnose complete ACL tears with 77% accuracy, while they could only diagnose AM bundle injuries with 13% accuracy (155). Interestingly, another study reported higher sensitivity in clinical examination (76.5%) compared to MRI (52.9%) for partial ACL tears confirmed by

arthroscopic examination (157). This study went on to report that the diagnostic performance of clinical examinations for ACL tears was not significantly different between children younger or older than 12 years of age, although the diagnostic performance of MRI examinations was worse in the younger cohort of children.

There were several limitations to this work. While the porcine model has been presented as a surrogate for the human knee in many studies (34, 41, 49, 109, 173), there are some differences between human joints and porcine joints. Notably in this study, porcine joints are limited in extension to approximately 40° of flexion while human knees can extend much further (0° of flexion). Additionally, the translation between porcine and human stages of growth requires consideration of multiple factors such as skeletal and sexual maturity, and as such, there is no confirmed direct correction factor between chronological ages in the two species. The calculation of load-translation curves were limited to data points at discrete load levels between maximum posterior and maximum anterior translation, which may impact curve fitting and resulting values for *in situ* slack and stiffness. These parameter estimates could be improved by using more continuous data points in the future. Nevertheless, inter-specimen variability observed in *in situ* slack values was very similar to that observed in total translation values (~10-35% standard deviation relative to the mean for both *in situ* slack and anterior-posterior tibial translation across ages and flexion angles) leading us to believe that the variability observed here represented biological variability, and was likely not a result of inaccurate curve fitting.

These findings motivate several avenues of future research. In order to assess sex-dependent changes in joint biomechanics at sub-maximum loads, we intend to repeat this study in the same age groups and injury conditions in a male porcine population. This work also motivates future *in vivo* studies analyzing changes in sub-maximum joint kinematics due to tissue remodeling following ACL injury and reconstruction in skeletally immature animals.

In conclusion, the biomechanical response of the porcine stifle joint to applied anterior tibial loads varies with age during skeletal growth due to increases in the *in situ* stiffness, but not slack, of the joint. Furthermore, *in situ* ACL stiffness increased during skeletal growth in a similar manner to *in situ* joint stiffness. Regardless of age, complete ACL injuries resulted in significant increases in the *in situ* slack length of the joint, and significant decreases in the *in situ* stiffness of the joint, with partial injury incurring these results in adolescent age groups. Clinically, these findings suggest that the kinematic response of knees to standard clinical exams may be age-dependent. As such, both patient age and specific ACL injury type are important factors to consider during clinical examinations to assess ACL function.

7.5. Conclusions and Broader Impact

Through this study, we were able to isolate the biomechanical function of skeletally immature knees in either the toe region or the linear portion of the anterior-posterior load-deformation curve. By separating these sections into *in situ* slack and *in situ* stiffness we found that the primary age-dependent changes under applied anterior loads are due to changes in the linear region, with increases in *in situ* stiffness occurring with growth. Additionally, we saw marked increases in *in situ* slack along with decreases in *in situ* stiffness due to both partial and complete ACL injury across ages. These changes are related to differences in kinematics prior to the engagement of secondary stabilizing tissues, and as such this study may lead to an improved understanding of chronic injuries following ACL rupture.

CHAPTER 8

Discussion, Conclusions, Implications, and Future Directions

8.1. Summary of Findings

The past five chapters describe a series of investigations into changes in the structure and function of the multi-bundle ACL throughout skeletal growth in a pre-clinical model, the Yorkshire cross-breed pig. By combining magnetic resonance imaging (MRI), anatomic and morphometric analysis techniques, a robotic biomechanical testing system, and computational analysis of the resulting kinematic-kinetic relationships, we are able to draw several conclusions about changes in the structure and function of the ACL during growth.

Through the analysis of magnetic resonance images, we were able to study changes in the orientation of the ACL and the AM and PL bundles throughout growth. Our findings in Chapter 3 reporting an increase in the angular orientation of the ACL were in agreement with human studies performed by other groups (1, 35) encouraging further investigation of the porcine model as a surrogate for the human ACL in skeletally immature populations. This method was again applied in Chapter 5, where we found that angular orientation changes are not bundle-specific, as the AM and PL bundles experience similar changes during growth.

Additional analysis of the MRI scans in Chapter 4 revealed a shift in the relative proportions of the ACL causing a change from a short, broad shape during youth to a longer, thinner ligament in skeletally mature limbs. In the same chapter we described allometric growth between the ACL and other ligaments and tendons in the knee, as the ACL did not grow proportionately to the other tissues. Later, in Chapter 5, we compared the growth of the AM and PL bundles and found that even within the ACL tissue growth occurs with varied timing as the AM bundle continued growing past the end of PL bundle growth.

Beyond studying changes in the structure of the ACL with growth, we aimed to characterize the biomechanical function to the ACL and its constituent bundles throughout skeletal growth. In Chapter 5 we first confirmed that the ACL is the primary restraint to anterior tibial loads throughout growth. Although this did not vary with age, our analysis of the individual AM and PL bundle contributions revealed age-specific changes in the function of the ACL. In pre-adolescent groups we found shared functional contributions of the AM and PL bundles under applied anterior tibial loads and varus moments, but in adolescent and late adolescent groups we found that the AM bundle dominates the function of the ACL in healthy cases. We expanded on these studies of healthy ACL function in Chapter 7, where we divided the load-deformation curve into the toe region and the linear region. Here we found consistent increases in the *in situ* stiffness of the knee and the ACL, calculated as the slope of the linear region of the load-deformation curve. The close relationship of knee stiffness and ACL stiffness across age groups highlighted our previous findings regarding the importance of the ACL in stabilizing the knee against applied anterior tibial loads throughout growth.

Finally, we aimed to assess changes in the biomechanics of the knee following partial and complete ACL injuries across age groups. Chapter 6 describes an increase in joint laxity in response to both anterior loads and varus-valgus moments following complete ACL injury regardless of age, and increased laxity due to partial ACL injury across ages in response to varus-valgus moments and in mature ages in response to anterior loads. We studied the *in situ* slack and *in situ* stiffness of these joints in injured states in Chapter 7, and found that both the toe region and linear region of load-deformation curves are impacted by ACL injuries.

8.2. Limitations and Challenges

The studies described in this dissertation were limited by several challenges. First, these studies are limited to a female, porcine sample. Pediatric studies involving invasive methods, such as the biomechanical studies described here, are frequently limited to pre-clinical models due to the paucity of pediatric cadaveric specimens. Wherever possible we aimed to compare our outcomes in the late adolescent group to values available in the literature for mature musculoskeletal studies in both human and porcine studies. Our general findings regarding decreased mechanical stiffness in young tissues are in line with recent data in the literature from a limited sample of pediatric cadaveric limbs (39). The inclusion of only female specimens was intended to isolate age- and sex-dependent changes in the ACL, and questions regarding the interaction of these effects will be addressed by ongoing studies in male specimens.

An additional limitation to these findings is related to the *ex vivo* approach used in our biomechanical studies. While the use of a robotic system to test joints *ex vivo* allows for high accuracy and repeatability and isolating the functional contribution of individual tissues, it does limit the study to a cross-sectional approach. This introduces animal-to-animal variability, whereas a less invasive biomechanical testing approach would allow for longitudinal studies, matching functional data within an animal across different age groups. Another impact from using this testing approach is the limitation of our injury studies to immediate functional changes. The changes we observed due to partial and complete ACL injuries may be amplified due to the lack of active stabilization from the muscles of the lower limb. Additionally, some patients with ACL injuries have been described as “copers” and are able to alter their lower limb kinematics to compensate for the lack of ACL function (174, 175). These compensations may not be evident immediately following ACL transection and without the proprioception and neuromuscular feedback loops which are present in patients.

A final challenge throughout this body of work was scaling methods and processes for specimens across a wide range of ages and sizes. Overall changes in the length of the ACL were ten-fold from birth through skeletal maturity, requiring the use of two MRI scanners in order to achieve adequate resolution for the smallest limbs while being able to physically contain the largest limbs. Specimens for mechanical testing experienced seven-fold increases in size from the youngest to oldest joints, requiring the development of protocols and methods which allowed for accurate preparation, analysis, and dissection of the full range of joints. Additionally, adjustment parameters were required for the load levels applied to this range of joints.

8.3. Clinical Implications

Many of the findings reported in this dissertation have potential applications in the diagnosis and treatment of ACL injuries in young populations. The angular orientation of the ACL has been reported to increase in human populations (1, 35) and through our study we have confirmed these changes in a pre-clinical model. The angular orientation of the ACL is readily altered by adjusting tunnel placement in the tibia and femur, making this parameter a straightforward target for tailoring reconstruction practices to individual age groups. Additionally, common variations of ACL reconstructions used in skeletally immature populations result in altered orientation angles for the graft tissues (30). The variation from healthy anatomy caused by this tissue orientation may be related to the poor outcomes often seen in physeal sparing techniques.

In addition to changes based on the orientation of the ACL, findings regarding age-specific tissue morphometry can be implemented in clinical studies and treatments for young populations. In Chapter 4 we demonstrated a shift in ACL shape from a greater CSA-to-length ratio in youth compared to adolescence, as the length of the ACL experienced more change with

age. A major decision made in ACL reconstruction is selection of graft size and length, and if reconstructions are performed in young patients without adapting for the age-specific geometry of the tissue, the resulting graft may be too elongated and thin for the patient's native anatomy. The timing of major changes in the morphometry of the ACL may be of interest to clinicians and tissue engineers working to develop ACL replacements, as we have shown that the majority of growth in the ACL occurs relatively early. Furthermore, when considering graft options for very young patients, it may be important to consider the age-specific proportions of the ACL, with greater CSA compared to length at young ages.

In addition to implications from our structural findings, functional outcomes from Chapter 5 may help tailor ACL reconstructions in young populations. Specifically, when considering graft placement in mature patients many clinical techniques suggest targeting the footprint of the AM bundle, as this bundle performs more significant functional roles in mature joints. However, our findings suggest that the AM and PL bundles both serve major roles in youth, suggesting that a shift in tunnel placement towards the midpoint of the two footprints may better replicate native function.

Finally, our findings regarding age-dependent changes in the kinematic response of the knee to applied loads following partial and complete ACL injuries may lead to improved sensitivity and specificity of clinical examinations for these injuries in young patients. Our findings in Chapter 6 suggest that while purely translational tests were only sensitive to partial ACL injury in the late adolescent group, rotational tests were sensitive to partial ACL injury across age groups. By improving our understanding of age-dependent responses to injuries we may be able to diagnose injuries more quickly and effectively, leading to earlier treatments and less risk of subsequent injuries.

While these findings have many exciting clinical implications, there are several intermediate steps between this research and changing surgical practices in the clinic. The structural findings reported here should be confirmed in human MRI studies, and suggest that consideration of tissue morphometry instead of reporting only length or CSA may help identify the timing of structural changes in the ACL. While many of the functional changes described in this work are not readily repeated in human *ex vivo* studies due to the paucity of cadaveric limbs from skeletally immature populations, many of the broad kinematic changes in response to applied tibial loads could be confirmed in an *in vivo* study. Additionally, computational modeling using subject-specific geometries and *in vivo* force data may be able to confirm our findings in human populations.

8.4. Basic Science and Engineering Implications

The methods and tools described in this body of work have been designed to use common approaches and techniques across a broad range of musculoskeletal joints. In addressing challenges related to applying imaging and mechanical testing systems to joints ranging in size by up to 10-fold differences, this dissertation includes methods for scaling applied loads based on bone size, repeatability of image processing techniques across multiple MRI scanners, and descriptions of tissue dissections that are applicable to small and large joints. The principles applied to scale these techniques could be further expanded when translating studies between small and large animal models, or animal models to cadaveric or *in vivo* human research.

In addition to validating the use of these techniques across joint sizes, the completion of this work involved developing a large portfolio of computational code. Within the structural studies, I have developed custom codes to analyze the morphometry of tissues and compare the proportions of tissue during growth. These tools could be used to compare the size and shape of

many tissues within the body either during healthy growth or following injury or healing responses. Within the field of biomechanical functional testing, we have developed a large collection of data processing and analysis code. Additionally, we have worked to confirm the independent function of many tissues in the knee across ages, and have established that the primary function of the ACL is consistent from youth through late adolescence in the porcine knee.

8.5. Future Directions

Moving forward from this body of work there are several avenues for additional study. Continuing in the porcine model, the interaction between age- and sex-dependent changes in ACL structure and function should be assessed. Analysis of human ACL injury patterns has shown that ACL injury incidence is similar in males and females during childhood with an increase in injury risk for females following the onset of adolescence (20). By repeating the studies described here in a male cohort it may be possible to isolate differences in native ACL structure or function between the sexes during growth, potentially improving our understanding of the mechanisms between this sex-dependent injury risk. Additionally, the age-dependent ACL morphometry and bundle-specific behavior described here could be used to develop longitudinal *in vivo* studies in the skeletally immature porcine model to study long-term outcomes from ACL reconstructions performed either with standard graft sizes and placement, or using clinical decisions which anticipate changes in ACL structure and function.

In addition to further studies in the porcine model, there are several opportunities for expanding this work through human studies. While some of the MRI studies described here have been applied to skeletally immature human cohorts, the analysis techniques described in Chapter 4 have not been applied to pediatric human scans. If these studies are repeated in humans and

reveal the same allometric growth patterns in the ACL, the case for using the porcine model as a surrogate for pediatric human knees would be strengthened. Additionally, MRI studies using state-of-the-art scanning technology such as high-field MRI and quantitative MRI with pediatric subjects may provide options for studying bundle-specific changes in the growing ACL and changes in the material properties of tissues *in vivo* (176). In addition to MRI-based studies, approaches involving non-invasive sensors may provide options for studying global changes in musculoskeletal soft tissues during growth (177). While the ACL is difficult to access non-invasively, many tendons and ligaments in the lower limb are located near the skin, and methods involving ultrasound and mechanical deflection could be used to study changes in tissue properties during growth. By combining these tools with common gait lab analysis techniques and the motivation provided through this dissertation, I think that there are many opportunities for expanding our understanding of age-related changes both in individual tissues and the musculoskeletal system in general.

REFERENCES

1. Kim HK, Laor T, Shire NJ, Bean JA, Dardzinski BJ. Anterior and Posterior Cruciate Ligaments at Different Patient Ages: MR Imaging Findings. Radiology. 2008;247(3):826-35. doi: doi:10.1148/radiol.2473071097. PubMed PMID: 18487537.

2. Petersen W, Zantop TJCO, Research® R. Anatomy of the anterior cruciate ligament with regard to its two bundles2007;454:35-47.

3. Cone SG, Warren PB, Fisher MB. Rise of the Pigs: Utilization of the Porcine Model to Study Musculoskeletal Biomechanics and Tissue Engineering During Skeletal Growth. Tissue Eng Part C Methods. 2017;23(11):763-80. doi: 10.1089/ten.TEC.2017.0227. PubMed PMID: 28726574; PMCID: PMC5689129.

4. Cone SG, Howe, D. H., Fisher, M. B. A Systematic Review of the Size and Shape of the Human Anterior Cruciate Ligament And the Impact of Sex and Skeletal Growth. JBJS Rev. 2019. In press.

5. Zantop T, Petersen W, Fu FHJOtio. Anatomy of the anterior cruciate ligament2005;15(1):20 -8.

6. Crawford C, Nyland J, Landes S, Jackson R, Chang HC, Nawab A, Caborn DN. Anatomic double bundle ACL reconstruction: a literature review. Knee Surg Sports Traumatol Arthrosc. 2007;15(8):946-64; discussion 5. doi: 10.1007/s00167-007-0343-7. PubMed PMID: 17534599.

7. Schreiber VM, van Eck CF, Fu FHJSm, review a. Anatomic double-bundle ACL reconstruction2010;18(1):27-32.

8. Kato Y, Ingham SJ, Maeyama A, Lertwanich P, Wang JH, Mifune Y, Kramer S, Smolinski P, Fu FH. Biomechanics of the human triple-bundle anterior cruciate ligament. Arthroscopy. 2012;28(2):247-54. doi: 10.1016/j.arthro.2011.07.019. PubMed PMID: 22019233.

9. Otsubo H, Shino K, Suzuki D, Kamiya T, Suzuki T, Watanabe K, Fujimiya M, Iwahashi T, Yamashita TJKS, Sports Traumatology, Arthroscopy. The arrangement and the attachment areas of three ACL bundles2012;20(1):127-34.

10. Livesay GA, Rudy TW, Woo SL, Runco TJ, Sakane M, Li G, Fu FH. Evaluation of the effect of joint constraints on the in situ force distribution in the anterior cruciate ligament. J Orthop Res. 1997;15(2):278-84. Epub 1997/03/01. doi: 10.1002/jor.1100150218. PubMed PMID: 9167632.

11. Fujie H, Mabuchi K, Woo SL, Livesay GA, Arai S, Tsukamoto Y. The use of robotics technology to study human joint kinematics: a new methodology. J Biomech Eng. 1993;115(3):211-7. PubMed PMID: 8231133.

12. Ishibashi Y, Rudy TW, Livesay GA, Stone JD, Fu FH, Woo SL. The effect of anterior cruciate ligament graft fixation site at the tibia on knee stability: evaluation using a

robotic testing system. Arthroscopy. 1997;13(2):177-82. Epub 1997/04/01. PubMed PMID: 9127075.

13. Kanamori A, Woo SL, Ma CB, Zeminski J, Rudy TW, Li G, Livesay GA. The forces in the anterior cruciate ligament and knee kinematics during a simulated pivot shift test: A human cadaveric study using robotic technology. Arthroscopy. 2000;16(6):633-9. Epub 2000/09/08. doi: 10.1053/jars.2000.7682. PubMed PMID: 10976125.

14. Li G, Rudy TW, Allen C, Sakane M, Woo SL. Effect of combined axial compressive and anterior tibial loads on in situ forces in the anterior cruciate ligament: a porcine study. J Orthop Res. 1998;16(1):122-7. Epub 1998/05/09. doi: 10.1002/jor.1100160121. PubMed PMID: 9565084.

15. Livesay GA, Fujie H, Kashiwaguchi S, Morrow DA, Fu FH, Woo SL. Determination of the in situ forces and force distribution within the human anterior cruciate ligament. Ann Biomed Eng. 1995;23(4):467-74. PubMed PMID: 7486353.

16. Takai S, Woo SL, Livesay GA, Adams DJ, Fu FH. Determination of the in situ loads on the human anterior cruciate ligament. J Orthop Res. 1993;11(5):686-95. doi: 10.1002/jor.1100110511. PubMed PMID: 8410469.

17. Woo SL, Fox RJ, Sakane M, Livesay GA, Rudy TW, Fu FHJTK. Biomechanics of the ACL: measurements of in situ force in the ACL and knee kinematics1998;5(4):267-88.

18. Bates NA, Nesbitt RJ, Shearn JT, Myer GD, Hewett TE. Sex-based differences in knee ligament biomechanics during robotically simulated athletic tasks. J Biomech. 2016;49(9):1429-36. doi: 10.1016/j.jbiomech.2016.03.001. PubMed PMID: 27083058.

19. Bell KM, Rahnemai-Azar AA, Irarrazaval S, Guenther D, Fu FH, Musahl V, Debski RE. In situ force in the anterior cruciate ligament, the lateral collateral ligament, and the anterolateral capsule complex during a simulated pivot shift test. J Orthop Res. 2018;36(3):847-53. doi: 10.1002/jor.23676. PubMed PMID: 28782837.

20. LaBella CR, Hennrikus W, Hewett TE, Council on Sports M, Fitness, Section on O. Anterior cruciate ligament injuries: diagnosis, treatment, and prevention. Pediatrics. 2014;133(5):e1437-50. doi: 10.1542/peds.2014-0623. PubMed PMID: 24777218.

21. Ardern CL, Ekas G, Grindem H, Moksnes H, Anderson A, Chotel F, Cohen M, Forssblad M, Ganley TJ, Feller JA, Karlsson J, Kocher MS, LaPrade RF, McNamee M, Mandelbaum B, Micheli L, Mohtadi N, Reider B, Roe J, Seil R, Siebold R, Silvers-Granelli HJ, Soligard T, Witvrouw E, Engebretsen L. 2018 International Olympic Committee consensus statement on prevention, diagnosis and management of paediatric anterior cruciate ligament (ACL) injuries. Knee Surg Sports Traumatol Arthrosc. 2018. doi: 10.1007/s00167-018-4865-y. PubMed PMID: 29455243.

22. Yang S, Werner BC, Gwathmey FW, Jr. Treatment trends in adolescent clavicle fractures. J Pediatr Orthop. 2015;35(3):229-33. Epub 2014/07/06. doi: 10.1097/BPO.0000000000000258. PubMed PMID: 24992356.

23. Queen RM. Infographic: ACL injury reconstruction and recovery. Bone Joint Res. 2017;6(11):621-2. doi: 10.1302/2046-3758.611.BJR-2017-0330. PubMed PMID: 29122748; PMCID: PMC5717074.

24. Millett PJ, Willis AA, Warren RF. Associated injuries in pediatric and adolescent anterior cruciate ligament tears: does a delay in treatment increase the risk of meniscal tear? Arthroscopy. 2002;18(9):955-9. PubMed PMID: 12426537.

25. Collins SL, Layde P, Guse CE, Schlotthauer AE, Van Valin SE. The Incidence and Etiology of Anterior Cruciate Ligament Injuries in Patients under the Age of 18 in the State of Wisconsin. Pediat Therapeut. 2014;4(196).

26. Dodwell ER, LaMont LE, Green DW, Pan TJ, Marx RG, Lyman S. 20 years of pediatric anterior cruciate ligament reconstruction in New York State. Am J Sports Med. 2014;42(3):675-80.

27. Freedman KB, Glasgow MT, Glasgow SG, Bernstein J. Anterior cruciate ligament injury and reconstruction among university students. Clin Orthop Relat Res. 1998(356):208-12. Epub 1999/01/26. PubMed PMID: 9917686.

28. Trentacosta NE, Vitale MA, Ahmad CS. The effects of timing of pediatric knee ligament surgery on short-term academic performance in school-aged athletes. Am J Sports Med. 2009;37(9):1684-91. Epub 2009/05/23. doi: 10.1177/0363546509332507. PubMed PMID: 19460815.

29. Dumont GD, Hogue GD, Padalecki JR, Okoro N, Wilson PL. Meniscal and chondral injuries associated with pediatric anterior cruciate ligament tears: relationship of treatment time and patient-specific factors. Am J Sports Med. 2012;40(9):2128-33. Epub 2012/06/26. doi: 10.1177/0363546512449994. PubMed PMID: 22729621.

30. McConkey MO, Bonasia DE, Amendola A. Pediatric anterior cruciate ligament reconstruction. Curr Rev Musculoskelet Med. 2011;4(2):37-44. Epub 2011/05/20. doi: 10.1007/s12178-011-9076-9. PubMed PMID: 21594689; PMCID: PMC3097323.

31. McCarthy MM, Tucker S, Nguyen JT, Green DW, Imhauser CW, Cordasco FA. Contact stress and kinematic analysis of all-epiphyseal and over-the-top pediatric reconstruction techniques for the anterior cruciate ligament. Am J Sports Med. 2013;41(6):1330-9. doi: 10.1177/0363546513483269. PubMed PMID: 23613444; PMCID: PMC4041132.

32. Diament MJ. The diagnosis of sinusitis in infants and children: x-ray, computed tomography, and magnetic resonance imaging. Diagnostic imaging of pediatric sinusitis. J Allergy Clin Immunol. 1992;90(3 Pt 2):442-4. Epub 1992/09/01. PubMed PMID: 1527334.

33. Kraff O, Theysohn JM, Maderwald S, Saylor C, Ladd SC, Ladd ME, Barkhausen J. MRI of the knee at 7.0 Tesla. Rofo. 2007;179(12):1231-5. Epub 2007/11/16. doi: 10.1055/s -2007-963607. PubMed PMID: 18004692.

34. Cone SG, Simpson SG, Piedrahita JA, Fordham LA, Spang JT, Fisher MB. Orientation changes in the cruciate ligaments of the knee during skeletal growth: A porcine model. J

Orthop Res. 2017;35(12):2725-32. doi: 10.1002/jor.23594. PubMed PMID: 28471537; PMCID: PMC5671372.

35. Reid JC, Yonke B, Tompkins M. The angle of inclination of the native ACL in the coronal and sagittal planes. Knee Surg Sports Traumatol Arthrosc. 2017;25(4):1101-5. doi: 10.1007/s00167-017-4419-8. PubMed PMID: 28246878.

36. Davidson SP, McLean SG. Effects of maturation on combined female muscle strength and ACL structural factors. J Sci Med Sport. 2016;19(7):553-8. doi: 10.1016/j.jsams.2015.07.016. PubMed PMID: 26387610.

37. Tuca M, Hayter C, Potter H, Marx R, Green DW. Anterior cruciate ligament and intercondylar notch growth plateaus prior to cessation of longitudinal growth: an MRI observational study. Knee Surg Sports Traumatol Arthrosc. 2016;24(3):780-7. doi: 10.1007/s00167-016-4021-5. PubMed PMID: 26860103.

38. Ford KR, Myer GD, Hewett TE. Longitudinal effects of maturation on lower extremity joint stiffness in adolescent athletes. Am J Sports Med. 2010;38(9):1829-37. Epub 2010/06/05. doi: 10.1177/0363546510367425. PubMed PMID: 20522830; PMCID: PMC3968426.

39. Schmidt EC, Chin M, Aoyama JT, Ganley TJ, Shea KG, Hast MW. Mechanical and Microstructural Properties of Pediatric Anterior Cruciate Ligaments and Autograft Tendons Used for Reconstruction. Orthop J Sports Med. 2019;7(1):2325967118821667. Epub 2019/02/06. doi: 10.1177/2325967118821667. PubMed PMID: 30719479; PMCID: PMC6348523.

40. Biercevicz AM, Murray MM, Walsh EG, Miranda DL, Machan JT, Fleming BC. T2 * MR relaxometry and ligament volume are associated with the structural properties of the healing ACL. J Orthop Res. 2014;32(4):492-9. doi: 10.1002/jor.22563. PubMed PMID: 24338640; PMCID: PMC3946219.

41. Proffen BL, McElfresh M, Fleming BC, Murray MM. A comparative anatomical study of the human knee and six animal species. The Knee. 2012;19(4):493-9.

42. Tantisricharoenkul G, Linde-Rosen M, Araujo P, Zhou J, Smolinski P, Fu FH. Anterior cruciate ligament: an anatomical exploration in humans and in a selection of animal species. Knee Surg Sports Traumatol Arthrosc. 2014;22(5):961-71. doi: 10.1007/s00167-013-2463-6. PubMed PMID: 23471530.

43. Zaino NL, Hedgeland MJ, Ciani MJ, Clark AM, Kuxhaus L, Michalek AJ. White-Tailed Deer as an Ex Vivo Knee Model: Joint Morphometry and ACL Rupture Strength. Ann Biomed Eng. 2017;45(4):1093-100. doi: 10.1007/s10439-016-1746-8. PubMed PMID: 27718092.

44. Xerogeanes JW, Fox RJ, Takeda Y, Kim H-S, Ishibashi Y, Carlin GJ, Woo SL. A functional comparison of animal anterior cruciate ligament models to the human anterior cruciate ligament. Ann Biomed Eng. 1998;26(3):345-52.

45. Proffen BL, Perrone GS, Fleming BC, Sieker JT, Kramer J, Hawes ML, Murray MM. Effect of low-temperature ethylene oxide and electron beam sterilization on the in vitro and in vivo function of reconstituted extracellular matrix-derived scaffolds. J Biomater Appl. 2015;30(4):435-49. doi: 10.1177/0885328215590967. PubMed PMID: 26088294; PMCID: PMC4670802.

46. Teuschl A, Heimel P, Nurnberger S, van Griensven M, Redl H, Nau T. A Novel Silk Fiber -Based Scaffold for Regeneration of the Anterior Cruciate Ligament: Histological Results From a Study in Sheep. Am J Sports Med. 2016;44(6):1547-57. doi: 10.1177/0363546516631954. PubMed PMID: 26957219.

47. Mahalingam VD, Behbahani-Nejad N, Horine SV, Olsen TJ, Smietana MJ, Wojtys EM, Wellik DM, Arruda EM, Larkin LM. Allogeneic versus autologous derived cell sources for use in engineered bone-ligament-bone grafts in sheep anterior cruciate ligament repair. Tissue Eng Part A. 2015;21(5-6):1047-54. doi: 10.1089/ten.TEA.2014.0422. PubMed PMID: 25397361; PMCID: PMC4356260.

48. Fisher MB, Liang R, Jung HJ, Kim KE, Zamarra G, Almarza AJ, McMahon PJ, Woo SL. Potential of healing a transected anterior cruciate ligament with genetically modified extracellular matrix bioscaffolds in a goat model. Knee Surg Sports Traumatol Arthrosc. 2012;20(7):1357-65. doi: 10.1007/s00167-011-1800-x. PubMed PMID: 22143425.

49. Boguszewski DV, Shearn JT, Wagner CT, Butler DL. Investigating the effects of anterior tibial translation on anterior knee force in the porcine model: is the porcine knee ACL dependent? J Orthop Res. 2011;29(5):641-6. doi: 10.1002/jor.21298. PubMed PMID: 21437942.

50. Atarod M, Frank CB, Shrive NG. Increased meniscal loading after anterior cruciate ligament transection in vivo: a longitudinal study in sheep. Knee. 2015;22(1):11-7. doi: 10.1016/j.knee.2014.10.011. PubMed PMID: 25487300.

51. Skelley NW, Castile RM, Cannon PC, Weber CI, Brophy RH, Lake SP. Regional Variation in the Mechanical and Microstructural Properties of the Human Anterior Cruciate Ligament. Am J Sports Med. 2016;44(11):2892-9. doi: 10.1177/0363546516654480. PubMed PMID: 27456027.

52. Takroni T, Laouar L, Adesida A, Elliott JA, Jomha NM. Anatomical study: comparing the human, sheep and pig knee meniscus. J Exp Orthop. 2016;3(1):35. doi: 10.1186/s40634 -016-0071-3. PubMed PMID: 27928740; PMCID: PMC5143332.

53. Gupte CM, Bull AM, Murray R, Amis AA. Comparative anatomy of the meniscofemoral ligament in humans and some domestic mammals. Anat Histol Embryol. 2007;36(1):47 -52. doi: 10.1111/j.1439-0264.2006.00718.x. PubMed PMID: 17266668.

54. Sweigart MA, Zhu CF, Burt DM, DeHoll PD, Agrawal CM, Clanton TO, Athanasiou KA. Intraspecies and interspecies comparison of the compressive properties of the medial meniscus. Ann Biomed Eng. 2004;32(11):1569-79. PubMed PMID: 15636116.

55. Joshi MD, Suh JK, Marui T, Woo SL. Interspecies variation of compressive biomechanical properties of the meniscus. J Biomed Mater Res. 1995;29(7):823-8. doi: 10.1002/jbm.820290706. PubMed PMID: 7593020.

56. Arnoczky SP, Cook JL, Carter T, Turner AS. Translational models for studying meniscal repair and replacement: what they can and cannot tell us. Tissue Eng Part B Rev. 2010;16(1):31-9. doi: 10.1089/ten.TEB.2009.0428. PubMed PMID: 19698055.

57. Baxter-Jones AD, Eisenmann JC, Sherar LB. Controlling for maturation in pediatric exercise science. Pediatr Exerc Sci. 2005;17(1):18-30.

58. Reiland S. Growth and skeletal development of the pig. Acta Radiol Suppl. 1978;358:15-22. PubMed PMID: 233594.

59. Greulich WW, Pyle SI. Radiographic atlas of skeletal development of the hand and wrist. The American Journal of the Medical Sciences. 1959;238(3):393.

60. Goetz JE, Fredericks D, Petersen E, Rudert MJ, Baer T, Swanson E, Roberts N, Martin J, Tochigi Y. A clinically realistic large animal model of intra-articular fracture that progresses to post-traumatic osteoarthritis. Osteoarthritis Cartilage. 2015;23(10):1797-805. doi: 10.1016/j.joca.2015.05.022. PubMed PMID: 26033166.

61. Radfar L, Sirois DA. Structural and functional injury in minipig salivary glands following fractionated exposure to 70 Gy of ionizing radiation: an animal model for human radiation-induced salivary gland injury. Oral Surg Oral Med Oral Pathol Oral Radiol Endod. 2003;96(3):267-74. doi: 10.1016/S107921040300369X. PubMed PMID: 12973282.

62. Jiang CC, Chiang H, Liao CJ, Lin YJ, Kuo TF, Shieh CS, Huang YY, Tuan RS. Repair of porcine articular cartilage defect with a biphasic osteochondral composite. J Orthop Res. 2007;25(10):1277-90. doi: 10.1002/jor.20442. PubMed PMID: 17576624.

63. Reisig G, Kreinest M, Richter W, Wagner-Ecker M, Dinter D, Attenberger U, Schneider-Wald B, Fickert S, Schwarz ML. Osteoarthritis in the Knee Joints of Gottingen Minipigs after Resection of the Anterior Cruciate Ligament? Missing Correlation of MRI, Gene and Protein Expression with Histological Scoring. PLoS One. 2016;11(11):e0165897. doi: 10.1371/journal.pone.0165897. PubMed PMID: 27820852; PMCID: PMC5098790.

64. Xia W, Liu W, Cui L, Liu Y, Zhong W, Liu D, Wu J, Chua K, Cao Y. Tissue engineering of cartilage with the use of chitosan-gelatin complex scaffolds. J Biomed Mater Res B Appl Biomater. 2004;71(2):373-80. doi: 10.1002/jbm.b.30087. PubMed PMID: 15386401.

65. Linkenhoker JR, Burkholder TH, Linton CG, Walden A, Abusakran-Monday KA, Rosero AP, Foltz CJ. Effective and safe anesthesia for Yorkshire and Yucatan swine with and without cardiovascular injury and intervention. J Am Assoc Lab Anim Sci. 2010;49(3):344-51. PubMed PMID: 20587167; PMCID: PMC2877308.

66. Eggleston TA, Roach WP, Mitchell MA, Smith K, Oler D, Johnson TE. Comparison of two porcine (Sus scrofa domestica) skin models for in vivo near-infrared laser exposure. Comp Med. 2000;50(4):391-7. PubMed PMID: 11020157.

67. Germscheid NM, Thornton GM, Hart DA, Hildebrand KA. A biomechanical assessment to evaluate breed differences in normal porcine medial collateral ligaments. J Biomech. 2011;44(4):725-31. doi: 10.1016/j.jbiomech.2010.10.036. PubMed PMID: 21092965.

68. Gotterbarm T, Breusch SJ, Schneider U, Jung M. The minipig model for experimental chondral and osteochondral defect repair in tissue engineering: retrospective analysis of 180 defects. Lab Anim. 2008;42(1):71-82. Epub 2008/03/20. doi: 10.1258/la.2007.06029e. PubMed PMID: 18348768.

69. McKnight LL, Myrie SB, Mackay DS, Brunton JA, Bertolo RF. Glucose tolerance is affected by visceral adiposity and sex, but not birth weight, in Yucatan miniature pigs. Appl Physiol Nutr Metab. 2012;37(1):106-14. doi: 10.1139/h11-142. PubMed PMID: 22236284.

70. Kiapour AM, Fleming BC, Proffen BL, Murray MM. Sex Influences the Biomechanical Outcomes of Anterior Cruciate Ligament Reconstruction in a Preclinical Large Animal Model. Am J Sports Med. 2015;43(7):1623-31. doi: 10.1177/0363546515582024. PubMed PMID: 25939612; PMCID: PMC4490080.

71. Lima FM, Debieux P, Astur DC, Luzo MVM, Cohen M, Cardoso FN, Aihara AY, Grimberg A, Fernandes ARC. The development of the anterior cruciate ligament in the paediatric population. Knee Surg Sports Traumatol Arthrosc. 2019. Epub 2019/01/24. doi: 10.1007/s00167-019-05349-x. PubMed PMID: 30671598.

72. Werner BC, Yang S, Looney AM, Gwathmey Jr FW. Trends in pediatric and adolescent anterior cruciate ligament injury and reconstruction. Journal of Pediatric Orthopaedics. 2016;36(5):447-52.

73. Gausden EB, Calcei JG, Fabricant PD, Green DW. Surgical options for anterior cruciate ligament reconstruction in the young child. Current opinion in pediatrics. 2015;27(1):82-91.

74. Pennock A, Murphy MM, Wu M. Anterior cruciate ligament reconstruction in skeletally immature patients. Current Reviews in Musculoskeletal Medicine. 2016:1-9.

75. Lohmander LS, Englund PM, Dahl LL, Roos EM. The long-term consequence of anterior cruciate ligament and meniscus injuries osteoarthritis. The American journal of sports medicine. 2007;35(10):1756-69.

76. Meller R, Brandes G, Drögemüller C, Fritz F, Schiborra F, Fehr M, Hankemeier S, Krettek C, Hurschler C. Graft remodeling during growth following anterior cruciate ligament reconstruction in skeletally immature sheep. Archives of orthopaedic and trauma surgery. 2009;129(8):1037-46.

77. Meller R, Schiborra F, Brandes G, Knobloch K, Tschernig T, Hankemeier S, Haasper C, Schmiedl A, Jagodzinski M, Krettek C, Willbold E. Postnatal maturation of tendon, cruciate ligament, meniscus and articular cartilage: a histological study in sheep. Ann Anat. 2009;191(6):575-85. doi: 10.1016/j.aanat.2009.08.005. PubMed PMID: 19800207.

78. Meller R, Haasper C, Westhoff J, Brand J, Knobloch K, Hankemeier S, Hesse E, Krettek C, Jagodzinski M. An animal model to study ACL reconstruction during growth. Technol Health Care. 2009;17(5-6):403-10. doi: 10.3233/THC-2009-0561. PubMed PMID: 20051620.

79. FederationofAnimalScienceSocieties. Guide for the Care and Use of Agricultural Animals in Teaching and Research, Third Edition. Champaign, IL2010.

80. Anderson AF, Dome DC, Gautam S, Awh MH, Rennirt GW. Correlation of anthropometric measurements, strength, anterior cruciate ligament size, and intercondylar notch characteristics to sex differences in anterior cruciate ligament tear rates. Am J Sports Med. 2001;29(1):58-66. PubMed PMID: 11206258.

81. Kiapour AM, Shalvoy MR, Murray MM, Fleming BC. Validation of porcine knee as a sex -specific model to study human anterior cruciate ligament disorders. Clin Orthop Relat Res. 2015;473(2):639-50. doi: 10.1007/s11999-014-3974-2. PubMed PMID: 25269532; PMCID: PMC4294889.

82. Lipps DB, Oh YK, Ashton-Miller JA, Wojtys EM. Morphologic characteristics help explain the gender difference in peak anterior cruciate ligament strain during a simulated pivot landing. Am J Sports Med. 2012;40(1):32-40. doi: 10.1177/0363546511422325. PubMed PMID: 21917612; PMCID: PMC4800982.

83. Dienst M, Schneider G, Altmeyer K, Voelkering K, Georg T, Kramann B, Kohn D. Correlation of intercondylar notch cross sections to the ACL size: a high resolution MR tomographic in vivo analysis. Arch Orthop Trauma Surg. 2007;127(4):253-60. doi: 10.1007/s00402-006-0177-7. PubMed PMID: 16807752.

84. Majewski M, Susanne H, Klaus S. Epidemiology of athletic knee injuries: A 10-year study. Knee. 2006;13(3):184-8. doi: 10.1016/j.knee.2006.01.005. PubMed PMID: 16603363.

85. Parkkari J, Pasanen K, Mattila VM, Kannus P, Rimpela A. The risk for a cruciate ligament injury of the knee in adolescents and young adults: a population-based cohort study of 46 500 people with a 9 year follow-up. Br J Sports Med. 2008;42(6):422-6. doi: 10.1136/bjsm.2008.046185. PubMed PMID: 18390920.

86. Swenson DM, Collins CL, Best TM, Flanigan DC, Fields SK, Comstock RD. Epidemiology of knee injuries among U.S. high school athletes, 2005/2006-2010/2011. Med Sci Sports Exerc. 2013;45(3):462-9. doi: 10.1249/MSS.0b013e318277acca. PubMed PMID: 23059869; PMCID: PMC3768257.

87. Wegmann H, Tschauner S, Singer G, Marterer R, Eberl R, Sorantin E. The pediatric knee: diagnosis and management of ligament injuries. Semin Musculoskelet Radiol. 2014;18(5):489-97. doi: 10.1055/s-0034-1389266. PubMed PMID: 25350827.

88. Samora W, Beran MC, Parikh SN. Intercondylar Roof Inclination Angle: Is It a Risk Factor for ACL Tears or Tibial Spine Fractures? J Pediatr Orthop. 2016;36(6):e71-4. doi: 10.1097/BPO.0000000000000631. PubMed PMID: 26327400.

89. Fujimaki Y, Thorhauer E, Sasaki Y, Smolinski P, Tashman S, Fu FH. Quantitative In Situ Analysis of the Anterior Cruciate Ligament: Length, Midsubstance Cross-sectional Area, and Insertion Site Areas. Am J Sports Med. 2016;44(1):118-25. doi: 10.1177/0363546515611641. PubMed PMID: 26564792.

90. Beveridge JE, Walsh EG, Murray MM, Fleming BC. Sensitivity of ACL volume and T2 * relaxation time to magnetic resonance imaging scan conditions. J Biomech. 2017. doi: 10.1016/j.jbiomech.2017.03.010. PubMed PMID: 28359570.

91. Biercevicz AM, Miranda DL, Machan JT, Murray MM, Fleming BC. In Situ, noninvasive, T2*-weighted MRI-derived parameters predict ex vivo structural properties of an anterior cruciate ligament reconstruction or bioenhanced primary repair in a porcine model. Am J Sports Med. 2013;41(3):560-6. doi: 10.1177/0363546512472978. PubMed PMID: 23348076; PMCID: PMC3593999.

92. Cone S, Piercy, HE., Lambeth, EP., Ru, H, Piedrahita, JA., Spang, JT., Fordham, LA., Fisher, MB. Tissue-Specific Changes in the Size and Shape of the Ligaments and Tendons of the Porcine Knee During Post-Natal Growth. Ann Biomed Eng. Under Review.

93. Done SL. Fetal and neonatal bone health: update on bone growth and manifestations in health and disease. Pediatr Radiol. 2012;42 Suppl 1:S158-76. doi: 10.1007/s00247-011-2251-8. PubMed PMID: 22395728.

94. Ferretti M, Levicoff EA, Macpherson TA, Moreland MS, Cohen M, Fu FH. The fetal anterior cruciate ligament: an anatomic and histologic study. Arthroscopy. 2007;23(3):278-83. Epub 2007/03/14. doi: 10.1016/j.arthro.2006.11.006. PubMed PMID: 17349471.

95. Felsenthal N, Zelzer E. Mechanical regulation of musculoskeletal system development. Development. 2017;144(23):4271-83. doi: 10.1242/dev.151266. PubMed PMID: 29183940.

96. Nguyen PK, Pan XS, Li J, Kuo CK. Roadmap of molecular, compositional, and functional markers during embryonic tendon development. Connect Tissue Res. 2018;59(5):495-508. doi: 10.1080/03008207.2018.1511710. PubMed PMID: 30231651.

97. Liu W, Watson SS, Lan Y, Keene DR, Ovitt CE, Liu H, Schweitzer R, Jiang R. The atypical homeodomain transcription factor Mohawk controls tendon morphogenesis. Mol Cell Biol. 2010;30(20):4797-807. doi: 10.1128/MCB.00207-10. PubMed PMID: 20696843; PMCID: PMC2950547.

98. Mienaltowski MJ, Birk DE. Mouse models in tendon and ligament research. Adv Exp Med Biol. 2014;802:201-30. Epub 2014/01/21. doi: 10.1007/978-94-007-7893-1_13. PubMed PMID: 24443029.

99. Huebner KD, O'Brien EJ, Heard BJ, Chung M, Achari Y, Shrive NG, Frank CB. Post-natal molecular adaptations in anteromedial and posterolateral bundles of the ovine anterior cruciate ligament: one structure with two parts or two distinct ligaments? Connect Tissue Res. 2012;53(4):277-84. doi: 10.3109/03008207.2011.637652. PubMed PMID: 22148917.

100.Marturano JE, Arena JD, Schiller ZA, Georgakoudi I, Kuo CK. Characterization of mechanical and biochemical properties of developing embryonic tendon. Proc Natl Acad Sci U S A. 2013;110(16):6370-5. doi: 10.1073/pnas.1300135110. PubMed PMID: 23576745; PMCID: PMC3631620.

101. Lee AH, Elliott DM. Comparative multi-scale hierarchical structure of the tail, plantaris, and Achilles tendons in the rat. J Anat. 2018. doi: 10.1111/joa.12913. PubMed PMID: 30484871.

102. Thompson DWJOg, form. On growth and form1942.

103. Huxley JS. Relative Growth and Form Transformation. Proc R Soc Ser B-Bio. 1950;137(889):465-9. doi: DOI 10.1098/rspb.1950.0055. PubMed PMID: WOS:A1950UJ62300006.

104. Brody S. Bioenergetics and growth: Reinhold Publishing Corporation: New York; 1945.

105. McMahon TA. Allometry and biomechanics: limb bones in adult ungulates. The American Naturalist. 1975;109(969):547-63.

106. Alexander R, Jayes A, Maloiy G, Wathuta E. Allometry of the limb bones of mammals from shrews (Sorex) to elephant (Loxodonta). Journal of Zoology. 1979;189(3):305-14.

107. Muller P, Dahners LE. A study of ligamentous growth. Clin Orthop Relat R. 1988;229:274-7.

108. Liu MF, He P, Aherne FX, Berg RT. Postnatal limb bone growth in relation to live weight in pigs from birth to 84 days of age. J Anim Sci. 1999;77(7):1693-701. PubMed PMID: 10438014.

109. Xerogeanes JW, Fox RJ, Takeda Y, Kim HS, Ishibashi Y, Carlin GJ, Woo SL. A functional comparison of animal anterior cruciate ligament models to the human anterior cruciate ligament. Ann Biomed Eng. 1998;26(3):345-52. PubMed PMID: 9570217.

110. Proffen BL, McElfresh M, Fleming BC, Murray MM. A comparative anatomical study of the human knee and six animal species. Knee. 2012;19(4):493-9. doi: 10.1016/j.knee.2011.07.005. PubMed PMID: 21852139; PMCID: PMC3236814.

111. Woo SL, Ohland KJ, Weiss JA. Aging and sex-related changes in the biomechanical properties of the rabbit medial collateral ligament. Mech Ageing Dev. 1990;56(2):129-42. Epub 1990/11/01. PubMed PMID: 2290352.

112. Woo SL, Orlando CA, Gomez MA, Frank CB, Akeson WH. Tensile properties of the medial collateral ligament as a function of age. J Orthop Res. 1986;4(2):133-41. Epub 1986/01/01. doi: 10.1002/jor.1100040201. PubMed PMID: 3712122.

113. Zember JS, Rosenberg ZS, Kwong S, Kothary SP, Bedoya MA. Normal Skeletal Maturation and Imaging Pitfalls in the Pediatric Shoulder. Radiographics. 2015;35(4):1108-22. Epub 2015/07/15. doi: 10.1148/rg.2015140254. PubMed PMID: 26172355.

114. Tschauner S, Sorantin E, Singer G, Eberl R, Weinberg AM, Schmidt P, Kraus T. The origin points of the knee collateral ligaments: an MRI study on paediatric patients during growth. Knee Surg Sports Traumatol Arthrosc. 2016;24(1):18-25. Epub 2014/04/20. doi: 10.1007/s00167-014-2991-8. PubMed PMID: 24744174.

115. Koob TJ, Pringle D, Gedbaw E, Meredith J, Berrios R, Kim HK. Biomechanical properties of bone and cartilage in growing femoral head following ischemic osteonecrosis. J Orthop Res. 2007;25(6):750-7. Epub 2007/02/24. doi: 10.1002/jor.20350. PubMed PMID: 17318897.

116. Haut RC, Wei F. Biomechanical Studies on Patterns of Cranial Bone Fracture Using the Immature Porcine Model. J Biomech Eng. 2017;139(2). Epub 2016/08/19. doi: 10.1115/1.4034430. PubMed PMID: 27537363.

117. Sun Z, Kennedy KS, Tee BC, Damron JB, Allen MJ. Establishing a critical-size mandibular defect model in growing pigs: characterization of spontaneous healing. J Oral Maxillofac Surg. 2014;72(9):1852-68. Epub 2014/05/13. doi: 10.1016/j.joms.2014.02.024. PubMed PMID: 24815793.

118. Goldblatt JP, Fitzsimmons SE, Balk E, Richmond JC. Reconstruction of the anterior cruciate ligament: meta-analysis of patellar tendon versus hamstring tendon autograft. Arthroscopy. 2005;21(7):791-803. doi: 10.1016/j.arthro.2005.04.107. PubMed PMID: 16012491.

119. Shea KG, Pfeiffer R, Wang JH, Curtin M, Apel PJ. Anterior cruciate ligament injury in pediatric and adolescent soccer players: an analysis of insurance data. J Pediatr Orthop. 2004;24(6):623-8. PubMed PMID: 15502559.

120. Cone S.G.: Lambeth, E.P.; Ru, H.; Fordham, L.A.; Piedrahita, J.P.; Spang, J.T.; Fisher, M.B. Biomechanical Function and Size of the Anteromedial and Posterolateral Bundles of the Anterior Cruciate Ligament Change Differently with Skeletal Growth in the Pig Model. Clin Orthop Relat Res. 2019. In Press.

121. Gabriel MT, Wong EK, Woo SL, Yagi M, Debski RE. Distribution of in situ forces in the anterior cruciate ligament in response to rotatory loads. J Orthop Res. 2004;22(1):85-9. doi: 10.1016/S0736-0266(03)00133-5. PubMed PMID: 14656664.

122. Skelley NW, Lake, S. P., Brophy, R. H. . Microstructural Properties of the Anterior Cruciate Ligament. Annals of Joint. 2017;2(19). doi: 10.21037/aoj.2017.05.08.

123. Chhabra A, Starman JS, Ferretti M, Vidal AF, Zantop T, Fu FH. Anatomic, radiographic, biomechanical, and kinematic evaluation of the anterior cruciate ligament and its two functional bundles. J Bone Joint Surg Am. 2006;88 Suppl 4:2-10. doi: 10.2106/JBJS.F.00616. PubMed PMID: 17142430.

124. Takeda Y, Xerogeanes JW, Livesay GA, Fu FH, Woo SL. Biomechanical function of the human anterior cruciate ligament. Arthroscopy. 1994;10(2):140-7. PubMed PMID: 8003139.

125. Xerogeanes JW, Takeda Y, Livesay GA, Ishibashi Y, Kim HS, Fu FH, Woo SL. Effect of knee flexion on the in situ force distribution in the human anterior cruciate ligament. Knee Surg Sports Traumatol Arthrosc. 1995;3(1):9-13. PubMed PMID: 7773824.

126. Hollis JM, Takai S, Adams DJ, Horibe S, Woo SL. The effects of knee motion and external loading on the length of the anterior cruciate ligament (ACL): a kinematic study. J Biomech Eng. 1991;113(2):208-14. PubMed PMID: 1875695.

127. Sakane M, Fox RJ, Woo SL, Livesay GA, Li G, Fu FH. In situ forces in the anterior cruciate ligament and its bundles in response to anterior tibial loads. J Orthop Res. 1997;15(2):285-93. Epub 1997/03/01. doi: 10.1002/jor.1100150219. PubMed PMID: 9167633.

128. Hewett TE, Myer GD. The mechanistic connection between the trunk, hip, knee, and anterior cruciate ligament injury. Exerc Sport Sci Rev. 2011;39(4):161-6. doi: 10.1097/JES.0b013e3182297439. PubMed PMID: 21799427; PMCID: PMC4168968.

129. Herzog MM, Marshall SW, Lund JL, Pate V, Mack CD, Spang JT. Incidence of Anterior Cruciate Ligament Reconstruction Among Adolescent Females in the United States, 2002 Through 2014. JAMA Pediatr. 2017;171(8):808-10. doi: 10.1001/jamapediatrics.2017.0740. PubMed PMID: 28604937.

130. Shaw L, Finch CF. Trends in Pediatric and Adolescent Anterior Cruciate Ligament Injuries in Victoria, Australia 2005-2015. Int J Environ Res Public Health. 2017;14(6). doi: 10.3390/ijerph14060599. PubMed PMID: 28587262; PMCID: PMC5486285.

131. Fabricant PD, Jones KJ, Delos D, Cordasco FA, Marx RG, Pearle AD, Warren RF, Green DW. Reconstruction of the anterior cruciate ligament in the skeletally immature athlete: a review of current concepts: AAOS exhibit selection. J Bone Joint Surg Am. 2013;95(5):e28. doi: 10.2106/JBJS.L.00772. PubMed PMID: 23467876.

132. Ardern CL, Ekas GR, Grindem H, Moksnes H, Anderson AF, Chotel F, Cohen M, Forssblad M, Ganley TJ, Feller JA, Karlsson J, Kocher MS, LaPrade RF, McNamee M, Mandelbaum B, Micheli L, Mohtadi N, Reider B, Roe J, Seil R, Siebold R, Silvers-Granelli HJ, Soligard T, Witvrouw E, Engebretsen L. 2018 International Olympic Committee consensus statement on prevention, diagnosis and management of paediatric anterior cruciate ligament (ACL) injuries. Br J Sports Med. 2018;52(7):422-38. doi: 10.1136/bjsports-2018-099060. PubMed PMID: 29478021; PMCID: PMC5867447.

133. Cone SG, Simpson SG, Piedrahita JA, Fordham LA, Spang JT, Fisher MB. Orientation Changes in the Cruciate Ligamnets of the Knee During Skeletal Growth: A Porcine Model. J Orthop Res. 2017;35(12):2725-32.

134. Murray MM, Magarian EM, Harrison SL, Mastrangelo AN, Zurakowski D, Fleming BC. The effect of skeletal maturity on functional healing of the anterior cruciate ligament. J Bone Joint Surg Am. 2010;92(11):2039-49. doi: 10.2106/JBJS.I.01368. PubMed PMID: 20810854; PMCID: PMC2924734.

135. Fisher MB, Jung HJ, McMahon PJ, Woo SL. Evaluation of bone tunnel placement for suture augmentation of an injured anterior cruciate ligament: effects on joint stability in a goat model. J Orthop Res. 2010;28(10):1373-9. doi: 10.1002/jor.21141. PubMed PMID: 20309958.

136. Howard RA, Rosvold JM, Darcy SP, Corr DT, Shrive NG, Tapper JE, Ronsky JL, Beveridge JE, Marchuk LL, Frank CB. Reproduction of in vivo motion using a parallel robot. J Biomech Eng. 2007;129(5):743-9. doi: 10.1115/1.2768983. PubMed PMID: 17887900.

137. Noble LD, Jr., Colbrunn RW, Lee DG, van den Bogert AJ, Davis BL. Design and validation of a general purpose robotic testing system for musculoskeletal applications. J Biomech Eng. 2010;132(2):025001. doi: 10.1115/1.4000851. PubMed PMID: 20370251.

138. Kato Y, Ingham SJ, Linde-Rosen M, Smolinski P, Horaguchi T, Fu FH. Biomechanics of the porcine triple bundle anterior cruciate ligament. Knee Surg Sports Traumatol Arthrosc. 2010;18(1):20-5. doi: 10.1007/s00167-009-0893-y. PubMed PMID: 19697011.

139. Stracciolini A, Stein CJ, Zurakowski D, Meehan WP, 3rd, Myer GD, Micheli LJ. Anterior cruciate ligament injuries in pediatric athletes presenting to sports medicine clinic: a comparison of males and females through growth and development. Sports Health. 2015;7(2):130-6. doi: 10.1177/1941738114554768. PubMed PMID: 25984258; PMCID: PMC4332643.

140. Sturnick DR, Vacek PM, DeSarno MJ, Gardner-Morse MG, Tourville TW, Slauterbeck JR, Johnson RJ, Shultz SJ, Beynnon BD. Combined anatomic factors predicting risk of anterior cruciate ligament injury for males and females. Am J Sports Med. 2015;43(4):839-47. doi: 10.1177/0363546514563277. PubMed PMID: 25583759.

141. Biercevicz AM, Proffen BL, Murray MM, Walsh EG, Fleming BC. T2* relaxometry and volume predict semi-quantitative histological scoring of an ACL bridge-enhanced primary repair in a porcine model. J Orthop Res. 2015;33(8):1180-7. doi: 10.1002/jor.22874. PubMed PMID: 25764143; PMCID: PMC4497917.

142. Darcy SP, Kilger RH, Woo SL, Debski RE. Estimation of ACL forces by reproducing knee kinematics between sets of knees: A novel non-invasive methodology. J Biomech. 2006;39(13):2371-7. Epub 2005/10/04. doi: 10.1016/j.jbiomech.2005.08.009. PubMed PMID: 16199046.

143. Kennedy A, Coughlin DG, Metzger MF, Tang R, Pearle AD, Lotz JC, Feeley BT. Biomechanical evaluation of pediatric anterior cruciate ligament reconstruction techniques. Am J Sports Med. 2011;39(5):964-71. Epub 2011/01/25. doi: 10.1177/0363546510390189. PubMed PMID: 21257848.

144. Kocher MS, Micheli LJ, Zurakowski D, Luke A. Partial tears of the anterior cruciate ligament in children and adolescents. Am J Sports Med. 2002;30(5):697-703. doi: 10.1177/03635465020300051201. PubMed PMID: 12239005.

145. Frank JS, Gambacorta PL. Anterior cruciate ligament injuries in the skeletally immature athlete: diagnosis and management. J Am Acad Orthop Surg. 2013;21(2):78-87. doi: 10.5435/JAAOS-21-02-78. PubMed PMID: 23378371.

146. Webster KE, Feller JA, Leigh WB, Richmond AK. Younger patients are at increased risk for graft rupture and contralateral injury after anterior cruciate ligament reconstruction. Am J Sports Med. 2014;42(3):641-7. doi: 10.1177/0363546513517540. PubMed PMID: 24451111.

147. Webster KE, Feller JA, Kimp AJ, Whitehead TS. Revision Anterior Cruciate Ligament Reconstruction Outcomes in Younger Patients: Medial Meniscal Pathology and High Rates of Return to Sport Are Associated With Third ACL Injuries. Am J Sports Med. 2018;46(5):1137-42. doi: 10.1177/0363546517751141. PubMed PMID: 29382207.

148. Rasmussen MT, Nitri M, Williams BT, Moulton SG, Cruz RS, Dornan GJ, Goldsmith MT, LaPrade RF. An In Vitro Robotic Assessment of the Anterolateral Ligament, Part 1: Secondary Role of the Anterolateral Ligament in the Setting of an Anterior Cruciate Ligament Injury. Am J Sports Med. 2016;44(3):585-92. doi: 10.1177/0363546515618387. PubMed PMID: 26684663.

149. Allen CR, Wong EK, Livesay GA, Sakane M, Fu FH, Woo SL. Importance of the medial meniscus in the anterior cruciate ligament-deficient knee. J Orthop Res. 2000;18(1):109-15. doi: 10.1002/jor.1100180116. PubMed PMID: 10716286.

150. Daniel DM, Stone ML, Dobson BE, Fithian DC, Rossman DJ, Kaufman KR. Fate of the ACL-injured patient. A prospective outcome study. Am J Sports Med. 1994;22(5):632-44. doi: 10.1177/036354659402200511. PubMed PMID: 7810787.

151. Haimes JL, Wroble RR, Grood ES, Noyes FR. Role of the medial structures in the intact and anterior cruciate ligament-deficient knee. Limits of motion in the human knee. Am J Sports Med. 1994;22(3):402-9. Epub 1994/05/01. doi: 10.1177/036354659402200317. PubMed PMID: 8037282.

152. Sakane M, Livesay GA, Fox RJ, Rudy TW, Runco TJ, Woo SL. Relative contribution of the ACL, MCL, and bony contact to the anterior stability of the knee. Knee Surg Sports Traumatol Arthrosc. 1999;7(2):93-7. doi: 10.1007/s001670050128. PubMed PMID: 10223530.

153. Fisher MB, Jung HJ, McMahon PJ, Woo SL. Suture augmentation following ACL injury to restore the function of the ACL, MCL, and medial meniscus in the goat stifle joint. J

Biomech. 2011;44(8):1530-5. Epub 2011/04/08. doi: 10.1016/j.jbiomech.2011.02.141. PubMed PMID: 21470612.

154. Rudy TW, Livesay GA, Woo SL, Fu FH. A combined robotic/universal force sensor approach to determine in situ forces of knee ligaments. J Biomech. 1996;29(10):1357-60. Epub 1996/10/01. PubMed PMID: 8884481.

155. Lintner DM, Kamaric E, Moseley JB, Noble PC. Partial tears of the anterior cruciate ligament. Are they clinically detectable? Am J Sports Med. 1995;23(1):111-8. Epub 1995/01/01. doi: 10.1177/036354659502300119. PubMed PMID: 7726340.

156. Li G, Papannagari R, DeFrate LE, Yoo JD, Park SE, Gill TJ. The effects of ACL deficiency on mediolateral translation and varus-valgus rotation. Acta Orthop. 2007;78(3):355-60. Epub 2007/07/06. doi: 10.1080/17453670710013924. PubMed PMID: 17611849.

157. Kocher MS, DiCanzio J, Zurakowski D, Micheli LJ. Diagnostic performance of clinical examination and selective magnetic resonance imaging in the evaluation of intraarticular knee disorders in children and adolescents. Am J Sports Med. 2001;29(3):292-6. Epub 2001/06/08. doi: 10.1177/03635465010290030601. PubMed PMID: 11394597.

158. Leblanc MC, Kowalczuk M, Andruszkiewicz N, Simunovic N, Farrokhyar F, Turnbull TL, Debski RE, Ayeni OR. Diagnostic accuracy of physical examination for anterior knee instability: a systematic review. Knee Surg Sports Traumatol Arthrosc. 2015;23(10):2805-13. Epub 2015/03/13. doi: 10.1007/s00167-015-3563-2. PubMed PMID: 25763847.

159. Cavinatto L, Gupta S, Morgan C, Bartolozzi AR. Value of Preoperative MRI and Examination under Anesthesia for Differentiating Complete from Partial Anterior Cruciate Ligament Tears. J Knee Surg. 2018. Epub 2018/07/11. doi: 10.1055/s-0038-1666827. PubMed PMID: 29991074.

160. Van Dyck P, Vanhoenacker FM, Gielen JL, Dossche L, Van Gestel J, Wouters K, Parizel PM. Three tesla magnetic resonance imaging of the anterior cruciate ligament of the knee: can we differentiate complete from partial tears? Skeletal Radiol. 2011;40(6):701-7. Epub 2010/10/12. doi: 10.1007/s00256-010-1044-8. PubMed PMID: 20931190.

161. Barton KI, Shekarforoush M, Heard BJ, Sevick JL, Martin CR, Frank CB, Hart DA, Shrive NG. Three-dimensional in vivo kinematics and finite helical axis variables of the ovine stifle joint following partial anterior cruciate ligament transection. J Biomech. 2019. Epub 2019/04/09. doi: 10.1016/j.jbiomech.2019.03.021. PubMed PMID: 30955851.

162. Adirim TA, Cheng TL. Overview of injuries in the young athlete. Sports Med. 2003;33(1):75-81. Epub 2002/12/13. doi: 10.2165/00007256-200333010-00006. PubMed PMID: 12477379.

163. Stracciolini A, Casciano R, Levey Friedman H, Meehan WP, 3rd, Micheli LJ. Pediatric sports injuries: an age comparison of children versus adolescents. Am J Sports Med. 2013;41(8):1922-9. Epub 2013/06/07. doi: 10.1177/0363546513490644. PubMed PMID: 23739684.

164. Dejour H, Bonnin M. Tibial translation after anterior cruciate ligament rupture. Two radiological tests compared. J Bone Joint Surg Br. 1994;76(5):745-9. Epub 1994/09/01. PubMed PMID: 8083263.

165. Torg JS, Conrad W, Kalen V. Clinical diagnosis of anterior cruciate ligament instability in the athlete. Am J Sports Med. 1976;4(2):84-93. Epub 1976/03/01. doi: 10.1177/036354657600400206. PubMed PMID: 961972.

166. Woo SL, Fisher MB. Evaluation of knee stability with use of a robotic system. J Bone Joint Surg Am. 2009;91 Suppl 1:78-84. Epub 2009/02/21. doi: 10.2106/JBJS.H.01371. PubMed PMID: 19182030; PMCID: PMC2663353.

167. Fujie H, Sekito T, Orita A. A novel robotic system for joint biomechanical tests: application to the human knee joint. J Biomech Eng. 2004;126(1):54-61. Epub 2004/06/03. PubMed PMID: 15171129.

168. Woo SL, Kanamori A, Zeminski J, Yagi M, Papageorgiou C, Fu FH. The effectiveness of reconstruction of the anterior cruciate ligament with hamstrings and patellar tendon . A cadaveric study comparing anterior tibial and rotational loads. J Bone Joint Surg Am. 2002;84-A(6):907-14. Epub 2002/06/14. PubMed PMID: 12063323.

169. Imhauser CW, Kent RN, 3rd, Boorman-Padgett J, Thein R, Wickiewicz TL, Pearle AD. New parameters describing how knee ligaments carry force in situ predict interspecimen variations in laxity during simulated clinical exams. J Biomech. 2017;64:212-8. doi: 10.1016/j.jbiomech.2017.09.032. PubMed PMID: 29078961.

170. Flynn JM, Mackenzie W, Kolstad K, Sandifer E, Jawad AF, Galinat B. Objective evaluation of knee laxity in children. J Pediatr Orthop. 2000;20(2):259-63. Epub 2000/03/30. PubMed PMID: 10739294.

171. Falciglia F, Guzzanti V, Di Ciommo V, Poggiaroni A. Physiological knee laxity during pubertal growth. Bull NYU Hosp Jt Dis. 2009;67(4):325-9. Epub 2009/12/17. PubMed PMID: 20001932.

172. Hinton RY, Rivera VR, Pautz MJ, Sponseller PD. Ligamentous laxity of the knee during childhood and adolescence. J Pediatr Orthop. 2008;28(2):184-7. Epub 2008/04/05. doi: 10.1097/BPO.0b013e3181652120. PubMed PMID: 18388713.

173. Kiapour AM, Sieker JT, Proffen BL, Lam TT, Fleming BC, Murray MM. Synovial fluid proteome changes in ACL injury-induced posttraumatic osteoarthritis: Proteomics analysis of porcine knee synovial fluid. PLoS One. 2019;14(3):e0212662. Epub 2019/03/02. doi: 10.1371/journal.pone.0212662. PubMed PMID: 30822327; PMCID: PMC6396923.

174. Alkjaer T, Simonsen EB, Jorgensen U, Dyhre-Poulsen P. Evaluation of the walking pattern in two types of patients with anterior cruciate ligament deficiency: copers and non -copers. Eur J Appl Physiol. 2003;89(3-4):301-8. doi: 10.1007/s00421-002-0787-x. PubMed PMID: 12736838.

175. Alkjaer T, Simonsen EB, Peter Magnusson SP, Aagaard H, Dyhre-Poulsen P. Differences in the movement pattern of a forward lunge in two types of anterior cruciate ligament deficient patients: copers and non-copers. Clin Biomech (Bristol, Avon). 2002;17(8):586-93. PubMed PMID: 12243718.

176. Biercevicz AM, Akelman MR, Fadale PD, Hulstyn MJ, Shalvoy RM, Badger GJ, Tung GA, Oksendahl HL, Fleming BC. MRI volume and signal intensity of ACL graft predict clinical, functional, and patient-oriented outcome measures after ACL reconstruction. Am J Sports Med. 2015;43(3):693-9. doi: 10.1177/0363546514561435. PubMed PMID: 25540298; PMCID: PMC4344859.

177. Martin JA, Brandon SCE, Keuler EM, Hermus JR, Ehlers AC, Segalman DJ, Allen MS, Thelen DG. Gauging force by tapping tendons. Nat Commun. 2018;9(1):1592. doi: 10.1038/s41467-018-03797-6. PubMed PMID: 29686281; PMCID: PMC5913259.

APPENDICES

Appendix 1

Table A-1-1. Both the sagittal and coronal angles of the ACL increase with increasing age. Different letters represent statistically significant differences between age groups ($p<0.05$).

Age [months]	Sagittal ACL Angle [deg]	Coronal ACL Angle [deg]
0	29.8±3.8[a]	36.0±4.7[a]
1.5	29.1±2.8[a]	45.7±4.9[b]
3	36.0±1.7[a]	54.4±6.5[c]
4.5	47.8±7.2[b]	69.4±3.3[d]
6	49.3±5.0[b]	72.6±4.9[d]
18	60.3±5.0[b]	77.6±4.1[d]

Table A-1-2. Both the PCL angle and the PCL horizontal-to-vertical ratio increase with increasing age. Different letters represent statistically significant differences between age groups ($p<0.05$).

Age [months]	PCL Angle [deg]	PCL H-to-V Ratio
0	112.3±4.6[a]	0.50±0.06[a]
1.5	114.7±2.6[a]	0.60±0.07[a,b]
3	126.6±4.4[b]	0.65±0.07[b]
4.5	135.6±3.1[c]	0.82±0.03[c,d]
6	140.1±2.9[c,d]	0.86±0.08[d,e]
18	142.6±3.1[d]	0.93±0.03[e]

Table A-1-3. The notch width index (calculated as the witch of the notch divided by the width of the femoral condyles) and the notch width aspect ratio (as described in Figure 3-5) decrease with increasing age. Different letters represent statistically significant differences between age groups ($p<0.05$).

Age [months]	Notch Width Index	Notch Width Aspect Ratio
0	0.21±0.02[a]	1.83±0.19[a]
1.5	0.21±0.04[a]	1.45±0.30[a]
3	0.12±0.02[b]	0.70±0.15[b]
4.5	0.13±0.01[b]	0.67±0.12[b]
6	0.15±0.02[b]	0.60±0.14[b]
18	0.12±0.02[b]	0.57±0.10[b]

Table A-1-4. The specific timing of orientation changes in the cruciate ligaments is similar between humans and the porcine model, with continued changes in the sagittal angle throughout adolescent growth, unlike the changes in the coronal ACL angle and the PCL angle which occur primarily during the early stages of growth. Age groups are as follows: [a]0-3 years, [b]1.5-3 months , [c]10-13 years, [d]4.5-6 months, [e]18-20 years, [f]18 months. Porcine data calculated from the current study by averaging age groups if needed. Approximate mean human data estimated from Kim et al (1).

Anatomic Feature	Human Early Youth[a]	Porcine Early Youth[b]	Human Pre-Adolescent[c]	Porcine Pre-Adolescent[d]	Human Late-Adolescent[e]	Porcine Late-Adolescent[f]
Sagittal ACL Angle	~48°	33°	~55°	49°	~62°	60°
Coronal ACL Angle	~52°	50°	~64°	71°	~69°	78°
PCL Angle	~110°	121°	~119°	138°	~122°	143°

Table A-1-5. Intraclass correlation coefficients (ICC) calculated for all measurements across images of both skeletally immature and mature pigs. Intrauser ICC values were calculated from 3 separate measurements performed by a single user, while interuser ICC values were calculated from measurements taken by 3 individuals. Calculation of ICC values were performed in JMP [SAS, Cary, NC] using the Measurement Systems Analysis tool. Intraclass correlation with bias and interactions reported for all values.

	ACL Sagittal Angle	ACL Coronal Angle	PCL Angle	PCL Horizontal Length	PCL Vertical Length	Intercondylar Roof Angle	Blumensaat-ACL Angle	Notch Width Index	Notch Width Aspect Ratio
Intrauser ICC [All Ages]	0.97	0.94	0.95	0.80	0.92	0.71	0.85	0.75	0.84
Interuser ICC [All Ages]	0.95	0.81	0.86	0.75	0.97	0.86	0.90	0.71	0.80

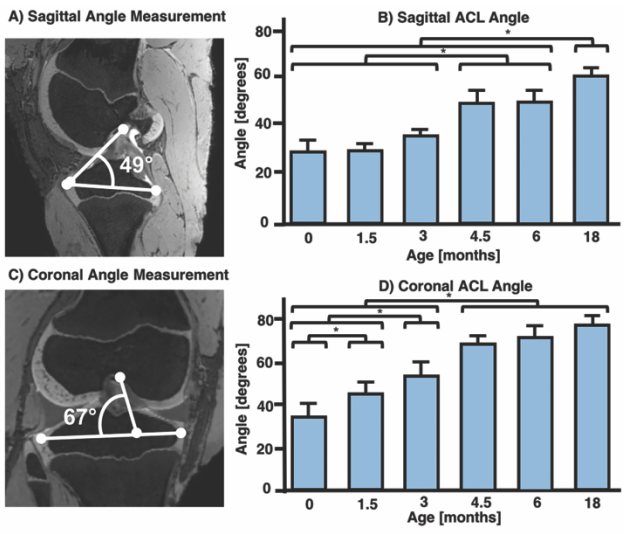

Figure A-1-1. Alternative representation of statistics from Figure 3-2. The angle of orientation of the ACL in both the sagittal and coronal planes is measured as shown in panels A and C. The sagittal angle (B) increases significantly between 3 and 18 months (late adolescence equivalent) while the changes in coronal angle (D) becomes insignificant after 4.5 months (early adolescence) in the porcine model. * represents statistical significance between age groups ($p<0.05$).

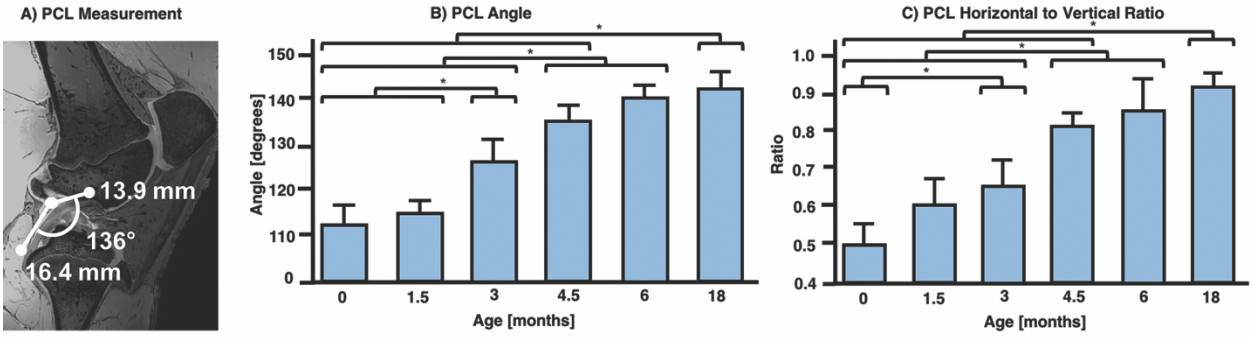

Figure A-1-2. Alternative representation of statistics from Figure 3-3. The PCL angle, measured between the horizontal and vertical components shown in panel A, increases with increasing age (B). Significant increases occur between consecutive age groups between 1.5 and 4.5 months of age, equivalent to an early adolescent age in humans. The horizontal-to-vertical ratio, calculated from these components, nearly doubles throughout skeletal growth, with significant changes occurring through late adolescence (18 months). * represents statistical significance between age groups ($p<0.05$).

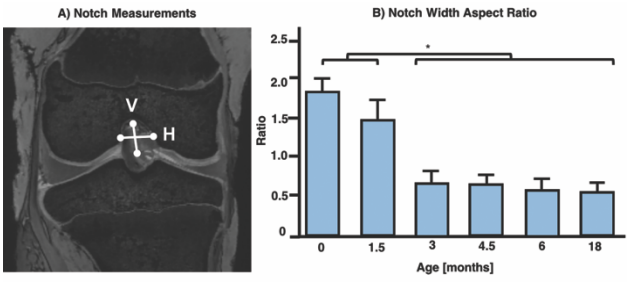

Figure A-1-3. Alternative representation of statistics from Figure 3-4. Notch width aspect ratio is calculated as a ratio of the horizontal ("H") and vertical ("V") notch measurements (A). Values decrease with increasing age, and statistically significant changes occur prior to early adolescence. * represents statistical significance between age groups ($p<0.05$).

Appendix 2

Table A-2-1. Tissue length data presented as mean ± standard deviation [95% C.I.].

Age (months)	ACL Length (mm)	PT Length (mm)	MCL Length (mm)	LCL Length (mm)
0	8.7 ± 1.4 [7.2-10.1]	14.2 ± 1.2 [13.0-15.4]	7.7 ± 1.8 [5.9-9.6]	7.8 ± 1.1 [6.6-9.0]
1.5	16.7 ± 3.0 [13.6-19.8]	25.8 ± 3.4 [21.6-30.0]	12.5 ± 2.2 [10.2-14.8]	12.5 ± 0.8 [11.7-13.3]
3	23.1 ± 2.1 [20.9-25.3]	41.3 ± 2.9 [38.3-44.3]	20.8 ± 2.1 [18.6-23.0]	22.2 ± 4.5 [17.5-26.9]
4.5	29.2 ± 2.4 [26.7-31.7]	54.9 ± 7.2 [47.4-62.4]	33.0 ± 3.2 [29.7-36.3]	29.4 ± 2.1 [27.2-31.5]
6	30.5 ± 1.0 [29.5-31.5]	58.0 ± 1.2 [56.5-59.5]	34.2 ± 2.6 [31.5-36.9]	34.5 ± 4.1 [30.3-38.8]
18	34.2 ± 2.3 [32.3-37.1]	73.8 ± 8.8 [64.5-83.0]	38.7 ± 3.4 [35.1-42.3]	35.6 ± 3.3 [32.2-39.0]

Table A-2-2. Tissue CSA data presented as mean ± standard deviation [95% C.I.].

Age (months)	ACL CSA (mm^2)	PT CSA (mm^2)	MCL CSA (mm^2)	LCL CSA (mm^2)
0	5.6 ± 0.7 [4.9-6.4]	2.9 ± 1.2 [1.6-4.1]	0.9 ± 0.3 [0.6-1.2]	1.7 ± 0.4 [1.2-2.1]
1.5	14.7 ± 4.7 [9.7-19.6]	15.6 ± 6.6 [7.4-23.8]	3.7 ± 1.2 [2.5-5.0]	6.3 ± 1.6 [4.6-7.9]
3	39.9 ± 4.5 [35.2-44.6]	24.5 ± 3.5 [20.9-28.2]	9.3 ± 1.8 [7.4-11.2]	13.3 ± 1.9 [11.3-15.2]
4.5	43.0 ± 7.5 [35.1-50.9]	36.0 ± 7.3 [28.3-43.6]	14.0 ± 2.3 [11.7-16.4]	18.5 ± 4.3 [13.9-23.0]
6	41.0 ± 6.4 [34.4-47.7]	52.3 ± 18.9 [28.8-75.7]	19.8 ± 2.9 [16.7-22.9]	26.3 ± 3.6 [22.6-30.0]
18	57.4 ± 8.9 [48.1-66.8]	70.5 ± 19.5 [50.0-91.0]	22.5 ± 3.5 [18.7-26.2]	31.3 ± 5.1 [25.9-36.7]

Table A-2-3. Tissue length normalized as a percentage of the average 18-month old value presented as mean ± standard deviation [95% C.I.].

Age (months)	ACL Length (%)	PT Length (%)	MCL Length (%)	LCL Length (%)
0	25.0 ± 4.1 [20.7-29.2]	19.3 ± 1.5 [17.6-20.9]	20.0 ± 4.6 [15.2-24.8]	21.8 ±3.2 [18.5-25.2]
1.5	48.1 ± 8.6 [39.2-57.1]	35.0 ± 4.6 [29.2-40.7]	32.3 ± 5.6 [26.5-38.2]	35.2 ± 2.1 [32.9-37.4]
3	66.5 ± 6.1 [60.1-72.9]	56.0 ± 3.9 [51.9-60.1]	53.7 ± 5.4 [48.1-59.4]	62.2 ± 12.6 [49.0-75.4]
4.5	84.1 ± 6.8 [76.9-91.3]	74.5 ± 9.7 [84.7-64.3]	85.3 ± 8.2 [76.7-93.9]	82.4 ± 5.8 [76.3-88.5]
6	87.8 ± 2.8 [84.8-90.8]	78.6 ± 1.7 [76.6-80.7]	88.5 ± 6.7 [81.5-95.5]	97.0 ± 11.4 [85.0-109.0]
18	100.0 ± 6.5 [93.2-106.8]	100.0 ± 12.0 [87.4-112.6]	100.0 ± 8.8 [90.7-109.3]	100.0 ± 9.2 [90.4-109.6]

Table A-2-4. Tissue cross-sectional area normalized as a percentage of the average 18-month old value presented as mean ± standard deviation [95% C.I.].

Age (months)	ACL CSA (%)	PT CSA (%)	MCL CSA (%)	LCL CSA (%)
0	9.8 ± 1.3 [8.5-11.1]	4.1 ± 1.7 [2.3-5.8]	4.0 ± 1.4 [2.5-5.4]	5.3 ± 1.3 [3.9-6.7]
1.5	25.6 ± 8.3 [16.9-34.2]	22.2 ± 9.4 [10.5-33.8]	16.6 ± 5.4 [10.9-22.3]	19.8 ± 5.0 [14.5-25.0]
3	69.5 ± 7.8 [61.3-77.7]	34.8 ± 4.9 [29.6-40.0]	41.5 ± 8.1 [33.0-50.1]	42.0 ± 5.9 [35.8-48.2]
4.5	74.8 ± 13.1 [61.2-88.6]	51.0 ± 10.4 [40.1-61.9]	62.5 ± 10.0 [52.0-73.0]	58.5 ± 13.8 [44.0-72.9]
6	71.5 ± 11.1 [59.9-83.1]	74.1 ± 26.8 [40.9-107.4]	88.2 ± 13.1 [74.5-102.0]	83.1 ± 11.3 [71.3-95.0]
18	100.0 ± 15.5 [83.7-116.3]	100.0 ± 27.7 [71.0-129.0]	100.0 ± 15.8 [83.4-116.6]	100.0 ± 16.2 [82.1-116.1]

Appendix 3

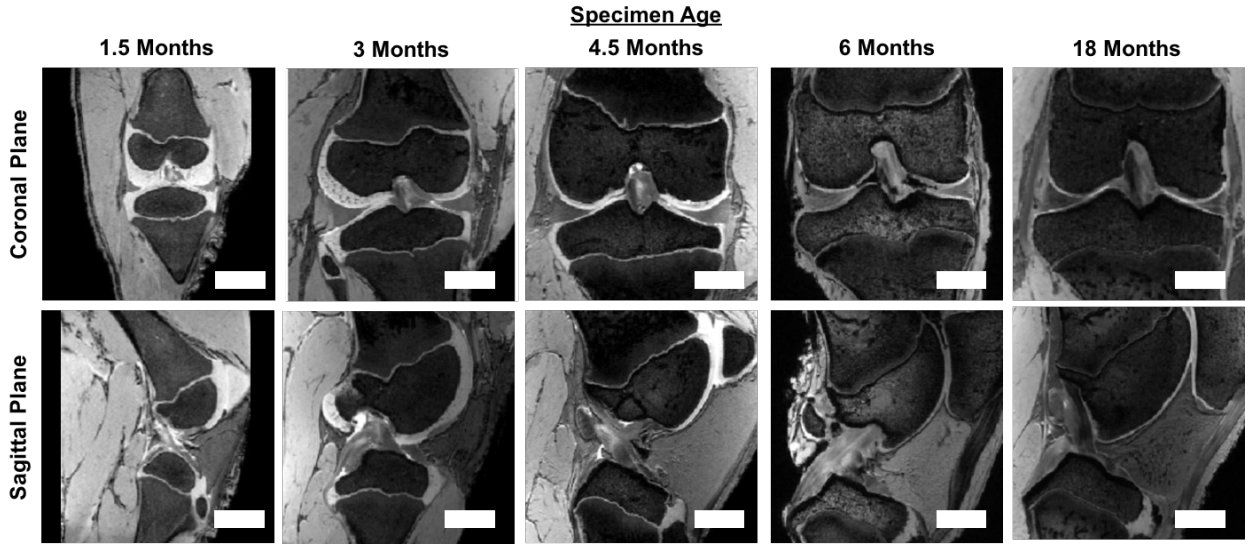

Figure A-3-1. MRI scans of porcine stifle joints (knee equivalent) ranging from 1.5 months through 18 months of age, scale bar is 20 mm.

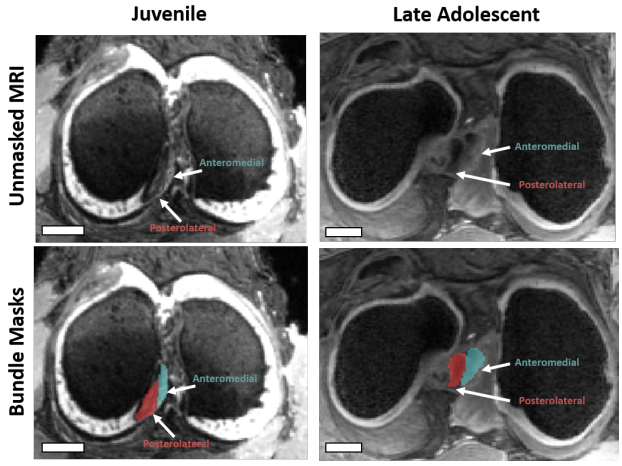

Figure A-3-2. Masking of the anteromedial and posterolateral bundles of the ACL via MRI. Sample images show for juvenile (3 months) and late adolescent (18 months) knee joints. Scale bars are 10 mm.

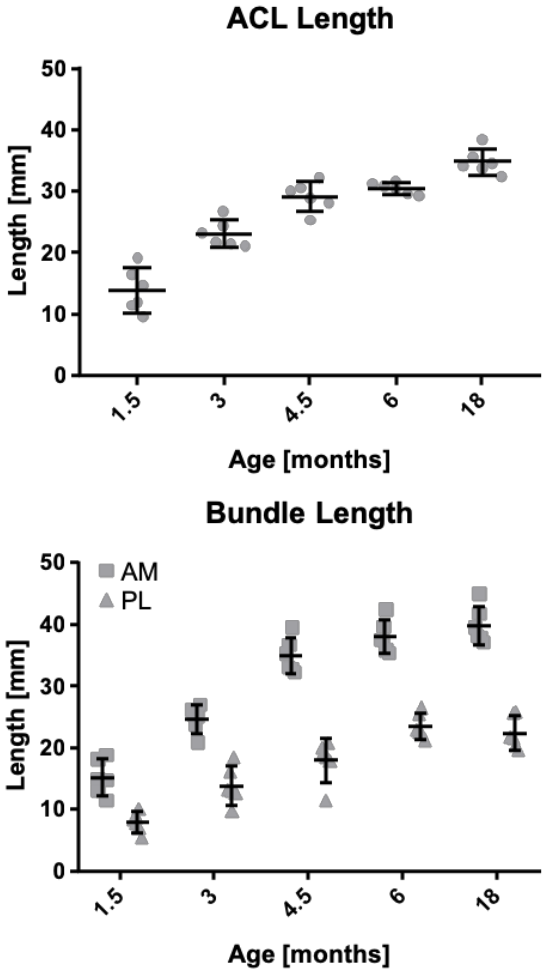

Figure A-3-3. The length of the ACL and its bundles increase similarly with age. Bars represent mean with a 95% confidence interval.

Table A-3-1. Applied Forces and Moments for Each Age Group

Age	Anterior-Posterior Load	Varus-Valgus Moment
1.5 Months	20 N	1 N*m
3 Months	40 N	2 N*m
4.5 Months	80 N	4 N*m
6 Months	100 N	5 N*m
18 Months	140 N	7 N*m

Raw Anterior-Posterior Tibial Translation (APTT) Summary Data

Direct measurements of anterior-posterior tibial translation (APTT) were not significantly affected by age ($p=0.64$) and varied significantly by flexion angle ($p=0.001$) with no interaction between the terms ($p=0.24$) via two-way ANOVA. Summary data presented as mean ± standard deviation [95% confidence interval of the mean].

Table A-3-2. APTT Summary Data [mm]

	40° of Flexion	60° of Flexion	90° of Flexion
1.5 Months	8.7 ± 1.6 [7.0-10.3]	8.6 ± 1.5 [7.1-10.2]	7.4 ± 0.5 [6.9-7.9]
3 Months	10.3 ± 4.6 [5.5-15.1]	10.2 ± 3.4 [6.7-13.7]	8.9 ± 1.9 [6.9-10.9]
4.5 Months	8.4 ± 1.1 [7.3-9.6]	9.2 ± 1.3 [7.9-10.5]	8.0 ± 1.2 [6.7-9.3]
6 Months	8.7 ± 3.1 [5.5-11.9]	9.8 ± 3.0 [6.7-13.0]	8.9 ± 2.5 [6.3-11.6]
18 Months	9.0 ± 0.8 [8.2-9.8]	10.1 ± 0.9 [9.1-11.1]	9.7 ± 1.2 [8.5-10.9]

Normalized APTT Summary Data and Statistics

Anterior-posterior tibial translation normalized to the anterior-posterior length of the tibial plateau decreased significantly with increasing age ($p<0.001$) and varied significantly by flexion angle ($p<0.001$) with no interaction between the terms ($p=0.14$) via two-way ANOVA. Summary data presented as mean ± standard deviation [95% confidence interval of the mean].

Table A-3-3. Normalized APTT Summary Data [A.U.]

	40° of Flexion	60° of Flexion	90° of Flexion
1.5 Months	0.34 ± 0.08 [0.26-0.43]	0.34 ± 0.08 [0.26-0.43]	0.29 ± 0.03 [0.26-0.33]
3 Months	0.28 ± 0.10 [0.1-0.39]	0.28 ± 0.08 [0.20-0.36]	0.25 ± 0.06 [0.19-0.31]
4.5 Months	0.29 ± 0.03 [0.17-0.23]	0.22 ±0.03 [0.18-0.25]	0.19 ±0.03 [0.15-0.22]
6 Months	0.19 ± 0.07 [0.12-0.25]	0.21 ± 0.07 [0.14-0.28]	0.19 ± 0.06 [0.13-0.25]
18 Months	0.17 ±0.01 [0.16-0.19]	0.19 ± 0.02 [0.18-0.21]	0.17 ±0.01 [0.16-0.19]

Varus-Valgus Rotation Summary Data and Statistics

Varus-valgus rotation at 60° of flexion decreased significantly with increasing age ($p<0.001$) in response to applied varus and valgus moments via one-way ANOVA. Summary data presented as mean ± standard deviation [95% confidence interval of the mean].

Table A-3-4. Varus-Valgus Rotation Summary Data [degrees]

	60° of Flexion
1.5 Months	25.4 ± 2.2 [23.1-27.8]
3 Months	20.0 ± 3.6 [16.2-23.7]
4.5 Months	12.1 ± 0.7 [11.4-12.8]
6 Months	11.6 ± 1.9 [9.6-13.5]
18 Months	6.3 ± 1.6 [4.6-8.0]

ACL Contribution to Anterior Load Summary Data and Statistics

The contribution of the ACL to resisting the applied anterior load was not significantly different across ages ($p=0.63$), although it varied by flexion angle ($p<0.001$), and there was an interaction between the two effects ($p<0.001$) via two-way ANOVA. Summary data presented as mean ± standard deviation [95% confidence interval of the mean].

Table A-3-5. ACL Contribution to Anterior Load Summary Data [% of Total Joint Force]

Age	40° of Flexion	60° of Flexion	90° of Flexion
1.5 Months	105 ± 14 [90-119]	109 ± 17 [92-127]	109 ± 19 [89-129]
3 Months	89 ± 20 [68-111]	101 ± 18 [82-120]	101 ± 25 [75-127]
4.5 Months	80 ± 26 [52-108]	110 ± 21 [87-132]	111 ± 18 [92-130]
6 Months	75 ± 14 [60-89]	97 ± 11 [86-108]	107 ± 11 [95-118]
18 Months	91 ± 14 [76-105]	100 ± 16 [83-117]	98 ± 11 [86-110]

Bundle Contributions to ACL Function Summary Data and Statistics

The relative functional contributions of the AM and PL bundles to overall ACL behavior varied as an effect of age ($p<0.001$) and flexion angle ($p<0.001$) with a significant interaction

between the two ($p<0.001$) via two-way ANOVA. Summary data presented as mean ± standard deviation [95% confidence interval of the mean].

Table A-3-6. AM Bundle Functional Contribution Summary Data [% of Total ACL Force]

Age	40° of Flexion	60° of Flexion	90° of Flexion
1.5 Months	44 ± 21 [22-66]	50 ± 19 [30-70]	49 ± 15 [34-65]
3 Months	31 ± 17 [13-48]	45 ± 21 [23-67]	48 ± 22 [25-71]
4.5 Months	49 ± 26 [21-76]	59 ± 22 [36-82]	41 ± 21 [19-62]
6 Months	65 ± 20 [45-86]	76 ± 19 [56-95]	63 ± 21 [40-85]
18 Months	89 ± 13 [75-103]	93 ± 12 [79-104]	86 ± 16 [70-103]

Table A-3-7. PL Bundle Functional Contribution Summary Data [% of Total ACL Force]

Age	40° of Flexion	60° of Flexion	90° of Flexion
1.5 Months	57 ± 21 [34-79]	50 ± 19 [30-71]	51 ± 16 [35-67]
3 Months	69 ± 17 [52-87]	55 ± 22 [33-78]	52 ± 22 [29-75]
4.5 Months	51 ± 26 [24-79]	41 ± 22 [18-64]	59 ± 21 [38-81]
6 Months	35 ± 20 [14-55]	24 ± 19 [5-44]	37 ± 21 [15-59]
18 Months	11 ± 13 [-3-25]	8 ± 12 [-4-21]	14 ± 16 [-3-30]

Bundle Contributions to ACL Function Under Applied Varus and Valgus Moments Summary Data and Statistics

The relative functional contributions of the AM and PL bundles to overall ACL behavior under applied varus loads at 60° of flexion varied as an effect of age ($p<0.001$) via one-way ANOVA. Age did not have a significant effect on bundle contributions under valgus loads ($p=0.15$) via one-way ANOVA. Summary data presented as mean ± standard deviation [95% confidence interval of the mean].

Table A-3-8. Bundle Specific Contributions to Resultant Force in the ACL Summary Data [% of total ACL Force]

Age	AM Varus	PL Varus	AM Valgus	PL Valgus
1.5 Months	46 ± 16 [30-63]	54 ± 16 [37-70]	47 ± 16 [31-63]	53 ± 16 [37-69]
3 Months	55 ± 14 [41-70]	45 ± 14 [30-59]	55 ± 26 [29-82]	45 ± 26 [18-71]
4.5 Months	71 ± 8 [62-79]	30 ± 8 [21-38]	72 ± 17 [54-90]	28 ± 17 [10-46]
6 Months	86 ± 3 [83-90]	14 ± 3 [11-17]	44 ± 21 [21-66]	56 ± 21 [34-79]
18 Months	80 ± 21 [57-102]	20 ± 21 [-2-43]	59 ± 20 [39-80]	41 ± 20 [20-61]

Tissue Cross-Sectional Area Summary Data and Statistics

The CSA of the ACL, AM, and PL bundles increased significantly with increasing age ($p<0.001$) via one-way ANOVA. The CSA values of the AM bundle became significantly greater than those of the PL bundle in adolescence. Summary data presented as mean ± standard deviation [95% confidence interval of the mean].

Table A-3-9. CSA Summary Data [mm^2]

	ACL CSA	AM Bundle CSA	PL Bundle CSA
1.5 Months	12 ± 3 [9-15]	5 ± 2 [3-7]	7 ± 2 [5-10]
3 Months	20 ± 4 [16-24]	9 ± 3 [7-12]	12 ± 2 [10-14]
4.5 Months	40 ± 5 [35-45]	22 ± 4 [18-25]	19 ± 5 [14-24]
6 Months	44 ± 11 [33-55]	28 ± 6 [21-34]	16 ± 4 [11-20]
18 Months	53 ± 13 [40-66]	35 ± 8 [27-44]	17 ± 7 [10-25]

Tissue Length Summary Data and Statistics

The length of the ACL, AM, and PL bundles increased significantly with increasing age ($p<0.001$) via one-way ANOVA. Summary data presented as mean ± standard deviation [95% confidence interval of the mean].

Table A-3-10. Tissue Length Summary Data [mm]

Age	ACL	AM Bundle	PL Bundle
1.5 Months	14 ± 4 [10-18]	15 ± 3 [12-18]	8 ± 2 [6-10]
3 Months	23 ± 2 [21-25]	25 ± 2 [22-27]	14 ± 3 [11-17]
4.5 Months	29 ± 2 [27-32]	35 ± 3 [32-38]	18 ± 3 [14-22]
6 Months	31 ± 1 [30-32]	38 ± 3 [35-41]	24 ± 2 [21-26]
18 Months	35 ± 2 [33-37]	40 ± 3 [37-43]	22 ± 3 [20-25]

Bundle Sagittal Angle Summary Data and Statistics

The sagittal orientation angle of the AM and PL bundles increased significantly with increasing age ($p<0.001$) and varied by specific bundle ($p<0.001$) via two-way ANOVA although there was no significant interaction ($p=0.06$). Summary data presented as mean ± standard deviation [95% confidence interval of the mean].

Table A-3-11. ACL Bundle Sagittal Angle Summary Data

Age	AM Bundle	PL Bundle
1.5 Months	32 ± 3 [29-35]	36 ± 3 [32-39]
3 Months	37 ± 3 [34-41]	43 ± 5 [38-47]
4.5 Months	48 ± 6 [42-53]	58 ± 7 [50-66]
6 Months	51 ± 5 [46-56]	63 ± 11 [52-75]
18 Months	55 ± 5 [50-61]	66 ± 4 [62-71]

Bundle Coronal Angle Summary Data and Statistics

The coronal orientation angle of the AM and PL bundles increased significantly with increasing age ($p<0.001$) and varied by specific bundle ($p<0.001$) via two-way ANOVA and

there was a significant interaction between the two (p=0.02). Summary data presented as mean ± standard deviation [95% confidence interval of the mean].

Table A-3-12. ACL Bundle Coronal Angle Summary Data

Age	AM Bundle	PL Bundle
1.5 Months	44 ± 3 [41-47]	47 ± 3 [44-50]
3 Months	54 ± 5 [49-59]	63 ± 3 [60-67]
4.5 Months	65 ± 4 [60-69]	70 ± 7 [63-78]
6 Months	71 ± 4 [67-76]	75 ± 6 [68-81]
18 Months	75 ± 3 [72-78]	74 ± 5 [69-80]

Appendix 4

Table A-4-1. Loading Protocol for Robotic Testing with Additional Calculations. Superscripts represent the joint state, subscripts represent the kinematic state.

Joint State	Loading Conditions	Data Acquired	Calculations
Intact Joint	Anterior-posterior tibial load (40°, 60°, 90°) and varus-valgus (60°) moment	Kinematics from intact joint (K_{intact}) In-situ force (F_{AMt}^{AMt})	
AM Bundle Transected	Anterior-posterior tibial load (40°, 60°, 90°) and varus-valgus (60°) moment	Kinematics from partial injury (K_{AMt})	
	Repeat (K_{intact})	In-situ force ($F_{intact}^{AMt}, F_{AMt}^{AMt}$)	AM bundle in-situ force ($F_{intact}^{intact} - F_{intact}^{AMt}$)
ACL Transected	Anterior-posterior tibial load (40°, 60°, 90°) and varus-valgus (60°) moment	Kinematics from ACL deficient knee (K_{ACLt})	
	Repeat (K_{intact}, K_{AMt})	In-situ force ($F_{intact}^{ACLt}, F_{AMt}^{ACLt}, F_{ACLt}^{ACLt}$)	ACL in-situ force ($F_{intact}^{intact} - F_{intact}^{ACLt}$) PL bundle in-situ force ($F_{intact}^{AMt} - F_{intact}^{ACLt}$) ($F_{AMt}^{AMt} - F_{AMt}^{ACLt}$)
MCL Transected	Repeat (K_{intact}, K_{AMt}, K_{ACLt})	In-situ force ($F_{intact}^{MCLt}, F_{AMt}^{MCLt}, F_{ACLt}^{MCLt}$)	MCL in-situ force ($F_{intact}^{ACLt} - F_{intact}^{MCLt}$) ($F_{AMt}^{ACLt} - F_{AMt}^{MCLt}$) ($F_{ACLt}^{ACLt} - F_{ACLt}^{MCLt}$)
LCL Transected	Repeat (K_{intact}, K_{AMt}, K_{ACLt})	In-situ force ($F_{intact}^{LCLt}, F_{AMt}^{LCLt}, F_{ACLt}^{LCLt}$)	LCL in-situ force ($F_{intact}^{MCLt} - F_{intact}^{LCLt}$) ($F_{AMt}^{MCLt} - F_{AMt}^{LCLt}$) ($F_{ACLt}^{MCLt} - F_{ACLt}^{LCLt}$)
Medial Meniscus Removed	Repeat (K_{intact}, K_{AMt}, K_{ACLt})	In-situ force ($F_{intact}^{MMENt}, F_{AMt}^{MMENt}, F_{ACLt}^{MMENt}$)	Medial Meniscus in-situ force ($F_{intact}^{LCLt} - F_{intact}^{MMENt}$) ($F_{AMt}^{LCLt} - F_{AMt}^{MMENt}$) ($F_{ACLt}^{LCLt} - F_{ACLt}^{MMENt}$)

Table A-4-1. (continued)

Lateral Meniscus Removed	Repeat (K_{intact}, K_{AMt}, K_{ACLt})	In-situ force (F_{intact}^{LMENt}, F_{AMt}^{LMENt}, F_{ACLt}^{LMENt})	Lateral Meniscus in-situ force ($F_{intact}^{MMENt} - F_{intact}^{LMENt}$) ($F_{AMt}^{MMENt} - F_{AMt}^{LMENt}$) ($F_{ACLt}^{MMENt} - F_{ACLt}^{LMENt}$)

Normalized APTT Summary Data

Anterior-posterior tibial translation normalized to the length of the tibial plateau varied with age ($p=0.003$), angle ($p<0.001$), and state ($p<0.001$) with significant interactions between age and angle ($p<0.001$), age and state ($p=0.027$) and angle and state ($p=0.001$) but not between age, angle, and state ($p=0.056$) via multi-way ANOVA and Tukey's post-hoc analysis. Summary data presented as mean ± standard deviation [95% confidence interval of the mean].

Table A-4-2. Normalized APTT Summary Data [mm/mm] ([a]p<0.05 vs. intact at a given flexion angle; [b]p<0.05 vs. AM-deficient at a given flexion angle; [c]p<0.05 vs. intact at a given age; [d]p<0.05 vs. AM-deficient at a given age).

40° of Flexion	Intact	AM-Deficient	ACL-Deficient[a,b]
1.5 Months	0.35 ± 0.08 [0.26-0.43]	0.40 ± 0.10 [0.30-0.50]	0.74 ± 0.14[c,d] [0.59-0.89]
3 Months	0.28 ± 0.10 [0.18-0.39]	0.32 ± 0.11 [0.20-0.43]	0.68 ± 0.13[c,d] [0.54-0.81]
4.5 Months	0.20 ± 0.03 [0.16-0.23]	0.23 ± 0.04 [0.18-0.27]	0.46 ± 0.14[c,d] [0.31-0.60]
6 Months	0.19 ± 0.07 [0.11-0.25]	0.23 ± 0.08 [0.15-0.31]	0.50 ± 0.15[c,d] [0.34-0.65]
18 Months	0.17 ± 0.01 [0.16-0.19]	0.24 ± 0.02[c] [0.22-0.26]	0.49 ± 0.05[c,d] [0.44-0.55]
60° of Flexion	Intact	AM-Deficient[a]	ACL-Deficient[a,b]
1.5 Months	0.34 ± 0.08 [0.26-0.43]	0.40 ± 0.09 [0.30-0.49]	0.66 ± 0.18[c,d] [0.48-0.85]
3 Months	0.28 ± 0.08 [0.20-0.36]	0.32 ± 0.09 [0.23-0.42]	0.64 ± 0.14[c,d] [0.49-0.79]
4.5 Months	0.22 ± 0.03 [0.18-0.25]	0.26 ± 0.03 [0.22-0.29]	0.50 ± 0.10[c,d] [0.40-0.60]
6 Months	0.21 ± 0.07 [0.14-0.28]	0.28 ± 0.07 [0.20-0.35]	0.57 ± 0.08[c,d] [0.49-0.65]
18 Months	0.19 ± 0.02 [0.18-0.21]	0.29 ± 0.03[c] [0.26-0.32]	0.52 ± 0.06[c,d] [0.46-0.58]
90° of Flexion	Intact	AM-Deficient	ACL-Deficient[a,b]
1.5 Months	0.29 ± 0.03 [0.26-0.33]	0.33 ± 0.04 [0.28-0.37]	0.42 ± 0.16[c,d] [0.25-0.58]
3 Months	0.25 ± 0.06 [0.19-0.31]	0.28 ± 0.07 [0.21-0.36]	0.53 ± 0.18[c,d] [0.34-0.72]
4.5 Months	0.19 ± 0.03 [0.15-0.22]	0.21 ± 0.03 [0.18-0.25]	0.45 ± 0.06[c,d] [0.39-0.52]
6 Months	0.19 ± 0.06 [0.13-0.25]	0.25 ± 0.07 [0.18-0.32]	0.52 ± 0.05[c,d] [0.47-0.58]
18 Months	0.18 ± 0.02 [0.17-0.20]	0.27 ± 0.03[c] [0.23-0.30]	0.47 ± 0.06[c,d] [0.40-0.53]

APTT Summary Data

Anterior-posterior tibial translation varied significantly with age (p=0.004), angle (p<0.001), and state (p<0.001) and there were significant interactions between age and angle

($p<0.001$), age and state ($p<0.001$) and angle and state ($p=0.007$) but not between age, angle, and state ($p=0.498$) via multi-way ANOVA and Tukey's post-hoc analysis. Summary data presented as mean ± standard deviation [95% confidence interval of the mean].

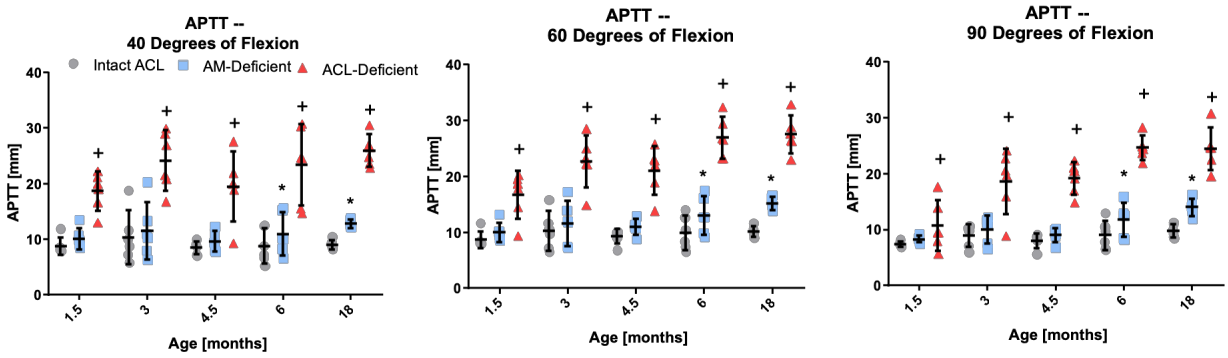

Figure A-4-1. Anterior-posterior tibial translation (APTT) increased following partial and complete ACL transection in response to an applied anterior-posterior tibial load. Data represented as points, with bars showing mean and 95% confidence interval. * denotes $p<0.05$ from intact state, + denotes $p<0.05$ from intact and AM deficient states.

Table A-4-3. APTT Summary Data [mm] ([a]p<0.05 vs. intact at a given flexion angle; [b]p<0.05 vs. AM-deficient at a given flexion angle; [c]p<0.05 vs. intact at a given age; [d]p<0.05 vs. AM-deficient at a given age).

40° of Flexion	Intact	AM-Deficient[a]	ACL-Deficient[a,b]
1.5 Months	8.7 ± 1.6 [7.0-10.3]	10.0 ± 1.8 [8.1-11.9]	18.6 ± 3.4[c,d] [15.1-22.1]
3 Months	10.3 ± 4.6 [5.5-15.1]	11.5 ± 4.9 [6.3-16.6]	24.1 ± 5.2[c,d] [18.6-29.6]
4.5 Months	8.4 ± 1.1 [7.3-9.6]	9.6 ± 1.8 [7.7-11.4]	19.4 ± 5.9[c,d] [13.1-25.6]
6 Months	8.7 ± 3.1 [5.5-12.0]	10.9 ± 3.7[c] [7.0-14.8]	23.3 ± 7.0[c,d] [16.0-30.7]
18 Months	9.0 ± 0.8 [8.2-9.8]	12.7 ± 0.7[c] [12.0-13.5]	25.8 ± 2.8[c,d] [22.9-28.7]
60° of Flexion	Intact	AM-Deficient[a]	ACL-Deficient[a,b]
1.5 Months	8.6 ± 1.5 [7.1-10.2]	9.9 ± 1.7 [8.1-11.7]	16.7 ± 1.7 [c,d] [12.3-21.0]
3 Months	10.2 ± 3.4 [6.7-13.7]	11.5 ± 3.8 [7.5-15.6]	22.6 ± 4.5 [c,d] [17.9-27.3]
4.5 Months	9.2 ± 1.3 [7.9-10.5]	10.9 ± 1.3 [9.5-12.3]	21.0 ± 4.2 [c,d] [16.6-25.4]
6 Months	9.8 ± 3.0 [6.7-13.0]	12.9 ± 3.3[c] [9.5-16.4]	26.9 ± 3.6 [c,d] [23.1-30.7]
18 Months	10.1 ± 0.9 [9.1-11.1]	15.1 ± 1.1[c] [13.9-16.3]	27.5 ± 3.3 [c,d] [24.0-30.9]
90° of Flexion	Intact	AM-Deficient[a]	ACL-Deficient[a,b]
1.5 Months	7.4 ± 0.5 [6.9-7.9]	8.2 ± 0.6 [7.6-8.8]	10.6 ± 4.4 [c,d] [6.1-15.2]
3 Months	8.9 ± 1.9 [6.9-10.9]	10.0 ± 2.4 [7.5-12.5]	18.6 ± 5.6 [c,d] [12.8-24.4]
4.5 Months	8.0 ± 1.2 [6.7-9.3]	9.0 ± 1.2 [7.7-10.3]	19.1 ± 2.8 [c,d] [16.2-22.0]
6 Months	8.9 ± 2.5 [6.3-11.6]	11.7 ± 2.9 [c] [8.6-14.8]	24.6 ± 2.1 [c,d] [22.4-26.8]
18 Months	9.7 ± 1.2 [8.5-11.0]	14.0 ± 1.5 [c] [12.4-15.5]	24.4 ± 3.7 [c,d] [20.6-28.3]

Varus-Valgus Rotation Summary Data

Varus-valgus rotation at 60° of flexion varied significantly with age (p<0.001) and state (p<0.001) with no significant interaction between age and state (p=0.523) via two-way ANOVA

and Tukey's post-hoc analysis. Summary data presented as mean ± standard deviation [95% confidence interval of the mean].

Table A-4-4. Varus-Valgus Rotation Summary Data [degrees] ([a]p<0.05 vs. intact; [b]p<0.05 vs. AM-deficient; [c]p<0.05 vs. 1.5 months; [d]p<0.05 vs. 3 months; [e]p<0.05 vs. 4.5 months; [f]p<0.05 vs. 6 months).

	Intact	AM-Deficient[a]	ACL-Deficient[a,b]
1.5 Months	25.4 ± 2.2 [23.1-27.8]	26.0 ± 2.5 [23.4-28.6]	30.1 ± 2.9 [27.1-33.1]
3 Months[c]	20.0 ± 3.6 [16.2-23.7]	21.4 ± 4.2 [17.0-25.8]	24.6 ± 6.3 [17.9-31.2]
4.5 Months[c,d]	12.1 ± 0.7 [11.4-12.8]	12.9 ± 1.0 [11.9-13.9]	14.7 ± 0.8 [13.8-15.6]
6 Months[c,d]	11.6 ± 1.9 [9.6-13.5]	12.7 ± 2.1 [10.5-15.0]	16.8 ± 4.5 [12.0-21.5]
18 Months[c,d,e,f]	6.3 ± 1.6 [4.6-8.0]	7.6 ± 2.1 [5.4-9.8]	10.6 ± 4.1 [6.3-14.9]

ACL Functional Contribution to Anterior Load in the Intact State Summary Data

The functional contribution of the ACL to resisting the applied anterior load was not significantly different across ages (p=0.630), although it varied by flexion angle (p<0.001), and there was an interaction between the two effects (p<0.001) via two-way ANOVA and Tukey's post-hoc analysis. Summary data presented as mean ± standard deviation [95% confidence interval of the mean].

Table A-4-5. ACL Functional Contribution to Anterior Load in the Intact State Summary Data [% of total anterior joint force].

Age	40° of Flexion	60° of Flexion	90° of Flexion
1.5 Months	104.5 ± 13.6 [90.3-118.7]	109.2 ± 16.8 [91.5-126.8]	108.8 ± 19.0 [88.9-128.8]
3 Months	89.3 ± 20.4 [67.9-110.7]	101.0 ± 18.3 [81.8-120.2]	101.2 ± 24.8 [75.1-127.2]
4.5 Months	79.8 ± 26.4 [52.1-107.5]	109.8 ± 21.4 [87.3-132.3]	111.0 ± 18.4 [91.7-130.3]
6 Months	74.7 ± 13.8 [60.2-89.1]	97.0 ± 10.6 [85.9-108.2]	106.5 ± 10.6 [95.4-117.6]
18 Months	90.7 ± 13.7 [76.3-105.1]	100.3 ± 16.1 [83.4-117.3]	98.2 ± 11.4 [86.2-110.2]

AM Bundle Functional Contribution to Anterior Tibial Load Summary Data

The relative functional contribution of the AM bundle to overall anterior tibial load resistance varied as an effect of age ($p=0.008$) and flexion angle ($p<0.001$) with a significant interaction between the two ($p=0.013$) via two-way ANOVA and Tukey's post-hoc analysis. Summary data presented as mean ± standard deviation [95% confidence interval of the mean].

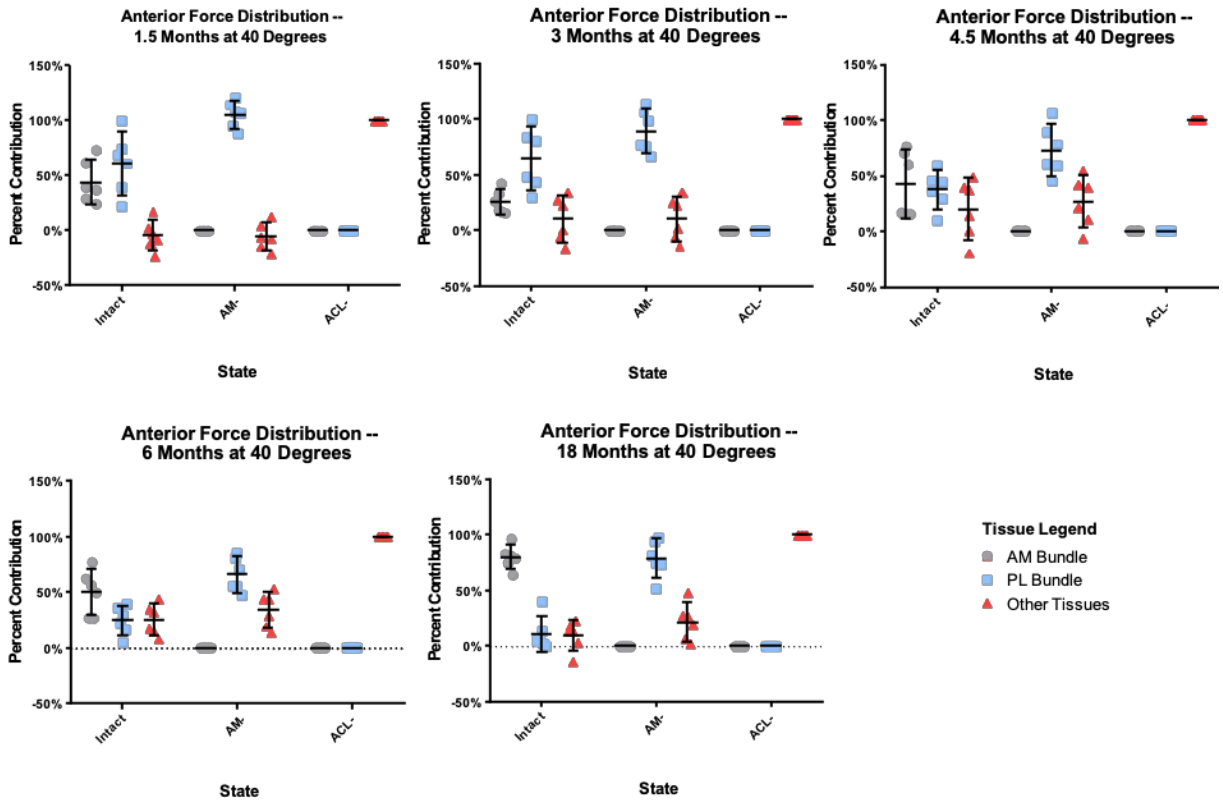

Figure A-4-2. In situ force contributions of the AM and PL bundles of the ACL relative to all other soft tissues shown at 40° of flexion across states and ages. Analyzing the in situ forces in response to an applied anterior-posterior tibial load, we see that the PL bundle resists the majority of the load across ages in the partial transection state, and other tissues carry all of the functional contributions in the ACL-transected state. Data represented as points, with bars showing mean and 95% confidence interval. Percent contribution is normalized to the total force resisted by the joint under an applied load.

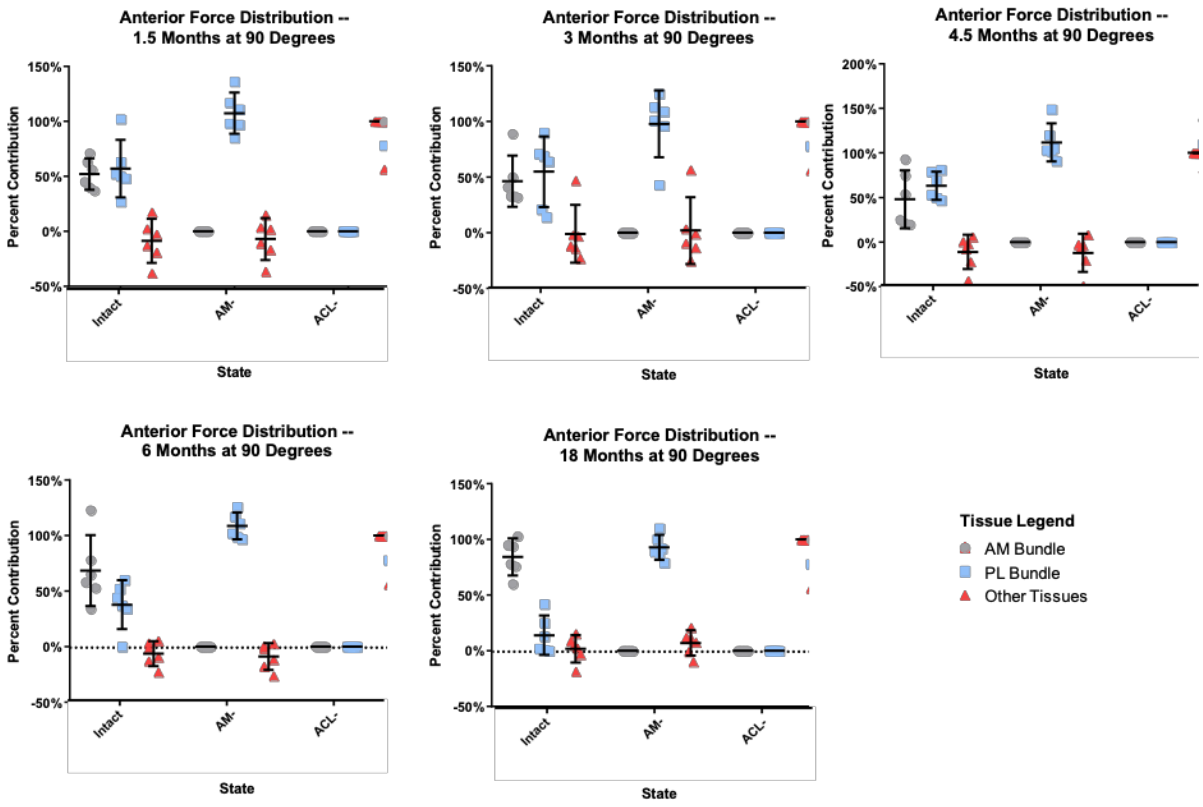

Figure A-4-3. In situ force contributions of the AM and PL bundles of the ACL relative to all other soft tissues shown at 90° of flexion across states and ages. Analyzing the in situ forces in response to an applied anterior-posterior tibial load, we see that the PL bundle resists the majority of the load across ages in the partial transection state, and other tissues carry all of the functional contributions in the ACL-transected state. Data represented as points, with bars showing mean and 95% confidence interval. Percent contribution is normalized to the total force resisted by the joint under an applied load.

Table A-4-6. AM Bundle Functional Contribution Summary Data [% total anterior joint force] ([a]$p<0.05$ vs. 1.5 months at a given flexion angle; [b]$p<0.05$ vs. 3 months at a given flexion angle; [c]$p<0.05$ vs. 4.5 months at a given flexion angle; [d]$p<0.05$ vs. 6 months at a given flexion angle).

Intact	40° of Flexion	60° of Flexion	90° of Flexion
1.5 Months	43.9 ± 19.1 [23.8-63.9]	52.0 ± 14.8 [36.4-67.5]	51.9 ± 13.6 [37.6-66.1]
3 Months	25.4 ± 10.6 [14.2-36.5]	43.9 ± 17.1 [25.9-61.8]	46.1 ± 21.9 [23.0-69.1]
4.5 Months	42.4 ± 29.6 [11.4-73.5]	67.3 ± 34.7 [30.9-103.7]	48.0 ± 31.3 [15.1-80.8]
6 Months	50.0 ± 20.0 [29.0-71.0]	74.4 ± 24.1 [49.1-99.7]	68.3 ± 30.2 [36.6-100.0]
18 Months	79.9 ± 10.7[b] [68.7-91.1]	90.7 ± 11.4[b] [78.7-102.7]	84.4 ± 15.8 [67.8-101.0]

PL Bundle Functional Contribution to Anterior Tibial Load Summary Data

The relative functional contribution of the PL bundle to overall anterior tibial load resistance varied significantly with age ($p=0.013$), angle ($p<0.001$), and state ($p<0.001$) and there was an interaction between age and angle ($p<0.001$), angle and state ($p=0.002$), and age and state ($p<0.001$) and no significant interaction between age, angle, and state ($p=0.669$) via multi-way ANOVA and Tukey's post-hoc analysis. Summary data presented as mean ± standard deviation [95% confidence interval of the mean].

Table A-4-7. PL Bundle Functional Contribution Summary Data [% total anterior joint force] ([a]$p<0.05$ vs. 1.5 months at a given state; [b]$p<0.05$ vs. 3 months at a given state; [c]$p<0.05$ vs. 4.5 months at a given state; [d]$p<0.05$ vs. 6 months at a given state; [e]$p<0.05$ vs. intact for a given age).

Intact	40° of Flexion	60° of Flexion	90° of Flexion
1.5 Months	60.5 ± 27.4 [31.8-89.2]	57.3 ± 27.4 [28.5-86.0]	56.9 ± 24.8 [30.8-82.9]
3 Months	64.0 ± 27.3 [35.4-92.7]	57.2 ± 26.2 [29.8-84.7]	54.9 ± 30.1 [23.3-86.5]
4.5 Months	17.0 ± 6.9 [19.6-55.3]	42.4 ± 19.0 [22.5-62.3]	63.2 ± 15.2 [47.2-79.1]
6 Months	24.7 ± 12.5 [11.5-37.8]	22.5 ± 16.3 [5.4-39.6]	37.9 ± 20.8 [16.1-59.7]
18 Months	10.7 ± 14.8[a,b,c] [-4.8-26.3]	9.5 ± 15.2[a,b,c] [-6.5-25.4]	13.8 ± 16.7[a,b,c] [-3.7-31.4]
AM-Deficient	**40° of Flexion**	**60° of Flexion**	**90° of Flexion**
1.5 Months[e]	105.3 ± 12.2 [92.4-118.2]	108.5 ± 16.8 [90.8-126.1]	107.3 ± 18.1 [88.3-126.2]
3 Months[e]	89.4 ± 19.1 [69.3-109.5]	89.0 ± 39.0 [48.1-129.9]	98.0 ± 28.7 [67.9-128.1]
4.5 Months[e]	72.9 ± 22.6 [49.2-96.7]	104.7 ± 17.5 [86.3-123.1]	112.0 ± 20.3 [90.7-133.3]
6 Months[e]	66.0 ± 15.5 [49.8-82.3]	88.1 ± 14.7 [72.6-103.5]	108.8 ± 11.6 [96.7-120.9]
18 Months[e]	78.5 ± 16.7 [60.9-96.0]	101.0 ± 16.3 [83.8-118.1]	92.9 ± 10.8 [81.6-104.2]

MCL Functional Contribution to Anterior Tibial Load Summary Data

The relative functional contribution of the MCL to overall anterior tibial load resistance varied significantly with angle ($p<0.001$), and state ($p<0.001$) but not age ($p=0.869$), and there

was an interaction between angle and state ($p<0.001$) but not age and angle ($p=0.999$), age and state ($p=0.201$) or age, angle, and state ($p=1.000$) via multi-way ANOVA and Tukey's post-hoc analysis. Summary data presented as mean ± standard deviation [95% confidence interval of the mean].

Table A-4-8. MCL Functional Contribution Summary Data [% total anterior joint force] ([a]$p<0.05$ vs. intact; [b]$p<0.05$ vs. AM-deficient; [c]$p<0.05$ vs. intact at 40° of flexion; [d]$p<0.05$ vs. AM-deficient at 60° of flexion).

Intact	40° of Flexion	60° of Flexion	90° of Flexion
1.5 Months	0.1 ± 1.4 [-1.3-1.5]	1.9 ± 4.8 [-3.2-7.0]	5.5 ± 5.6 [-0.4-11.3]
3 Months	2.0 ± 4.2 [-2.4-6.3]	0.3 ± 0.9 [-0.6-1.3]	6.0 ± 8.4 [-2.8-14.8]
4.5 Months	0.5 ± 0.8 [-0.3-1.3]	0.2 ± 0.5 [-0.4-0.7]	0.6 ± 0.6 [0.0-1.2]
6 Months	-0.3 ± 0.5 [-0.8-0.3]	0.3 ± 0.7 [-0.4-1.0]	0.5 ± 1.2 [-0.8-1.8]
18 Months	-0.5 ± 1.0 [-1.8-0.8]	0.6 ± 1.0 [-0.5-1.6]	4.6 ± 6.9 [-2.6-11.8]
AM-Deficient	**40° of Flexion**	**60° of Flexion**	**90° of Flexion**
1.5 Months	0.9 ± 2.5 [-1.6-3.5]	2.0 ± 2.1 [-0.3-4.2]	4.0 ± 5.8 [-2.2-10.1]
3 Months	5.1 ± 9.0 [-4.4-14.5]	2.5 ± 3.0 [-0.6-5.7]	8.7 ± 11.9 [-3.8-21.2]
4.5 Months	0.2 ± 0.4 [-0.2-0.6]	0.7 ± 1.0 [-0.3-1.8]	3.2 ± 0.7 [-0.4-1.0]
6 Months	0.8 ± 1.7 [-1.0-2.6]	1.0 ± 2.2 [-1.4-3.3]	0.4 ± 0.9 [-0.6-1.3]
18 Months	1.2 ± 2.4 [-1.3-3.8]	1.4 ± 2.4 [-1.1-3.8]	9.4 ± 11.8 [-2.9-21.8]
ACL-Deficient[a,b]	**40° of Flexion[c,d]**	**60° of Flexion[c,d]**	**90° of Flexion[c,d]**
1.5 Months	56.7 ± 30.4 [24.8-88.6]	70.7 ± 34.3 [34.6-106.7]	84.4 ± 34.7 [48.0-120.9]
3 Months	51.5 ± 19.6 [30.9-72.1]	64.5 ± 22.1 [41.4-87.7]	75.8 ± 21.5 [53.2-98.4]
4.5 Months	59.8 ± 34.8 [23.2-96.3]	68.5 ± 37.0 [29.6-107.4]	89.6 ± 44.8 [42.6-136.6]
6 Months	44.7 ± 23.7 [19.8-69.6]	58.7 ± 22.1 [35.6-81.9]	75.0 ± 22.2 [51.7-98.3]
18 Months	48.2 ± 23.9 [23.1-73.3]	54.8 ± 21.8 [31.9-77.7]	70.1 ± 28.5 [40.2-100.0]

Medial Meniscus Functional Contribution to Anterior Tibial Load Summary Data

The relative functional contribution of the medial meniscus to overall anterior tibial load resistance varied significantly with angle ($p=0.002$), and state ($p<0.001$) but not age ($p=0.448$), and there was an interaction between angle and state ($p=0.013$) and age and state ($p=0.003$), but not between age and angle ($p=0.708$) or age, angle, and state ($p=0.926$) via multi-way ANOVA and Tukey's post-hoc analysis. Summary data presented as mean ± standard deviation [95% confidence interval of the mean].

Table A-4-9. Medial Meniscus Functional Contribution Summary Data [% total anterior joint force] ([a]p<0.05 vs. intact; [b]p<0.05 vs. AM-deficient; [c]p<0.05 vs. intact at a given age; [d]p<0.05 vs. AM-deficient at a given age).

Intact	40° of Flexion	60° of Flexion	90° of Flexion
1.5 Months	0.2 ± 1.4 [-1.3-1.7]	1.0 ± 2.7 [-1.9-3.8]	-2.1 ± 5.5 [-7.9-3.7]
3 Months	-0.2 ± 0.8 [-1.0-0.6]	-0.2 ± 0.9 [-1.1-0.7]	-1.3 ± 1.1 [-2.4 - -0.1]
4.5 Months	0.6 ± 0.8 [-1.4-0.3]	-2.2 ± 1.8 [-4.0 - -0.3]	-3.3 ± 3.6 [-7.0-0.5]
6 Months	0.0 ± 0.4 [-0.4-0.4]	-0.8 ± 1.6 [-2.5-0.9]	-1.1 ± 1.2 [-2.4-0.2]
18 Months	-1.1 ± 2.2 [-3.4-1.1]	-1.5 ± 2.5 [-4.2-1.2]	-1.1 ± 3.6 [-4.8-2.7]
AM-Deficient	**40° of Flexion**	**60° of Flexion**	**90° of Flexion**
1.5 Months	-0.1 ± 1.5 [-1.7-1.5]	-1.3 ± 4.7 [-6.3-3.7]	-1.8 ± 3.8 [-5.8-2.2]
3 Months	-0.6 ± 0.6 [-1.2-0.1]	-0.2 ± 0.8 [-1.0-0.6]	-1.7 ± 1.0 [-2.4- -0.1]
4.5 Months	0.0 ± 0.6 [-0.6-0.6]	-2.4 ± 2.6 [-5.0-0.3]	-4.9 ± 4.4 [-9.5 - -0.3]
6 Months	0.2 ± 0.2 [0.0-0.3]	-0.2 ± 1.5 [-1.9-1.4]	-2.1 ± 2.6 [-4.8-0.7]
18 Months	0.9 ± 1.0 [-1.9-0.2]	-2.2 ± 3.8 [-6.2-1.8]	-3.1 ± 6.8 [-10.2-4.0]
ACL-Deficient[a,b]	**40° of Flexion**	**60° of Flexion**	**90° of Flexion**
1.5 Months[c,d]	28.0 ± 28.0 [-2.5-56.4]	21.8 ± 24.1 [-3.5-47.1]	18.5 ± 22.1 [-4.7-41.6]
3 Months[c,d]	24.2 ± 20.5 [2.6-45.7]	23.4 ± 23.2 [-0.9-47.7]	16.0 ± 23.9 [-9.1-41.1]
4.5 Months	13.9 ± 13.5 [-0.2-28.0]	14.8 ± 17.6 [-3.7-33.2]	-9.0 ± 13.2 [-22.9-4.9]
6 Months[c,d]	16.3 ± 16.5 [-1.1-33.6]	26.0 ± 13.5 [11.8-40.2]	11.5 ± 9.1 [1.9-21.1]
18 Months[c,d]	23.6 ± 17.3 [5.4-41.8]	34.7 ± 21.3 [12.3-57.1]	20.7 ± 27.2 [-7.8-49.2]

Appendix 5

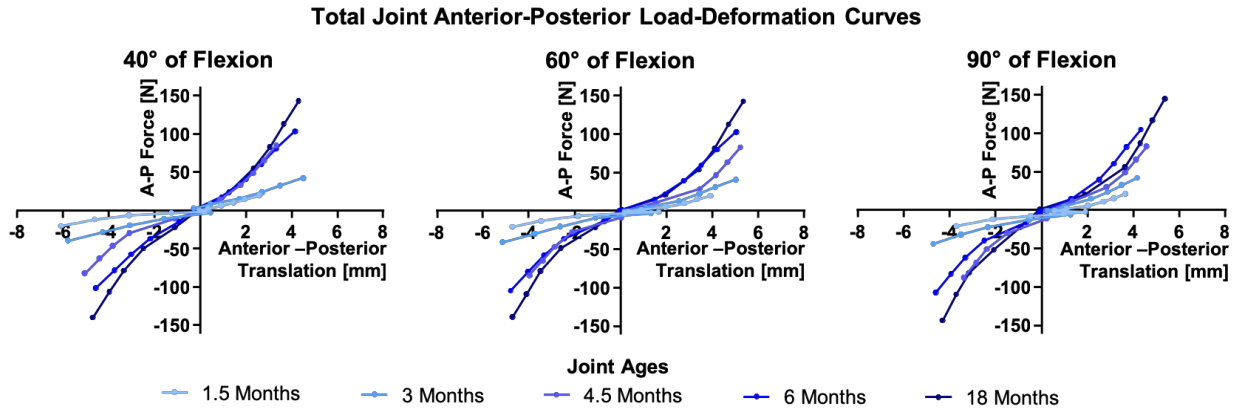

Figure A-5-1. The anterior-posterior (A-P) load-deformation curves of intact joints vary with age. Individual points represent group averages. Y-axis values range from negative (posterior tibial force) to positive (anterior tibial force) while x-axis values range from negative (posterior tibial translation) to positive (anterior tibial translation). Data presented at 40°, 60°, and 90° of flexion.

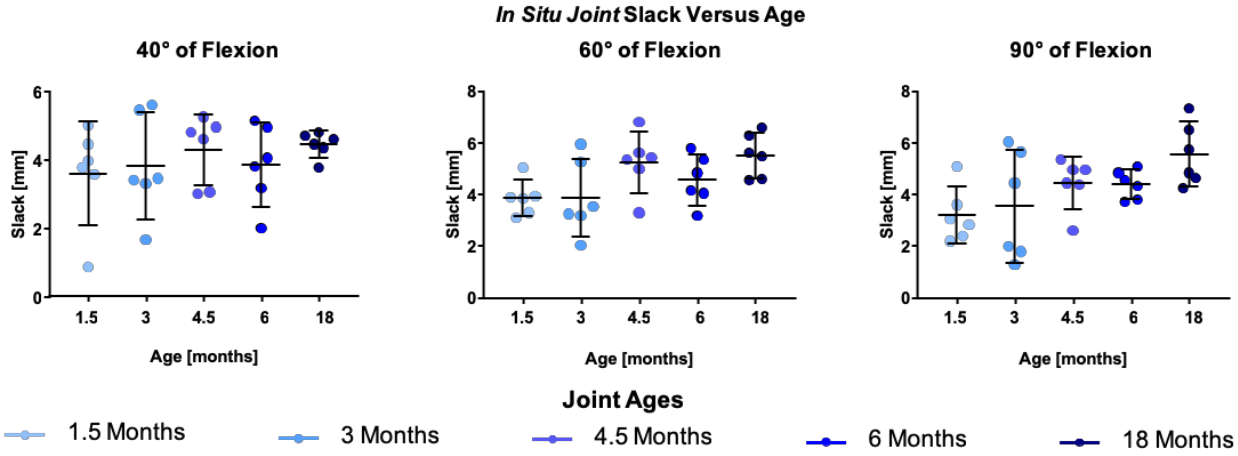

Figure A-5-2. In situ joint slack does not change substantially across age groups. Points represent data from separate specimens, bars represent mean ± 95% C.I. Data presented at 60° of flexion.

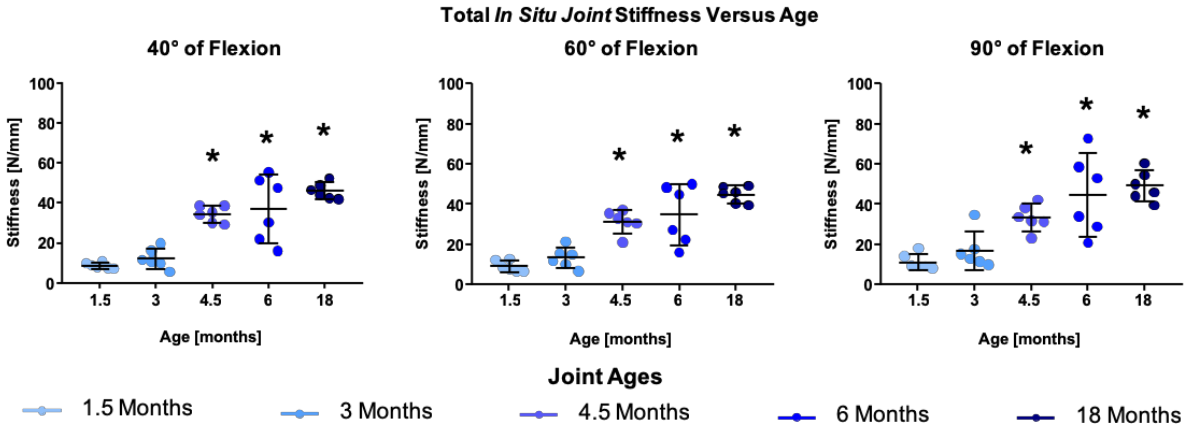

Figure A-5-3. In situ joint stiffness increases with increasing age across flexion angles. Points represent data from separate specimens, bars represent mean ± 95% C.I. * represents statistically significant difference from both 1.5 and 3 months. Data presented at 60° of flexion.

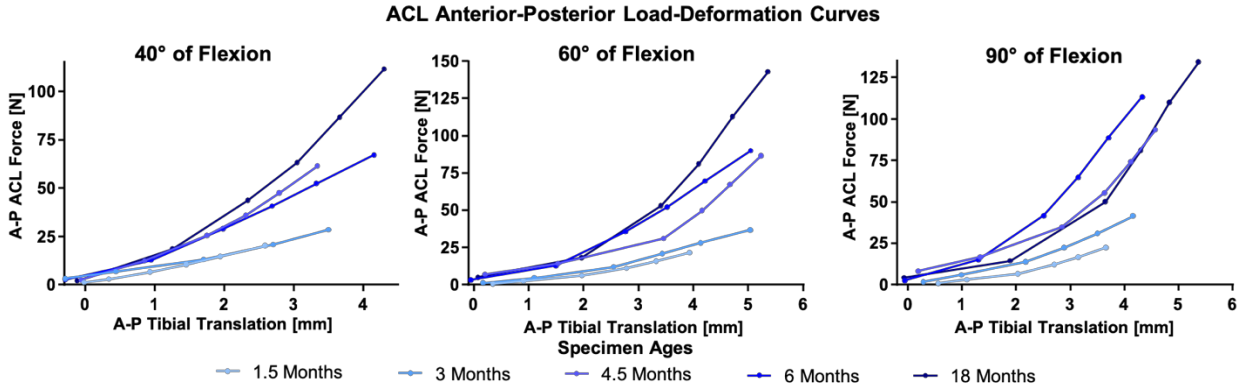

Figure A-5-4. The anterior-posterior (A-P) load-deformation curves of ACLs vary with age. Individual points represent group averages. Y-axis values range from negative (posterior force) to positive (anterior force) and x-axis values range from negative (posterior translation) to positive (anterior translation). Data presented at 60° of flexion.

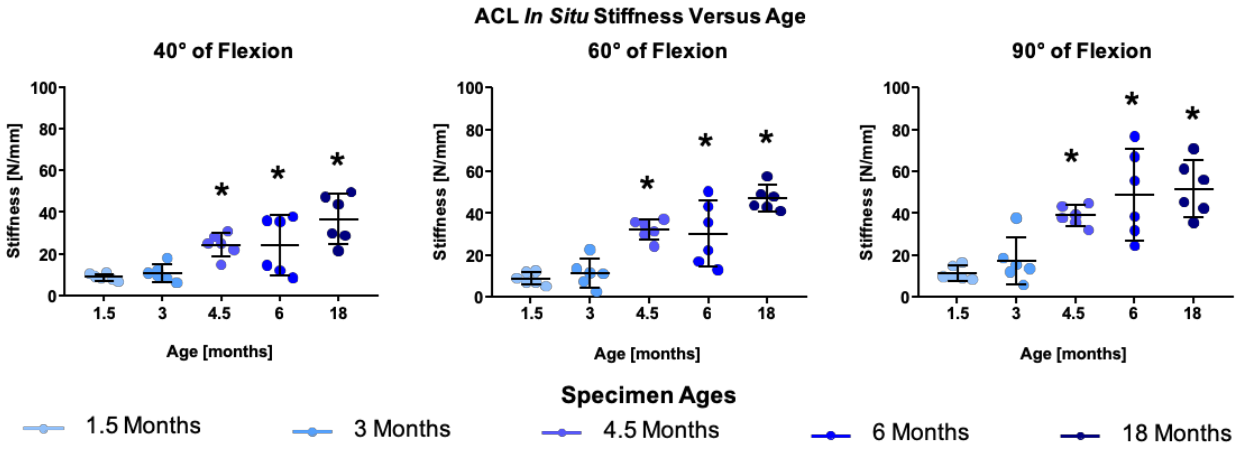

Figure A-5-5. ACL stiffness versus age. Points represent data from separate specimens, bars represent mean ± 95% C.I. * represents statistically significant difference from both 1.5 and 3 months.

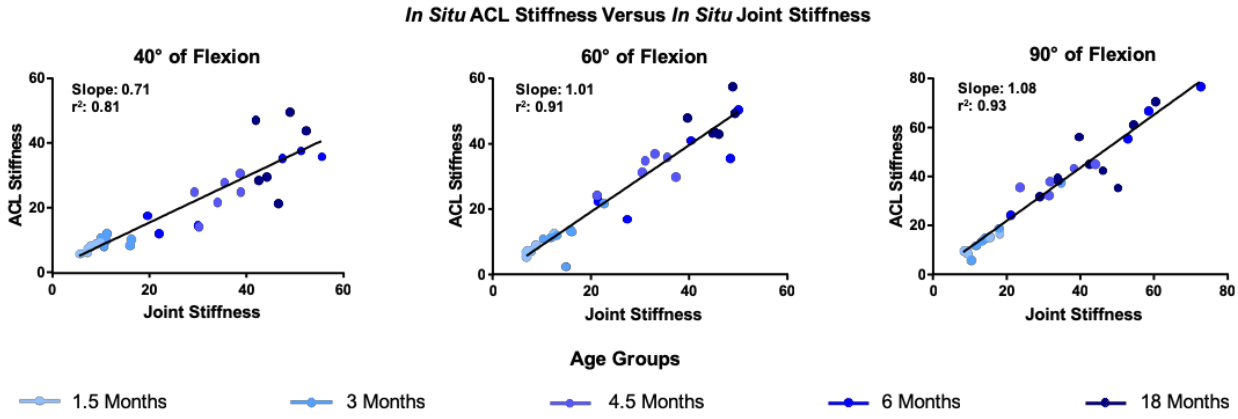

Figure A-5-6. Line of best fit for ACL stiffness versus joint stiffness at 60° of flexion.

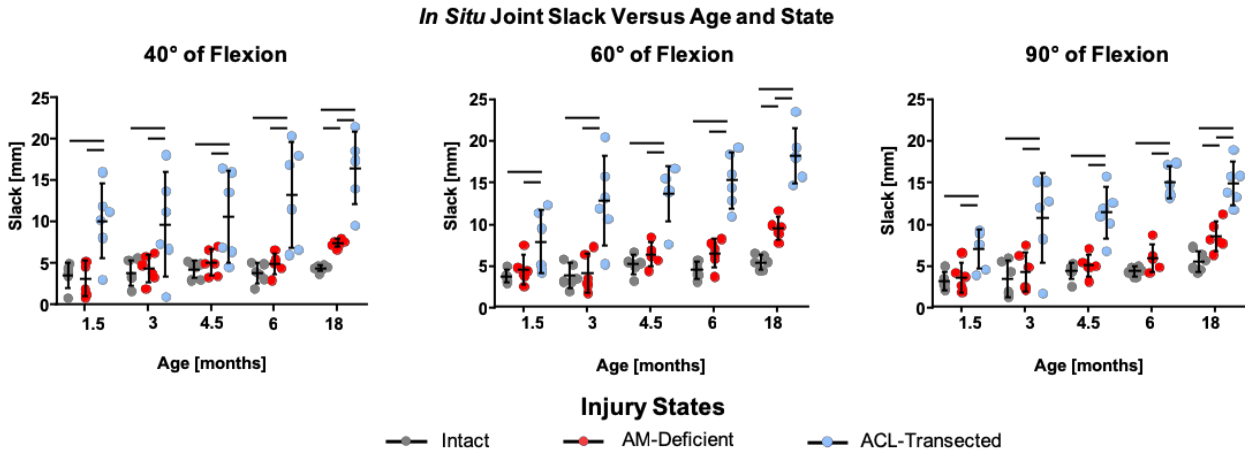

Figure A-5-7. In situ joint slack increases as a result of both partial and complete ACL injury. Points represent data from individual specimens, lines connect data within specimens across states. Bars represent statistically significant differences between states.

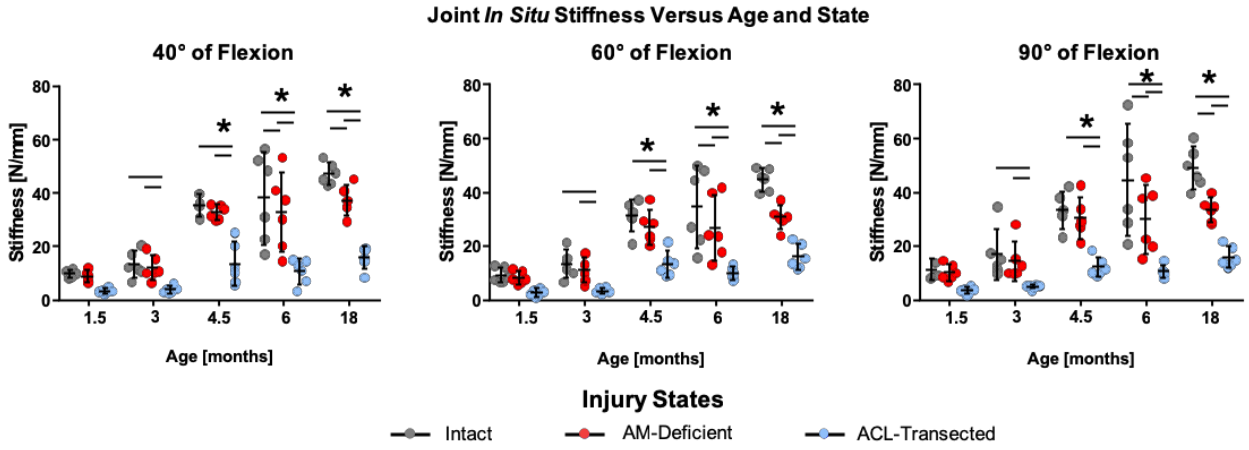

Figure A-5-8. In situ joint stiffness increases with age, but decreases as a result of complete ACL injury and partial injury in older groups. Points represent data from individual specimens, lines connect data within specimens across states. Bars represent significant differences between states ($p<0.05$). * represents significant difference from both 1.5 and 3 months ($p<0.05$).

Table A-5-1. Total joint *in situ* slack length varied significantly as an effect of age ($p<0.001$) and angle ($p=0.008$), with no interactions between age and angle ($p=0.767$).

In Situ Slack Length in mm			
Age [months]	40° of Flexion	60° of Flexion	90° of Flexion
1.5	4 ± 1 [2 – 5]	4 ± 1 [3 – 5]	3 ± 1 [2 – 4]
3	4 ± 2 [2 – 5]	4 ± 1 [2 – 5]	3 ± 2 [1 – 6]
4.5	4 ± 1 [3 – 5]	5 ± 1 [4 – 6]	4 ± 1 [3 – 5]
6	4 ± 1 [3 – 5]	5 ± 1 [4 – 6]	4 ± 1 [4 – 6]
18	4 ± 1 [4 – 5]	5 ± 1 [5 – 6]	6 ± 1 [6 – 7]

Table A-5-2. Normalized total joint *in situ* slack length varied significantly as an effect of angle (p=0.008), but not by age (p=0.188), with no interactions between age and angle (p=0.489).

	Normalized *In Situ* Slack Length		
Age [months]	40° of Flexion	60° of Flexion	90° of Flexion
1.5	0.14 ± 0.06 [0.08 – 0.20]	0.15 ± 0.03 [0.11 – 0.18]	0.12 ± 0.03 [0.09 – 0.16]
3	0.11 ± 0.05 [0.06 – 0.15]	0.11 ± 0.05 [0.06 – 0.16]	0.10 ± 0.06 [0.03 – 0.17]
4.5	0.10 ± 0.02 [0.08 – 0.12]	0.12 ±0.03 [0.10 – 0.15]	0.10 ± 0.02 [0.08 – 0.13]
6	0.08 ± 0.02 [0.06 – 0.11]	0.10 ± 0.02 [0.07 – 0.12]	0.09 ± 0.01 [0.08 – 0.11]
18	0.08 ± 0.01 [0.08 – 0.09]	0.14 ± 0.09 [0.05 – 0.23]	0.10 ± 0.02 [0.08 – 0.13]

Table A-5-3. Total joint *in situ* stiffness varied significantly as an effect of age (p<0.001) but not angle (p=0.323), with no interactions between age and angle (p=0.997).

	Joint *In Situ* Stiffness in N/mm		
Age [months]	40° of Flexion	60° of Flexion	90° of Flexion
1.5	9 ± 2 [7 – 10]	9 ± 3 [6 – 12]	11 ± 4 [7 – 15]
3	12 ± 5 [7 – 17]	13 ± 5 [8 – 18]	17 ± 9 [7 – 26]
4.5	34 ± 4 [30 – 39]	31 ± 6 [25 – 37]	33 ± 7 [27 – 40]
6	37 ± 17 [20 – 54]	35 ± 15 [19 – 50]	45 ± 20 [24 – 65]
18	46 ± 4 [42 – 50]	45 ± 4 [41 – 49]	49 ± 8 [41 – 57]

Table A-5-4. ACL *in situ* stiffness varied significantly as an effect of age (p<0.001) and angle (p<0.001), with no interactions between age and angle (p=0.219).

	ACL *In Situ* Stiffness in N/mm		
Age [months]	40° of Flexion	60° of Flexion	90° of Flexion
1.5	9 ± 2 [10 – 7]	9 ± 3 [6 – 12]	11 ± 3 [8 – 15]
3	11 ± 4 [6 – 15]	11 ± 7 [4 – 19]	17 ± 11 [29 – 6]
4.5	24 ± 6 [18 – 30]	32 ± 5 [27 – 37]	39 ± 5 [34 – 44]
6	24 ± 14 [10 – 38]	30 ± 15 [14 – 46]	49 ± 21 [27 – 71]
18	37 ± 12 [25 – 49]	47 ± 6 [41 – 53]	52 ± 13 [38 – 66]

Table A-5-5. Joint *in situ* slack length varied significantly as an effect of age ($p<0.001$), state ($p<0.001$), and angle ($p=0.008$), with an interactions between age and state ($p<0.001$), but no interactions between age and angle ($p=0.767$), state and angle ($p=0.641$), or age, state, and angle ($p=0.903$).

Joint *In Situ* Slack in mm			
Intact State	40° of Flexion	60° of Flexion	90° of Flexion
1.5	3.5 ± 1.4 [2.0 – 5.1]	3.8 ± 0.7 [3.1 – 4.5]	3.2 ± 1.1 [2.0 – 4.3]
3	3.8 ± 1.5 [2.2 – 5.3]	3.8 ± 1.4 [2.3 – 5.3]	3.5 ± 2.1 [1.3 – 5.7]
4.5	4.2 ± 1.0 [3.2 – 5.3]	5.3 ± 1.1 [4.0 – 6.4]	4.4 ± 1.0 [3.4 – 5.4]
6	3.8 ± 1.2 [2.6 – 5.0]	4.5 ± 1.0 [3.5 – 5.5]	4.3 ± 0.6 [3.8 – 4.9]
18	4.4 ± 0.4 [4.0 – 4.8]	5.5 ± 0.8 [4.6 – 6.4]	5.5 ± 1.2 [4.3 – 6.8]
AM- State	40° of Flexion	60° of Flexion	90° of Flexion
1.5	3.1 ± 2.0 [1.0 – 5.3]	4.5 ± 1.7 [2.8 – 6.3]	3.5 ± 1.7 [1.7 – 5.4]
3	4.4 ± 1.6 [2.6 – 6.0]	4.1 ± 2.2 [1.8 – 6.5]	4.3 ± 2.3 [1.9 – 6.7]
4.5	5.1 ± 1.6 [3.4 – 6.7]	6.4 ± 1.4 [5.0 – 7.9]	5.1 ± 1.3 [3.8 – 6.4]
6	4.9 ± 1.2 [3.7 – 6.2]	6.5 ± 1.6 [4.8 – 8.2]	6.0 ± 1.6 [4.3 – 7.6]
18	7.4 ± 0.5 [6.9 – 7.9]	9.5 ± 1.3 [10.9 – 8.2]	8.6 ± 1.7 [6.7 – 10.4]
ACL- State	40° of Flexion	60° of Flexion	90° of Flexion
1.5	10.1 ± 4.3 [5.5 – 14.6]	7.9 ± 3.6 [4.1 – 11.7]	7.0 ± 2.2 [4.6 – 9.3]
3	9.7 ± 6.0 [3.3 – 16.0]	12.9 ± 5.1 [7.5 – 18.3]	10.8 ± 5.1 [5.5 – 16.2]
4.5	10.6 ± 5.3 [5.1 – 16.2]	13.7 ± 3.2 [10.3 – 17.0]	11.4 ± 3.0 [8.3 – 14.5]
6	13.2 ± 6.1 [6.8 – 19.6]	15.3 ± 3.2 [11.9 – 18.7]	15.0 ± 1.9 [13.0 – 16.9]
18	16.4 ± 4.1 [12.1 – 20.8]	18.2 ± 3.1 [15.0 – 21.5]	14.9 ± 2.5 [12.3 – 17.6]

Table A-5-6. Normalized total joint *in situ* slack length varied significantly as an effect of age ($p<0.001$), state ($p<0.001$), and angle ($p=0.047$), with an interaction between age and state ($p<0.001$), but no interactions between age and angle ($p=0.916$), state and angle ($p=0.381$), or age, state, and angle ($p=0.999$).

Joint *In Situ* Stiffness in N/mm			
Intact State	40° of Flexion	60° of Flexion	90° of Flexion
1.5	9 ± 2 [7 – 10]	9 ± 3 [6 – 12]	11 ± 4 [7 – 15]
3	12 ± 5 [7 – 17]	13 ± 5 [8 – 18]	17 ± 9 [7 – 26]
4.5	34 ± 4 [30 – 39]	31 ± 6 [25 – 37]	33 ± 7 [27 – 40]
6	37 ± 17 [20 – 54]	35 ± 15 [19 – 50]	45 ± 20 [24 – 65]
18	46 ± 4 [42 – 50]	45 ± 4 [41 – 49]	49 ± 8 [41 – 57]
AM- State	40° of Flexion	60° of Flexion	90° of Flexion
1.5	8 ± 2 [6 – 10]	8 ± 2 [6 – 11]	10 ± 3 [7 – 14]
3	11 ± 5 [6 – 16]	11 ± 5 [6 – 16]	14 ± 7 [7 – 22]
4.5	32 ± 3 [29 – 35]	27 ± 6 [21 – 34]	30 ± 7 [23 – 38]
6	32 ± 14 [17 – 47]	27 ± 12 [15 – 39]	30 ± 12 [17 – 43]
18	36 ± 5 [30 – 41]	31 ± 4 [26 – 35]	34 ± 4 [29 – 38]
ACL- State	40° of Flexion	60° of Flexion	90° of Flexion
1.5	2 ± 1 [1 – 3]	3 ± 1 [1 – 4]	4 ± 1 [2 – 5]
3	3 ± 1 [1 – 4]	3 ± 1 [2 – 5]	5 ± 1 [4 – 6]
4.5	12 ± 8 [4 – 21]	13 ± 5 [8 – 18]	12 ± 4 [9 – 16]
6	10 ± 5 [5 – 14]	10 ± 2 [7 – 12]	11 ± 2 [8 – 13]
18	15 ± 4 [10 – 19]	16 ± 5 [11 – 21]	16 ± 4 [12 – 20]